UNIVERSITY OF KWAZULU-NATAL

PERFORMANCE ANALYSIS OF OPTICAL WIRELESS COMMUNICATION SYSTEMS IN A WARM-SUMMER MEDITERRANEAN CLIMATIC REGION

Olabamidele O. Kolawole

Supervised by:

Professor Thomas J.O. Afullo

Dr. Pius A. Owolawi

2017

PERFORMANCE ANALYSIS OF OPTICAL WIRELESS COMMUNICATION SYSTEMS IN A WARM-SUMMER MEDITERRANEAN CLIMATIC REGION

Olabamidele O. Kolawole

Supervised by:

Professor Thomas J.O. Afullo

Dr. Pius A. Owolawi

Submitted in fulfilment of the academic requirements

for the degree of MSc. Engineering

in the Faculty of Engineering

at the University of KwaZulu-Natal, Durban, South Africa

June 2017

As the candidate's supervisor, I agree to the submission of this dissertation.

Date of Submission: _____

Supervisor: _____

Professor Thomas J.O. Afullo

To the all-knowing God,

Acknowledgements

I wish to express my sincere gratitude to my supervisor, Professor Thomas J.O. Afullo, for his invaluable support, encouragement, and guidance all through the course of this work. I appreciate his efforts in proofreading this dissertation and for giving me the invaluable opportunity to undertake my studies in his research group.

I deeply appreciate my parents, Pastor and Mrs. O. A. Kolawole and my ever lovely sisters – Gbemisola, Ololade and Toluwalase for their unwavering support, prayers, understanding, encouragement, and patience all through my master's degree program.

Lastly, I wish to thank all my friends, colleagues and academic mentors at the University of KwaZulu-Natal for all their encouragements and insightful advice.

Declaration

I, Olabamidele Kolawole, declare that,

i. The research reported in this dissertation, except where otherwise indicated, is my original work.

ii. This dissertation has not been submitted for any degree or examination at any other university.

iii. This dissertation does not contain other persons' data, pictures, graphs or other information unless specifically acknowledged as being sourced from other persons.

iv. This dissertation does not contain other persons' writing unless specifically acknowledged as being sourced from other researchers. Where other written sources have been quoted, then:

   a. Their words have been re-written but the general information attributed to them has been referenced;

   b. Where their exact words have been used, their writing has been placed inside quotation marks and referenced.

v. Where I have reproduced a publication of which I am an author, co-author or editor, I have indicated in detail which part of the publication was actually written by myself alone and have fully referenced such publications.

vi. This dissertation does not contain text, graphics or tables copied and pasted from the Internet, unless specifically acknowledged, and the source being detailed in the dissertation and in the References sections.

Signed: _____

Abstract

Optical Wireless Communication (OWC) involves the propagation of information-carrying optical signals through the free space channel. This technology promises high modulation bandwidths over the unlicensed spectrum with cost-effective deployment and quick installation. The performance of OWC systems is heavily dependent on the state of atmospheric conditions in a given environment. Optical signals are known to experience scattering attenuation in foggy weather and in clear weather conditions while turbulence losses of optical signals occur as a result of fluctuations in the atmosphere's refractive index.

In this dissertation, an in-depth performance analysis is carried out on OWC systems in a warm-summer Mediterranean climatic region using Cape Town, city of South Africa as a case study. Regression Models for predicting visibilities in such climatic regions from other weather parameters such as relative humidity, maximum temperature and fraction of sunshine hours are investigated. The atmospheric scattering attenuation coefficients are estimated using different models such as the Kim, Kruse, Ferdinandov et al, Naboulsi, Ijaz, and Grabner et al models over visibilities ranging from 0 - 50 km. These estimated scattering attenuation computations amongst others are carried out on commonly used commercial OWC systems transmitting at 850, 950 and 1550 nm wavelengths. Scintillation effects leading to power losses in OWC systems as well as the required link budget analysis are also investigated. The minimum required visibility relations and their corresponding link availability estimations from various models are then derived. Finally, the analyzed results are applied to cross M-ary QAM OWC systems and their bit error rate performance analysis is presented.

From the results obtained, the average multiple regression model is adjudged to be the best and most suitable model for determining the visibility in Cape Town based on the fact that it results in the highest correlation coefficient and the lowest standard error result. This regression model is then used to estimate the minimum, average and maximum monthly visibility ranges for a six year period (2010 – 2015). The aerosol scattering attenuation models considered in this work predict that OWC systems will encounter high attenuation values of up to 150 dB/km on 850 nm, 950 nm and 1550 nm optical transmission wavelengths. Scintillation losses are determined to have a contribution of over 90% to the total atmospheric losses on selected wavelengths and link distances up to 15 km. It is also determined that the optical signals being transmitted on the 1550 nm wavelength have better link availability over a specific propagation distance as compared to the 850 and 950 nm wavelengths.

As an application, the bit error rate (BER) performance analysis conducted on the proposed cross M-QAM OWC systems indicate that in order to attain a certain BER value, transmitting wavelengths of 850 nm and 950 nm result in higher Signal-to-noise ratios (SNR) than the 1550 nm wavelength. This shows that it is more power efficient to transmit optical signals on the 1550 nm wavelength using the spectral efficient cross M-QAM OWC system. Implementing the results of this work on the design of OWC systems produces a highly sophisticated, but cost-effective system which has ~99.999% link availability while still maintaining eye safety standards in warm-summer Mediterranean climatic regions.

Table of Contents

List of Figures

List of Tables

List of Acronyms

OWC	Optical wireless communication
APD	Avalanche photodetector
BER	Bit error rate
bps	Bits per second
CDRH	Centre for Devices and Radiological Health
CENELEC	European Committee for Electrotechnical Standardization
GaAs	Gallium arsenide
IEC	International Electrotechnical Commission
LED	Light emitting diode
LOS	Line of sight
MLCD	Mars Laser Communication Demonstration
pdf	Probability density function
PIN	p-type-intrinsic-n-type photodetector
QAM	Quadrature amplitude modulation
RF	Radio frequency
S.I.	Scintillation index
SILEX	Semiconductor-Laser Inter-Satellite Link Experiment
SNR	Signal to noise ratio

List of Symbols

$T(\lambda, L)$	Transmittance of the atmospheric channel
α_{ext}	Coefficient of atmospheric attenuation
L	Propagation length.
V	Atmospheric visibility
T_{th}	Transmission threshold
a_c, b_c, c_c and d_c	Coefficients of regression
$R.H.$	Relative humidity
$T_{\max}$	Maximum temperature
$\frac{n}{N}$	Fraction of sunshine hours
$A_\alpha(L,V)$	Atmospheric attenuation (dB)
$\alpha_a(V)$	Total extinction coefficient
$\sigma_m(\lambda)$	Molecular absorption coefficient
$\sigma_a(\lambda)$	Aerosol absorption coefficient
$\beta_m(\lambda)$	Raleigh scattering coefficient
$\beta_{as}(\lambda)$	Aerosol scattering coefficient
λ	Optical signal wavelength
λ_o	Maximum spectrum wavelength of the solar band
q_o	Particle size distribution parameter
$\sigma_{S.I.}$	Scintillation index
k	Optical wave number
$C_n^2\left[m^{-2/3}\right]$	Refractive index profile parameter
a	Altitude
w_v	Wind velocity
α_{turb}	Atmospheric turbulence loss
$\sigma_{P-S.I.}$	Power scintillation index
D	Diameter of the receiver lens

$A_{tl}(L)$	Fading loss due irradiance fluctuations
P_{up}	Upper bound probability
$L_M(L)$	Optical link margin
P_{tx}	Transmitted optical power
S_{tx}	Total losses in the transmitter
S_{rx}	Aggregate losses in the receiver
θ	Beam divergence angle in radians,
R_s	Receiver sensitivity in dB
M_o	84 dB when L is measured in meters
L_{Geo}	Geometric or optical divergence loss
$V_{\min}(L)$	Minimum required visibility
L_A	Link availability
P_I	Probability density function of the received light intensity (irradiance)
I	Irradiance at the receiver
I_0	Turbulence-free irradiance
M_I	In-phase signals
M_Q	Quadrature signals
$A_I(t)$	In-phase signal components
$A_Q(t)$	Quadrature signal components respectively;
α_i	In-phase information signal components of the i th amplitude symbol
β_i	Quadrature information signal components of the i th amplitude symbol
$g(t)$	Signal shaping pulse

T_s	Symbol time interval
I_m	Modulation index
$P(t)$	Radiated optical intensity
a_L	Signal link loss factor
$X_s(t)$	Stationary random processed signal scintillation
A_r	Area of the receiver
$\Re$	Photodetector's responsivity
G	Average gain
$n(t)$	Total noise at the receiver
BER_{inst}	Instantaneous bit error rate of the system
$P_I(I)$	Probability distribution function of I
$P_{M(BER)}$	BER expression for the general cross M-ary QAM
BER	BER of the OWC system

Chapter 1
INTRODUCTION

1.1 Background of OWC

Optical Wireless Communication (OWC) involves the propagation of information-carrying optical signals through the free space channel. The first free space communication through a wireless media was carried out by Alexander Graham Bell in 1880. In his famous Photo-phone experiment, the sun's radiation was modulated with voice signals and transmitted over 0.2 kilometers. Due to the crudity of the transmitter and receiver and the unstable fluctuation of the sun's radiation, the results obtained were not valid [1, 2].

The popularity of OWC began to gather momentum in the 1960s with the discovery of the laser. Novel research breakthroughs such as the use of GaAs light emitting diodes to propagate a television signal over a distance of 48 kilometers by some researchers, a 190 kilometers transmission of voice using the HE-NE laser beam as the optical carrier wave in the USA amongst others sparked great interest in OWC systems [3]. The military developed a keen interest in OWC and began using it for discreet communication during covert operations. NASA and the ESA researched greatly into OWC and used it successfully for two of its deep space programmes namely: Semiconductor-laser Inter-satellite Link Experiment (SILEX) and Mars Laser Communication Demonstration (MLCD) as reported in[4, 5].

OWC has witnessed rapid development with the advent of highly sophisticated optoelectronic devices. With the ever increasing demand for data bandwidth, telecommunication companies are now exploring alternative/backup access network options to connect end users together. Field trials involving the deployment and use of OWC systems to back up the already existing access networks have been carried out successfully in various parts of the world [6-9]. This has led to the emergence of OWC systems as a viable complementary technology to millimeter-wave and radio frequency (RF) wireless systems for the reliable deployment of multimedia signals within the access networks.

1.2 Research Motivation

Warm-summer Mediterranean climatic regions are regions that experience warm and dry summers. No mean monthly temperatures exceed 22 ^{o}C during its warmest month and there is an average temperature range of -3 to 18 ^{o}C in its coldest month. Mild to chilly rainy weather is experienced during winter which may sometimes be accompanied by snowfall. Places with this type of weather include Spain, Portugal, Western Washington, Central Chile, Southern Australia, Cape Town, etc. A common feature of all the places aforementioned is that they are all urban, industrialized areas with large human population. This definitely translates to a high number of communication devices which results in a huge demand for

bandwidth. This has prompted Telecommunication companies to look for viable alternative/backup links to the already existing microwave and RF links. It is highly expensive laying fiber optic cables and a cost effective alternative with very high and secure bandwidths will be a viable option. The optical wireless communication system (OWCS) possesses these desirable qualities. It is important to have a thorough performance analysis of the OWCS given the available scattering and turbulence loss models which will aid in designing highly sophisticated, but cost-effective systems having ~99.999% link availability while maintaining eye safety standards. Using some meteorological data for Cape Town, South Africa, the results can be extended to OWCS design in other regions with similar climatic characteristics.

1.3 Research Objectives

The main objectives of this work are:

1. To determine the visibility of Cape Town from various weather parameters such as Relative Humidity, Maximum Temperature, and Fraction of Sunshine Hours using Regression Analysis.

2. To estimate the minimum, maximum and average atmospheric attenuation values of Optical Wireless Communication (OWC) systems in Cape Town using various models.

3. To approximate the probability of encountering various atmospheric attenuation conditions.

4. To determine the power loss caused by scintillation effects using the lognormal model.

5. To perform and analyze the link budget and availability of Optical Wireless Communication Systems in a warm-summer Mediterranean environment.

1.4 Dissertation Organization

The rest of this dissertation is organized as follows: Chapter Two presents an in-depth literature review of OWC systems which includes an overview, features, areas of application, design and eye safety standards considered in OWC. Chapter Three examines the models and equations used for computing the aerosol scattering attenuation, turbulence losses, optical link margin, and system availability. An elaborate discussion of the results is carried out in chapter Four. Insightful applications of some of the results in chapter four are used to evaluate the bit error rate (BER) performance of cross M-QAM OWC systems in chapter Five. Chapter Six concludes the dissertation.

1.5 Publication

O. O. Kolawole, T. J. Afullo and P. A. Owolawi **"**Performance Analysis of Cross M-QAM over Weak Atmospheric Turbulence Channel" SATNAC Conference, George, Western Cape, South Africa, 4-7 September 2016.

Chapter 2
LITERATURE REVIEW

2.1 Introduction

This chapter presents an overview of the OWC technology with a review of the existing related works done in the field. Major features and applications of OWC systems are itemized. The chapter is concluded with a depiction and explanation of the blocks making up the OWCS and a discussion on eye safety and standards.

2.2 Overview of OWC Technology

OWC involves the use of lasers in transferring information/data between two nodes via unguided media. The unguided media may include one or a combination of water, space or the atmosphere. Since this work is based on terrestrial OWC, the channel of focus is the atmosphere. The information signal to be transmitted may be impinged on any of the optical carrier wave characteristic property which includes its intensity, frequency, and phase. The OWCS is a line-of-sight (LOS) technology which requires the direct alignment of the transceivers with no form of obstacle in between them.

The conventional OWC system is for point-to-point communication with two cognate transceivers placed at each end of the link. This communication configuration allows for a high data rate full duplex throughput in which information exchange can be achieved simultaneously between the two transceivers. A review of existing related work, the features, applications as well as the delineating of the blocks of the OWCS are discussed in the following sections

2.3 Review of Existing Related Work

In [10], Usman et al used meteorological parameters such as relative humidity, sunshine hours and maximum temperature to estimate the monthly average visibility at Sokoto, Nigeria. This was achieved using three linear regression models which focused on establishing their direct relationships with the visibility. Measurements and analysis of relative humidity (R.H.), fraction of sunshine hours and maximum temperature for a period of five years were sorted and used to predict the visibility of subsequent years using the obtained regression equations. On comparing the correlation coefficients and absolute errors of the three linear regression equations, the best model was accepted to be: $V = 7.02 + 0.16$ (R.H). It was concluded that the relative humidity had the best linear relationship with the visibility in Sokoto, Nigeria.

Kim et al in [11] sought to correct the misconception that 1550 nm wavelength of optical signals were less affected by aerosol scattering attenuation than the shorter wavelengths (780 and 850 nm) for all weather conditions. After exhaustive literature search and in-depth computations using the Mie scattering theory, it was discovered that the attenuation of laser beams for visibility less than 500 meters is wavelength independent in fog, rain and snowy weather. A new modification of the scattering attenuation equation which described the power loss level of the optical signal more accurately was proposed. It was concluded that short optical wireless communication links will meet the demand requirement for high link availability in the communication industry after adopting the proposed modification.

Using the FASCOD computation, Al Naboulsi investigated the optical wireless system performance in the presence of advection and convection fog for wavelengths in the range of 400 - 1550 nm. A high transmission gain was observed for a lasercom system working at shorter wavelengths as compared to the one transmitting at 1550 nm. New scattering attenuation equations derived from the exact Mie scattering theory calculations and valid for a wavelength range of 690 – 1550 nm were thereafter proposed in [12]. It was concluded that the new equations would predict the fog attenuation through visibility measurements without reliance on computer programs.

In [13], Ferdinandov et al proposed new empirical models for the aerosol and molecular scattering coefficients in the lower troposphere using analytical methods. The models were found to be valid for a visibility range of 100 – 50000 meters and a wavelength interval 0.3 – 1.1 μm. The results of the proposed equations were compared and validated by the experimental results of other works. It was concluded that the modeling of the scattering loss in the troposphere would aid the analysis and design of optoelectronic optical wireless communication systems. Models developed from the empirical data of fog for determining the total extinction coefficient were developed for the 830 and 1550 nm wavelengths in [14]. The models were concluded to be valid locally with root mean square error values close to the Naboulsi convection model.

In [15], Ijaz designed and built an indoor atmospheric chamber to mimic the heterogeneous fluctuations of a real outdoor atmosphere. This was done to investigate fog and smoke attenuations of optical signals at visibilities between 0 – 1000 meters. The results obtained indicated that the fog attenuation is wavelength dependent for all ranges of visibility. This negates the claim by Kim which suggested that for visibility less than 500 meters, the fog attenuation is independent of all ranges of wavelength. The particle size distribution parameter value was modified by reconsidering it as a function of wavelength rather than visibility and a

new empirical model was proposed to estimate the wavelength dependent fog and smoke attenuation of optical signals pronounced in urban industrial areas.

From the visibility data collected at various airports in France, Germany, and Italy over a four-year period, a statistical evaluation was conducted by Prokes in [16] to determine the attenuation due to scattering of optical signals in Europe. The scintillation loss was modeled using the Rytov turbulence theory and an exhaustive link budget analysis and availability was computed from specified optical wireless communication link parameters.

2.4 Features of OWC

High Modulation Bandwidth – The optical carrier waves have very high-frequency bandwidths of up to 2000 THz. Since there is a direct relationship between the amount of data transmitted and the bandwidth of the carrier, high data rates of up to 20% of the carrier frequency is achievable in OWC technology.

Unlicensed Spectrum – The optical wireless spectrum is unlicensed and free. This poses an advantage over the congested RF spectrum that is being faced by bureaucratic bottlenecks and stringent government regulations before a part of the spectrum is allocated for use.

Quick Installation and Deployment – With the right installation tools available, the optical wireless communication system (OWCS) can be installed and deployed in very few hours. The pertinent instruction to note is that there must be no obstruction in the line of sight between the transmitter and the receiver.

Cost Effectiveness – It is cheaper to deploy an OWCS than its RF counterpart with a similar data rate of transmission. By eliminating the extra costs of trenching when laying optical fibers, OWC is an ideal alternative to delivering the same bandwidth.

Weather Dependence – The performance of OWC systems are heavily dependent on the state of atmospheric conditions present in the environment. Optical signals are known to experience scattering attenuation in Foggy weather and in clear weather situations while turbulence losses of optical signals occur as a result of fluctuations in the atmosphere's refractive index.

2.5 Areas of Application

The features of OWC highlighted above makes it very attractive in many areas of application namely:

Last Mile Access – The OWC technology bridges the bandwidth gap existing between the optical fiber backbone and the end users. OWC links transmitting data rates of up to 10 Gbps with link lengths of up to few kilometers are available in the market [17, 18].

Backup to Fiber Optic Links – In situations where the optical fiber communication link is damaged or unavailable, OWC systems can be deployed as a backup to fill the gap [19, 20].

Temporal Links – In situations of disaster, OWC systems can serve as temporary links since they are easy to install and use [21, 22].

Difficult Topography – In difficult terrains, it is cost effective to deploy OWC systems instead of laying optic fiber cables [23].

High-Definition Television – OWC systems can be used to broadcast live high definition video signals in remote places to the television stations [17, 24].

2.6 Block Diagram of OWC System

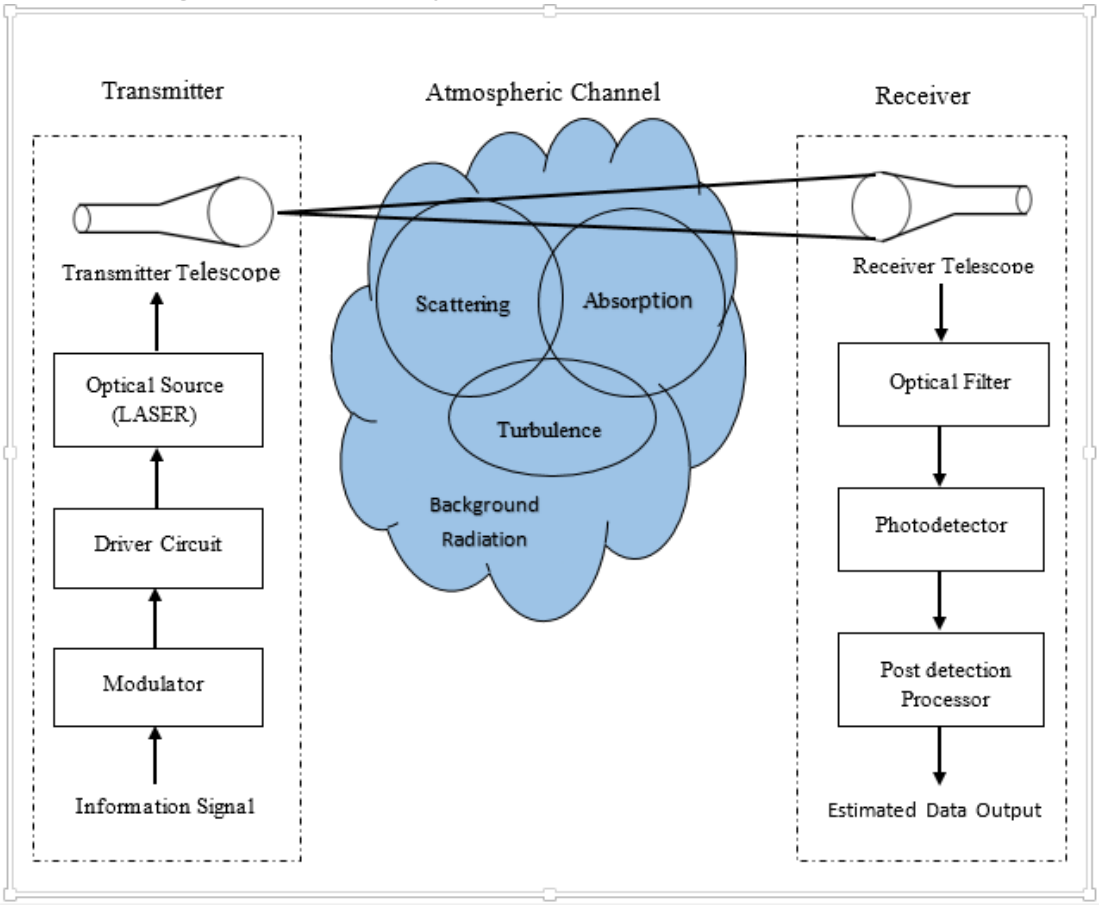

Figure 2.1 Block diagram of a terrestrial OWC system

The block diagram of a conventional terrestrial OWC link is shown in Figure 2.1. The OWCS comprises the transmitter, atmospheric channel and receiver. Each of these blocks will be discussed in the next sections below:

2.6.1 The Transmitter

In this part of the OWCS, the information signal is being modulated onto the optical carrier wave and sent via the atmospheric channel to the receiver. The intensity modulation (IM) is commonly employed in most OWCS. It involves the direct variation of the current driving the optical carrier wave in line with the information signal to be transmitted. This could also be achieved through an external modulator such the Mach-Zehnder interferometer. Apart from modulating the optical carrier wave through its intensity, other characteristic properties such as frequency, phase, and state of polarization (SOP) of the carrier wave can also be modulated with the information signal. Optical sources commonly employed in OWC systems include vertical cavity surface emitting laser (850 nm), Fabry-Perot lasers (~1300 nm), Distributed-feedback lasers (~1500 nm), LED (near Infrared) etc. These sources are reliable, very cheap, readily

available and, can achieve data rates up to 40 Gbps. The Transmitter telescope collimates and transmits the optical modulated radiation towards the receiver at the opposite end of the channel [25, 26].

2.6.2. The Atmospheric Channel

The atmosphere comprises gases such as Nitrogen, Oxygen, Argon, Carbon dioxide, water vapor etc. and minute particles suspended in the air (aerosols). Rain, haze, fog and other weather conditions are also present in the atmosphere. These weather conditions are seasonal and location dependent. The concentration of aerosols are higher near the earth surface (troposphere) and reduce with increasing altitude. These atmospheric constituents cause scattering and absorption of the optical signals propagating through the atmosphere leading to a reduction in the power levels of the signal reaching the receiver [27].

During sunny and clear sky conditions, the temperature inhomogeneity of the atmosphere resulting from the turbulent mixture of the warm, light air close to the earth surface and the cooler air mass at higher altitudes causes intense fluctuations in the refractive index of the atmosphere [2]. This leads to the full or partial deviation of optical beams traversing through the varying refractive prisms of air packets or eddies. The optical information signal thus experiences random fading in its irradiance and phase. Atmospheric turbulence effects on optical signals include: beam steering, beam spreading, spatial coherence degradation, polarization fluctuation etc. [28].

2.6.3. The Receiver

Here, the transmitted information signal is recovered from the incident optical radiation. The incident optical beam is collected and focused onto the photodetector via the optical bandpass filter. The larger the aperture of the receiver telescope, the more the collection of the incoming uncorrelated optical beams. It should, however, be noted that, the wider the aperture, the more the background noise being transferred to the detector. The optical bandpass filter reduces the amount of background noise and sends its output to the Photodetector. The incoming optical signals are being converted into electrical signals by the photodetector. The commonly used photodetectors in OWCS receivers are the p-i-n diode (PIN) and the avalanche photodiode. Examples of photodetectors commonly employed are Silicon PIN (300 – 1100 nm), Silicon APD (400 – 1000 nm), InGaAs APD (1000-1700 nm) etc. These photodetectors have gains ranging from 1 – 150 at up to 1.25 Gbps data rates. The post-detection processor also known as the decision circuit, amplifies, filters and processes the electrical signal output of the photodetector in order to recover the information signal sent from the transmitter [25].

The two main receiver detection processes are the direct and coherent detection methods. In the former, the intensity or power of the incoming optical beam impinging on the photodiode is detected [28]. On the other hand, in the coherent detection receiver, the incident optical field is mixed with the signal output from a local oscillator on the surface of the photodiode. The merits of the coherent detection process include easy amplification of the signal at a known intermediate frequency and improved signal-to-noise ratio as compared to the direct detection method [29].

2.7 Eye Safety and Standards

When designing OWC systems, tremendous care has to be taken in ensuring that the optical radiation field is safe and poses no health threats to humans and animals that may come in contact with it knowingly or otherwise. The skin, and most especially the eyes can experience significant damage if there is a direct focus on the optical beams. Optical wavelengths of about 400 – 1400 nm can be focused by the eye's retina while the cornea part of the eyes simply absorbs the energy of other wavelengths. Various international standard bodies such as the Center for Devices and Radiological Health (CDRH), International Electrotechnical Commission (IEC), European Committee for Electrotechnical Standardization (CENELEC) etc. provide safety guidelines on the use of optical beams, some of which are enforced by law [25].

According to the IEC standard classification of lasers, Class 1 lasers include low power radiation emitting devices of wavelengths ranging from 0.3025 – 4 μm which poses no danger under all reasonably foreseeable conditions of use. Class 1M lasers are similar to class 1 lasers, but there exists a possibility of danger when viewing the optical radiation emanating from them with optical equipment such as microscopes, telescopes, binoculars etc. Other laser classes include Class 2, Class 2M, Class 3B etc. [30, 31]. Since the laser classification is determined by the output power, it should be noted that no optical wavelength is immanently dangerous or safe for the eyes. The OWCS can, therefore, be designed to transmit at any choice wavelength and still be relatively harmless to the eyes [25].

2.8 Summary

In this chapter, a concise description of OWC and a review of existing related work was done. Features and areas of application for OWCS were also discussed. Key blocks of the OWCS such as the transmitter, atmospheric channel and the receiver were also examined. This dissertation seeks to perform an in-depth performance analysis of OWCS in Cape Town, South Africa, with a view to implement the results in other regions of similar climatic characteristics as will be shown in the next chapters.

Chapter 3
METHODOLOGY

3.1 Introduction

Different models used in this dissertation are presented in this chapter. They include models for the propagation of laser beams through the atmosphere and the study of irradiance fluctuation effects on transmitted optical signals. In investigating the effects of irradiance fluctuations, the lognormal model is employed. The regression equations for determining visibility and other equations used for estimating the losses in OWC systems are stated. This chapter will also present a discussion on OWC systems link budget analysis and availability.

3.2 Model of the Propagation of Optical Beams through the Atmospheric Channel

The Beer Lambert's law describes the propagation of optical signals via the turbulent atmospheric channel. It is stated in [16] as:

$$T(\lambda, L) = e^{-(\alpha_{ext} L)} \tag{1}$$

where $T(\lambda, L)$ represents the transmittance of the atmospheric channel, α_{ext} denotes the coefficient of atmospheric attenuation and L is the propagation length. The Transmittance is dependent on the meteorological visibility (V) which basically defines the transparency of the atmosphere. The visibility is defined as the path length at which the transmittance drops to a certain transmission threshold value [i.e. $T(\lambda, L) = T_{th}$]. The transmission threshold also known as the optical threshold is set at 2% for optical wireless communication systems and 5% for Runway Visual Range at Airports [16, 32].

At $T_{th} = 2\%$, the coefficient of atmospheric attenuation is expressed as:

$$\alpha_{ext} = \frac{-\ln(0.02)}{V} = \frac{3.912}{V} \tag{2}$$

Here V is the atmospheric visibility in kilometers.

Visibility (V) may be defined as the propagation length that an optical beam must travel through the atmospheric channel for its luminous flux to reduce to, in this case, 2% of its original value [32, 33]. In [10], visibility was estimated from the relative humidity, maximum temperature and fraction of sunshine hours using single regression equations listed below:

$$V = a_c + b_c(R.H.) \tag{3}$$

$$V = a_c + b_c(T_{\max}) \tag{4}$$

$$V = a_c + b_c\left(\frac{n}{N}\right) \tag{5}$$

where a_c, b_c, c_c and d_c are the coefficients of regression, $R.H.$ is the relative humidity, $T_{\max}$ is the maximum temperature, *n* is the actual amount of sunshine hours in a day, *N* is the maximum possible amount of daylight hours and (*n/N*) represents the fraction of sunshine hours. However, a slightly different approach was taken to estimate minimum, average and maximum visibility in this work. A multiple regression model is proposed and is expressed in the form:

$$V = a_c + b_c(R.H.) + c_c\left(\frac{n}{N}\right) + d_c(T_{\max}) \tag{6}$$

The atmospheric attenuation in decibels may then be calculated using the expression [16]:

$$A_\alpha(L,V) = 10\log_{10}(e)\alpha_{ext}(V)L \tag{7}$$

Therefore, in decibel per unit length, the coefficient of atmospheric attenuation is approximately:

$$\alpha_a(V) = 4.343\alpha_{ext} \tag{8}$$

Discontinuities in the atmospheric channel such as aerosols and gas molecules serve as sources of reduced signal strength for optical signals as they transverse through the free space media. These channel impediments lead to scattering losses which may also be expressed as atmospheric attenuation and calculated using [34]:

$$A_\alpha = \alpha_a(V) \times L \quad \text{[dB]} \tag{9}$$

where $\alpha_a(V)$ is the total extinction coefficient and it comprises atmospheric absorption and scattering parameters. It may be further evaluated by the expression:

$$\alpha_a(V) = \sigma_m(\lambda) + \sigma_a(\lambda) + \beta_m(\lambda) + \beta_{as}(\lambda) \tag{10}$$

where $\sigma_m(\lambda)$ represents the molecular absorption coefficient, $\sigma_a(\lambda)$ is the aerosol absorption coefficient, $\beta_m(\lambda)$ denotes the Raleigh scattering coefficient and $\beta_{as}(\lambda)$ is the aerosol scattering coefficient. Since the aerosol scattering coefficient is the main atmospheric channel parameter that is responsible for scattering losses in the optical signal, equation (10) may, therefore, be approximated to [32]:

$$\alpha_a(V) \cong \beta_{as}(\lambda) \tag{11}$$

From visible to near–infrared wavelengths, the total extinction coefficient can be calculated by the Kruse formula [35] and is modified for $T_{th} = 2\%$ as:

$$\alpha_{a,scat}(V) \cong \beta_{as}(\lambda) = \frac{10\log_{10} T_{th}}{V[km]} \times \left(\frac{\lambda(nm)}{\lambda_o\, nm}\right)^{-q_o(V)} = \frac{17}{V[km]} \times \left(\frac{\lambda(nm)}{550nm}\right)^{-q_o(V)} \text{ [dB/km]} \tag{12}$$

where λ is the optical signal wavelength in nanometers, λ_o is the maximum spectrum wavelength of the solar band and q_o is the particle size distribution parameter and is presented as:

$$q_o(V) = \begin{cases} 1.6 & for \quad V > 50\,\text{km} \\ 1.3 & for \quad 6\,\text{km} < V < 50\,\text{km} \\ 0.585V^{\frac{1}{3}} & for \quad 0\,\text{km} < V < 6\,\text{km} \end{cases} \tag{13}$$

The Kruse model has been widely employed to estimate the aerosol scattering coefficient. However, it was discovered in [11] that for visibility less than 6 km in foggy weather, the particle size distribution parameter in the Kruse model cannot accurately estimate the values of the scattering attenuation coefficient. Therefore, a new modification for the particle size-related coefficient was proposed by [11] in order to estimate $\beta_{as}(\lambda)$ more accurately and is given as:

$$q_o(V) = \begin{cases} 1.6 & for \quad V > 50\,\text{km} \\ 1.3 & for \quad 6 < V < 50\,\text{km} \\ 0.16V + 0.34 & for \quad 1 < V < 6\,\text{km} \\ V - 0.5 & for \quad 0.5 < V < 1\,\text{km} \\ 0 & for \quad V < 0.5\,\text{km} \end{cases} \tag{14}$$

In [12], Al Naboulsi proposed equations for calculating the scattering attenuation caused by convection and advection fog for a visibility range of 0.05 to 1 km and for wavelengths ranging from 690 to 1550 nm. They are:

$$\beta_{as-con}(\lambda) = 4.343\left(\frac{0.11478\lambda + 3.8367}{V}\right) \quad \text{[dB/km]} \tag{15}$$

$$\beta_{as-adv}(\lambda) = 4.343\left(\frac{0.18126\lambda^2 + 0.13709\lambda + 3.7205}{V}\right) \quad \text{[dB/km]} \tag{16}$$

A model for the scattering attenuation of optical signals in the troposphere is presented by [13]. It is valid for a visibility span of 100 – 50 000 m and developed for a wavelength range 0.3 - 1.1 µm. It is given as:

$$\beta_{as-Fer}(\lambda) = \{-2.656\ln(\lambda[\mu m]) + 2.449\} \times V[km]^{-\{0.199\ln(\lambda[\mu m])+1.157\}} \quad \text{[dB/km]} \tag{17}$$

In [14], Grabner et al proposed another model for calculating the scattering attenuation coefficient. The model was developed from the empirical data of fog and used for a wavelength of 1550 nm with a valid visibility span of 50 – 1000 m. They are expressed as:

$$\beta_{as-Grab-P}(1.55\mu m) = 22.44V^{-0.8616} \quad \text{(Power Law)} \quad \text{[dB/km]} \tag{18}$$

$$\beta_{as-Grab-In}(1.55\mu m) = \frac{18.22}{V} \quad \text{(Inverse Law)} \quad \text{[dB/km]} \tag{19}$$

In 2013, Ijaz proposed a new model for the estimation of the scattering attenuation coefficient due to fog and smoke. It is valid for a visibility range of 15 – 1000 m and a wavelength span of 600 – 1600 nm. It is given as [15]:

$$\beta_{as}(\lambda) = \frac{17}{V[km]} \times \left(\frac{\lambda(nm)}{550nm}\right)^{-q_o(\lambda)} \quad \text{[dB/km]} \tag{20}$$

Where

$$q_o(\lambda) = \begin{cases} 0.1428\lambda - 0.0947 & Fog \\ 0.8467\lambda - 0.5212 & Smoke \end{cases} \tag{21}$$

3.3 Power loss due to Atmospheric Turbulence

During clear sky periods, the power levels of optical signals have been known to undergo significant reduction. This is as a result of temperature inhomogeneity and rapid fluctuations in the pressure, density and humidity of the atmosphere. This invariably leads to rapid changes in the refractive index from which Scintillation or Irradiance fluctuations emanate. Scintillation results in the performance deterioration of

OWC systems which leads to beam broadening, phase deviations of received information signals, beam wander, and even total disruption of communication link lengths [36]. In this dissertation, a spherical wave is assumed and the scintillation index which is a measure of the irradiance fluctuation strength of the atmospheric channel is given as:

$$\sigma_{S.I.} = 0.50 \times C_n^2 \times k^{7/6} \times L^{11/6} \tag{22}$$

where k is the optical wave number and is given as:

$$k = \frac{44}{7\lambda} \tag{23}$$

L is the propagation link length in meters and $C_n^2\left[m^{-2/3}\right]$ is the refractive index profile parameter. The Hufnagel-Valley model estimates $C_n^2\left[m^{-2/3}\right]$in an expression given as:

$$C_n^2\left[m^{-2/3}\right] = \frac{297}{50000}\left(\frac{w_v}{27}\right)^2\left(\frac{a}{10^5 m}\right)\exp\left(-\frac{a}{1000\text{m}}\right) + \left(2.7\times 10^{-16}\right)\exp\left(-\frac{a}{1500\text{m}}\right) + 1.7\times 10^{-14}\exp\left(-\frac{a}{100\text{m}}\right) \tag{24}$$

where a is the altitude above the earth surface in meters and w_v is the wind velocity in m/s.

The atmospheric turbulence loss resulting from irradiance fluctuations as proposed by Rytov is given as [34]:

$$\alpha_{turb} = 2\times\sqrt{23.17\times C_n^2 \times k^{7/6} \times L^{11/6}} \qquad \text{[dB]} \tag{25}$$

The power scintillation index used in this work as derived from [16] is calculated from the equation given as:

$$\sigma_{P-S.I.} = \sigma_{S.I.}\left[1 + 0.333\left(\frac{k D^2}{4L}\right)^{5/6}\right]^{-7/5} \tag{26}$$

where D denotes the diameter of the lens at the receiver.

The expression for estimating the fading loss due to irradiance fluctuations is given as:

$$A_{tl}(L) = 10\log\left[\exp\left[erfc^{-1}\left(2P_{up}\right)\sqrt{2\ln\left(\sigma_{P-S.I.}+1\right)}\right]\sqrt{\sigma_{P-S.I.}+1}\right] \quad \text{[dB]} \tag{27}$$

where P_{up} is the upper bound probability. A_{tl} is needed for calculating the link margin necessary for compensating for losses due to scintillation.

3.4 Optical Link Margin

The link margin is the yardstick for evaluating the OWC system performance and is presented in the following equations:

$$L_M(L) = P_{tx} - S_{tx} - 20\log\left(\frac{\sqrt{2}L\theta}{D}\right) - S_{rx} - R_s \quad \text{[dB]} \tag{28}$$

$$L_M(L) = M_o - 20\log L \quad \text{[dB]} \tag{29}$$

$$P_{rx} = P_{tx} - \beta_{as}(\lambda) \times L - L_{Geo} - A_{tl}(L) - S_{tx} - S_{rx} \quad \text{[dB]} \tag{30}$$

$$L_{Geo} = -20\log\left(\frac{D}{L\theta}\right) \quad \text{[dB]} \tag{31}$$

where P_{tx} is the transmitted optical power, S_{tx} represents the total losses at the transmitter, S_{rx} denotes the aggregate losses at the receiver, θ is the beam divergence angle in radians, R_s is the receiver sensitivity in dB, M_o is a constant calculated from our proposed system specifications with a value of 84 dB when L is measured in meters and 24 dB when L is measured in kilometers and L_{Geo} is the geometric or optical divergence loss.

The proposed OWC system parameters used in this work are listed below:

Table 3.1 Typical OWC system parameters

Parameter	Value
Wavelength	850 nm, 950 nm and 1550 nm
Transmit Power	16 dBm (40 mW)
Light Source	Laser
Receiver Sensitivity	-38 dBm
Transmitter and Receiver System Losses	2 dB
Receiver Aperture Diameter	16 cm
Eye Safety	Class 1M
Receiver Field of View	10 mrad
Detector	Avalanche Photodiode (APD)
Transmit Beam Divergence Angle	2.8 mrad
Data Rate	1.25 Gbps

3.5 OWC System Link Availability

For the correct operation of the OWC system, the minimum required visibility $V_{\min}(L)$ must be calculated. The minimum required visibility is important for estimating the OWC system's availability. It is usually expressed in the form $V \geq V_{\min}(L)$. For a link to be available, the following condition must be achieved:

$$L_M \geq A_\alpha(L,V) \tag{32}$$

Substituting equations (9), (12), (15), (16), (17), (18), (19) and (20) into equation (32) and solving for visibility V in kilometers, we obtain the inequality equations as shown below in the order corresponding to the aforementioned equations. The right-hand side of these equations (i.e. equations (33) to (39)) represent the minimum visibility for the aerosol scattering attenuation models considered previously in this chapter.

$$V \geq \frac{17L}{L_M(L)} \times \left(\frac{\lambda(nm)}{550nm}\right)^{-q_o(V)} \quad \text{[km]} \tag{33}$$

$$V \geq 4.343 \times L \times \left(\frac{0.11478\lambda + 3.8367}{L_M(L)}\right) \quad \text{[km]} \tag{34}$$

$$V \geq 4.343 \times L \times \left(\frac{0.18126\lambda^2 + 0.13709\lambda + 3.7205}{L_M(L)}\right) \quad \text{[km]} \tag{35}$$

$$V \geq 4.343 \times L \times \{-2.656\ln(\lambda[\mu m]) + 2.449\} \times L_M^{-\{0.199\ln(\lambda[\mu m])+1.157\}} \quad \text{[km]} \tag{36}$$

$$V \geq 22.44 \times L \times L_M^{-0.8616} \quad \text{(Power Law)} \quad \text{[km]} \tag{37}$$

$$V \geq \frac{18.22 \times L}{L_M(L)} \quad \text{(Inverse Law)} \quad \text{[km]} \tag{38}$$

$$V \geq \frac{17L}{L_M(L)} \times \left(\frac{\lambda(nm)}{550nm}\right)^{-q_o(\lambda)} \quad \text{[km]} \tag{39}$$

The OWC system link availability for the various models considered in this work is defined as:

$$L_A = \Pr obability[V \geq V_{\min}(L)] \tag{40}$$

3.6 Summary

The different models for the propagation of optical signals through the free space media and the resultant attenuation caused by discontinuities in the atmosphere were presented in this chapter. The effects of irradiance fluctuations on laser beams were discussed and the various parameters for determining the link budget were stated. The equations for determining the minimum visibility for different scattering attenuation models were also derived. The chapter ends with expressions used for finding the link margin and availability of OWC systems.

Chapter 4
RESULTS AND DISCUSSIONS

4.1 Introduction

Determination of monthly minimum, average and maximum visibility for six years (2010-2015) from relative humidity, maximum temperature and fraction of sunshine hours using different regression models will be carried out in this chapter. Various models will also be used to present the aerosol scattering attenuation from minimum, average and maximum visibility results for Cape Town. Results on power loss due to turbulence, power scintillation index, link margin and minimum required visibility will be discussed. Finally, the link availability for OWC systems transmitting at 850 nm, 950 nm and 1550 nm will be estimated for Cape Town.

4.2 Determination of Visibility using various Regression models

The average monthly visibility for the period of four years, starting from January 2011 to December 2014 were obtained from the South African Weather Services (SAWS). Other associated weather parameters such as relative humidity, temperature and sunshine hours from January 2010 to December 2015 (6 years) were also obtained from the same source. The mean monthly relative humidity (R.H.), maximum temperature (T_{max}) and fraction of sunshine hours (*n/N*) were extracted from the data set and used for this work. Typical computation and sorting of the monthly data for the years 2011 - 2014 are shown in Tables 4.1 - 4.4.

Table 4.1 Measured values of the average monthly visibility, relative humidity, maximum temperature and fraction of sunshine hours for the year 2011.

2011				
Month	**Visibility (km)**	**R.H. (%)**	**T_{max} (^{0}C)**	**n/N**
January	25	70	27.8	0.797503
February	25	75	28.6	0.856292
March	21	76	26.8	0.709163
April	22	73	23.4	0.788346
May	18	80	20.3	0.536062
June	16	85	17.7	0.580000
July	23	76	19.1	0.743961
August	21	74	19.0	0.666075
September	20	76	19.2	0.623420
October	25	70	21.8	0.653846
November	29	68	22.3	0.742857
December	30	68	24.3	0.828571

Table 4.2 Measured values of the average monthly visibility, relative humidity, maximum temperature and fraction of sunshine hours for the year 2012.

2012				
Month	**Visibility (km)**	**R.H. (%)**	**T_{max} (^{0}C)**	**n/N**
January	26	70	28.3	0.842857
February	31	68	26.7	0.819188
March	28	73	26.1	0.808333
April	26	74	23.0	0.705073
May	23	78	19.5	0.688995
June	20	73	17.9	0.570000
July	23	74	17.3	0.583090
August	23	74	16.4	0.596616
September	24	69	19.0	0.645432
October	29	65	21.1	0.756173
November	28	65	23.7	0.742857
December	28	66	27.4	0.785714

Table 4.3 Measured values of the average monthly visibility, relative humidity, maximum temperature and fraction of sunshine hours for the year 2013.

2013				
Month	**Visibility (km)**	**R.H. (%)**	**T_{max} (^{0}C)**	**n/N**
January	30	63	26.5	0.857143
February	31	66	26.4	0.829091
March	30	66	26.2	0.750000
April	25	70	23.2	0.726016
May	20	74	21.1	0.660287
June	21	70	17.6	0.610000
July	24	71	18.2	0.631681
August	20	67	17.5	0.584007
September	25	67	17.3	0.641667
October	26	68	21.1	0.704441
November	26	68	23.7	0.742857
December	33	64	27.0	0.828571

Table 4.4 Measured values of the average monthly visibility, relative humidity, maximum temperature and fraction of sunshine hours for the year 2014.

2014				
Month	**Visibility (km)**	**R.H. (%)**	**T_{max} (^{0}C)**	**n/N**
January	30	69	27.0	0.778571
February	29	67	28.2	0.814286
March	27	71	24.0	0.750000
April	26	67	25.5	0.836207
May	22	76	20.2	0.567854
June	21	73	18.0	0.570000
July	20	78	17.3	0.556098
August	21	76	19.2	0.575022
September	25	71	20.2	0.666667
October	29	67	25.5	0.800000
November	28	67	24.3	0.785714
December	35	64	25.8	0.835714

In the following subsections, different single and multiple regression models based on equations (3) - (6) for determining visibility from the aforementioned weather parameters will be extracted from the data set. The regression relationship between the values of the cumulative monthly weather parameters from January 2011 to December 2013 will be examined. Thereafter, the regression relationship for the average monthly weather parameters for years 2011-2013 for the same set of weather parameters previously examined will also be obtained. The correlation coefficients and standard errors between the values of these parameters will then be determined. Monthly visibility values for the year 2014 will be predicted from the derived regression models and compared to the measured values. The regression model with the highest correlation coefficient and lowest standard error value will be adjudged to be the best. This regression model will then be used to predict visibility values of Cape Town for years 2010 and 2015. Having obtained a 6 year (2010 -2015) visibility data set, a thorough performance analysis of OWCS in Cape Town will be carried out. The results may also be implemented in the design of OWC systems in other regions of similar climate characteristics (warm-summer Mediterranean climates).

4.2.1 Cumulative Visibility (km) against Cumulative Relative Humidity (%)

As shown in Table 4.5 and Figure 4.1, one-to-one monthly visibility values are plotted against relative humidity values from January 2011 to December 2013.

Table 4.5 Three years measured values of the cumulative monthly relative humidity and visibility.

2011-2013	
R.H. (%)	**Visibility (km)**
70	25
75	25
76	21
73	22
80	18
85	16
76	23
74	21
76	20
70	25
68	29
68	30
70	26
68	31
73	28
74	26
78	23
73	20
74	23
74	23
69	24
65	29
65	28
66	28
63	30
66	31
66	30
70	25
74	20
70	21
71	24
67	20
67	25
68	26
68	26
64	33

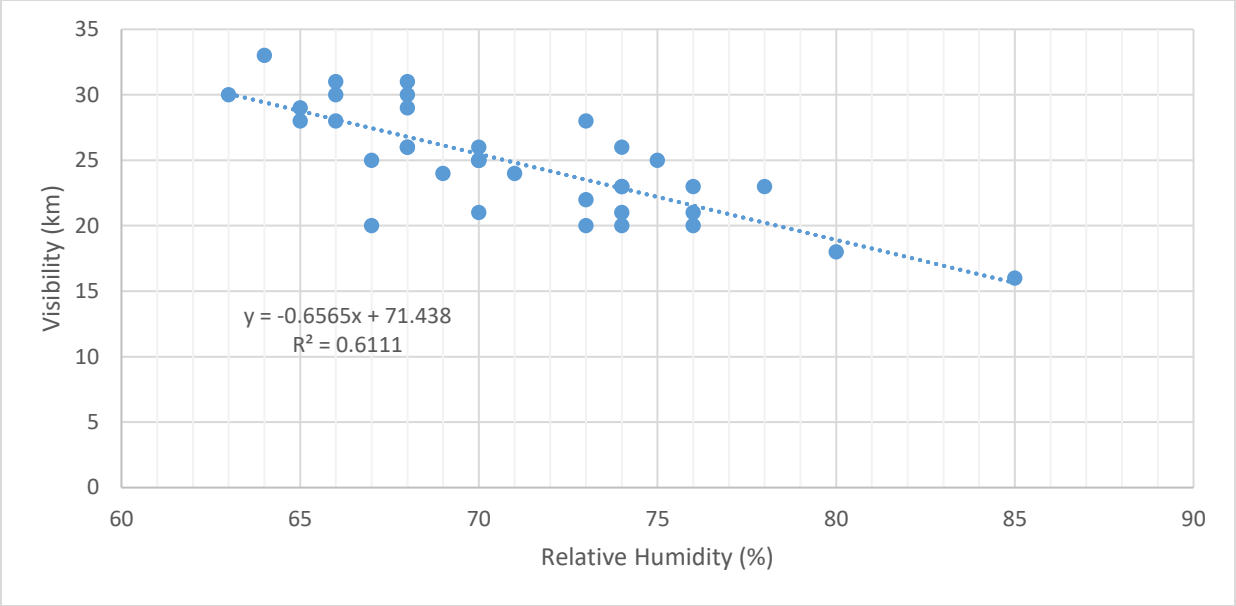

Figure 4.1 Cumulative visibility (km) against cumulative relative humidity (%)

The regression equation obtained is:

$$V = -0.65653(R.H.) + 71.43793 \tag{41}$$

The correlation coefficient and the standard error obtained from this regression model are 0.78172 and 2.27198 respectively.

Table 4.6 Measured and predicted visibility values using the cumulative relative humidity regression model along with their RMSE difference for the year 2014

2014				
Months	**Measured Relative Humidity R.H. (%)**	**Measured Visibility V_m (km)**	**Predicted Visibility $V_{Cum\text{-}R.H.}$ (km)**	**RMSE (km)**
January	69	30	26	**2.516611478**
February	67	29	27	
March	71	27	25	
April	67	26	27	
May	76	22	22	
June	73	21	24	
July	78	20	20	
August	76	21	22	
September	71	25	25	
October	67	29	27	
November	67	28	27	
December	64	35	29	

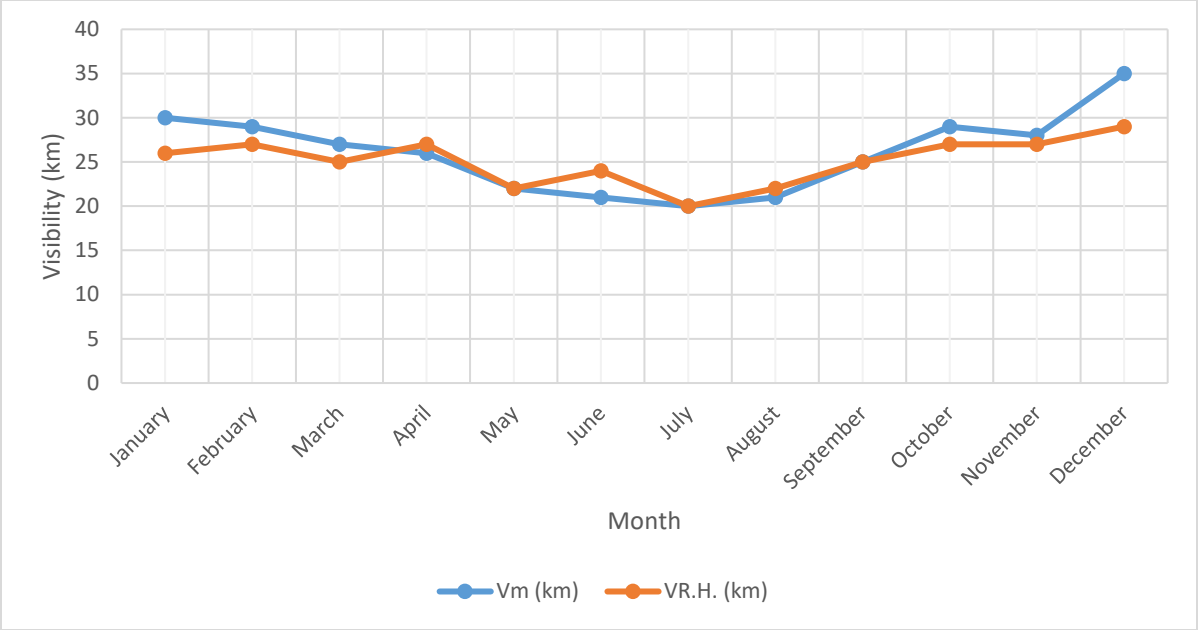

Figure 4.2 Variation of the measured and the predicted values of visibility using the cumulative relative humidity regression model with the months of the year 2014.

4.2.2 Average Visibility (km) against Average Relative Humidity (%)

In Table 4.7 and Figure 4.3, three years average monthly visibilities plotted against corresponding relative humidity values are presented.

Table 4.7 Average monthly measured relative humidity and visibility values for three years.

2011-2013	
Average R.H. (%)	**Average Visibility (km)**
67.67	27.00
69.67	29.00
71.67	26.33
72.33	24.33
77.33	20.33
76.00	19.00
73.67	23.33
71.67	21.33
70.67	23.00
67.67	26.67
67.00	27.67
66.00	30.33

The correlation coefficient and standard error obtained from this regression model in Figure 4.3 are 0.86813 and 1.84635 respectively.

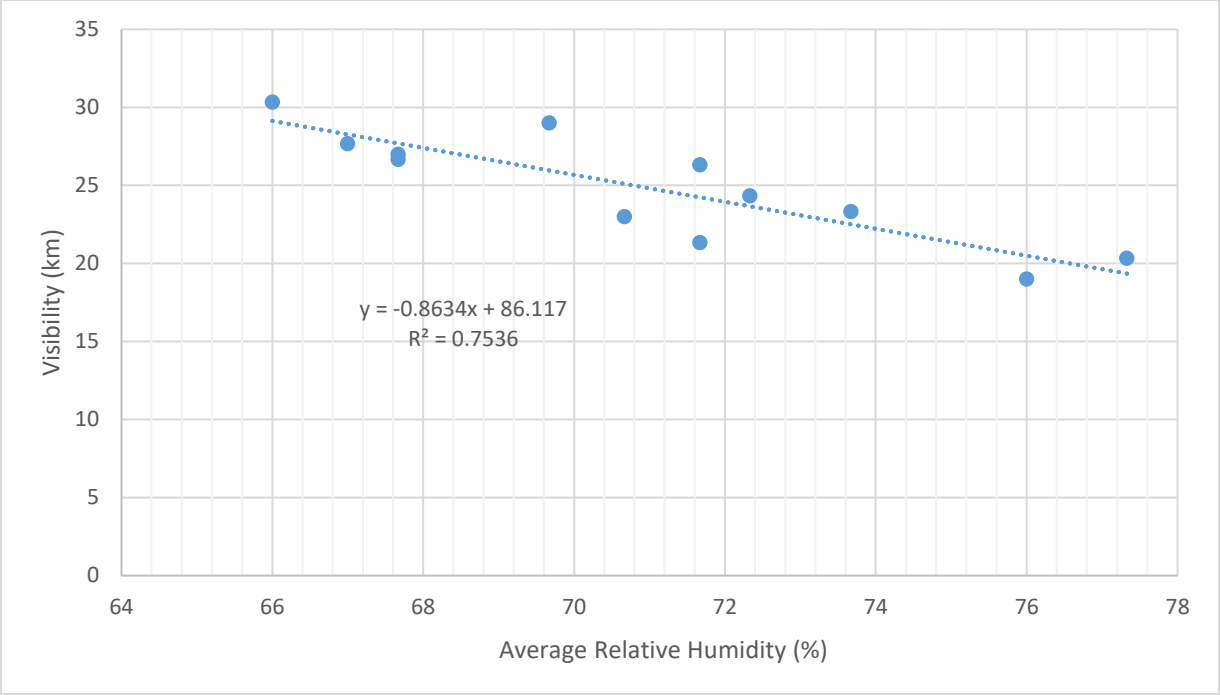

Figure 4.3 Average visibility (km) against average relative humidity (%)

The average relative humidity regression equation is:

$$V = -0.86343(R.H.) + 86.11686 \tag{42}$$

Table 4.8 Measured and predicted visibility values using the average relative humidity regression model along with their RMSE difference for the year 2014

2014				
Months	**Measured Relative Humidity R.H. (%)**	**Measured Visibility V_m (km)**	**Predicted Visibility $V_{Ave\text{-}R.H.}$ (km)**	**RMSE (km)**
January	69	30	27	**1.936491673**
February	67	29	28	
March	71	27	25	
April	67	26	28	
May	76	22	20	
June	73	21	23	
July	78	20	19	
August	76	21	20	
September	71	25	25	
October	67	29	28	
November	67	28	28	
December	64	35	31	

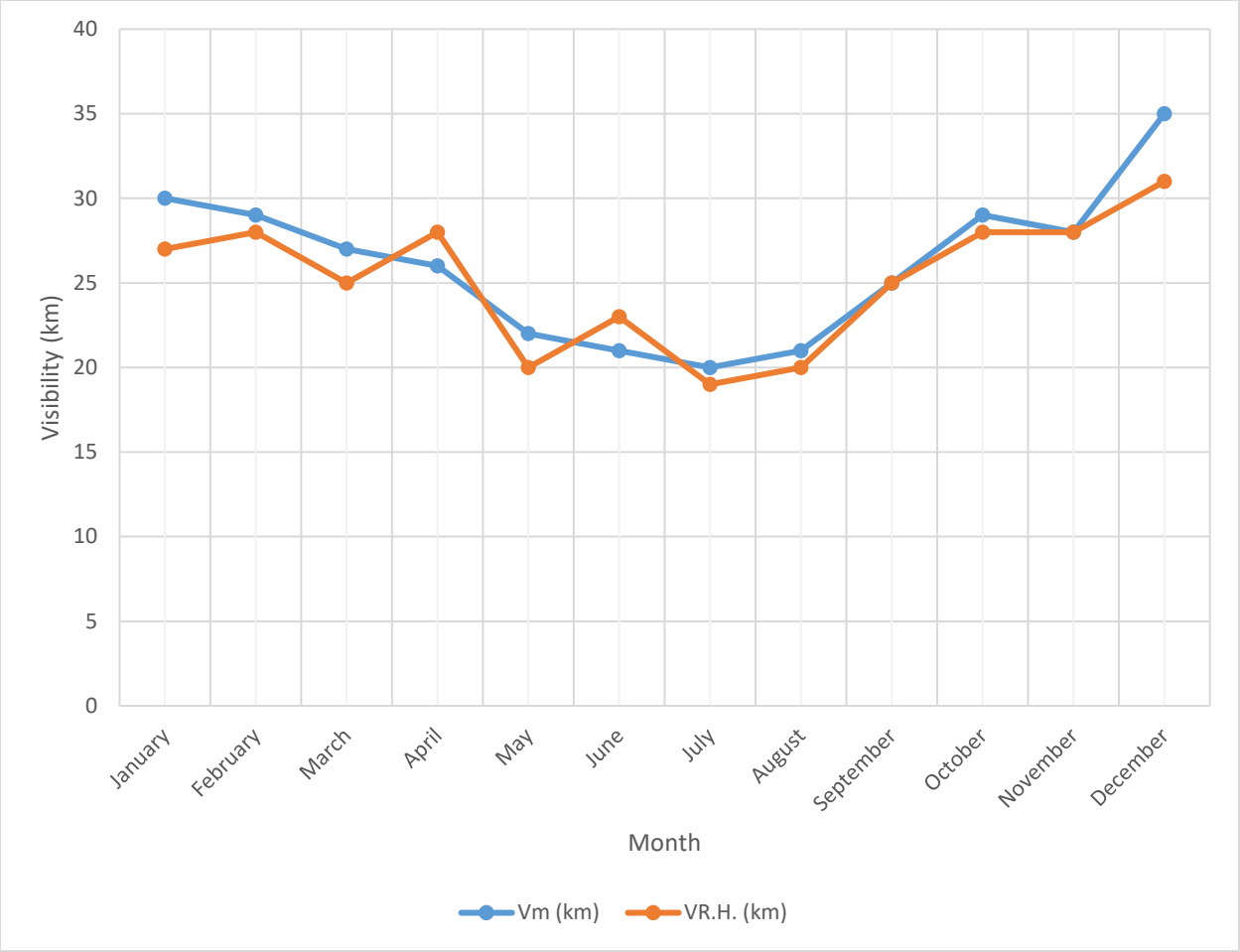

Figure 4.4 Variation of the measured and the predicted values of visibility using the average relative humidity regression model with the months of the year 2014.

4.2.3 Cumulative Visibility (km) against Cumulative Maximum Temperature (ºC)

One-to-one monthly visibility values are plotted against maximum temperature values from January 2011 to December 2013 as shown in Table 4.9 and Figure 4.5.

Table 4.9 Three years measured values of cumulative monthly maximum temperature and visibility

2011-2013	
T_{max} (^{0}C)	Visibility (km)
27.80	25
28.60	25
26.80	21
23.40	22
20.30	18
17.70	16
19.10	23
19.00	21
19.20	20
21.80	25
22.30	29
24.30	30
28.30	26
26.70	31
26.10	28
23.00	26
19.50	23
17.90	20
17.30	23
16.40	23
19.00	24
21.10	29
23.70	28
27.40	28
26.50	30
26.40	31
26.20	30
23.20	25
21.10	20
17.60	21
18.20	24
17.50	20
17.30	25
21.10	26
23.70	26
27.00	33

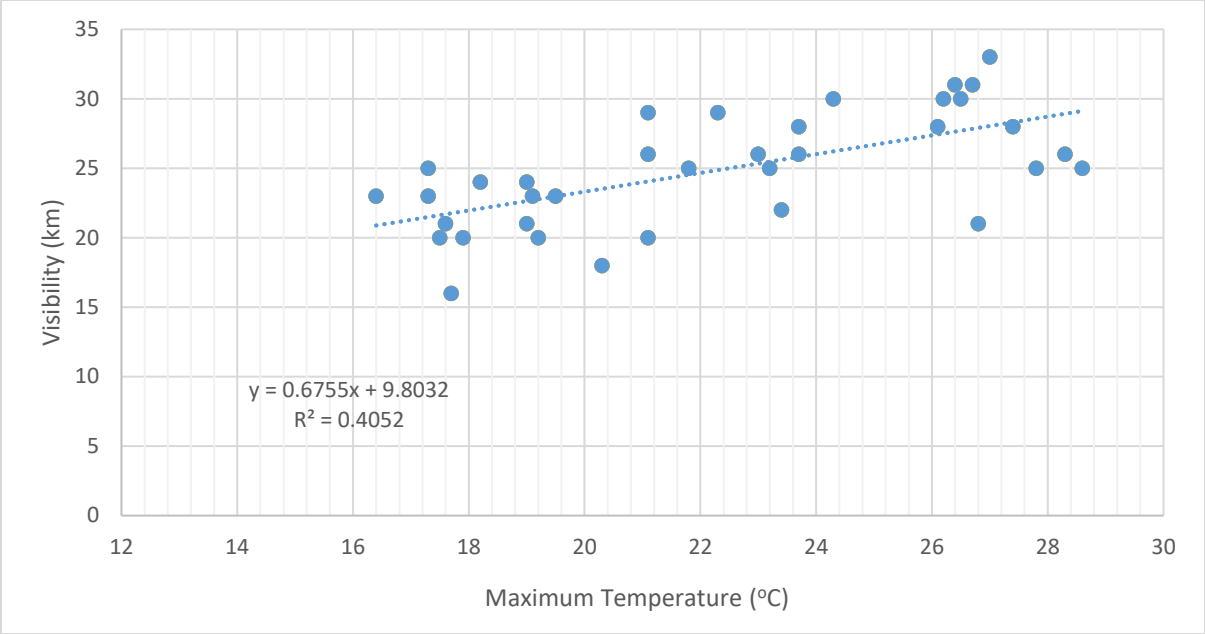

Figure 4.5 Cumulative visibility against cumulative maximum temperature (°C)

The correlation coefficient obtained from Figure 4.5 is 0.63651 while the standard error is 3.18085. The cumulative maximum temperature regression equation is:

$$V = 0.67550(T_{\max}) + 9.80320 \tag{43}$$

Table 4.10 Measured and predicted visibility values using the cumulative maximum temperature regression model along with their RMSE difference for the year 2014

Months	**Measured Maximum Temperature T_{max} (°C)**	**Measured Visibility V_m (km)**	**Predicted Visibility $V_{Cum\ Tmax}$ (km)**	**RMSE (km)**
January	27.00	30	28	**2.723355773**
February	28.20	29	29	
March	24.00	27	26	
April	25.50	26	27	
May	20.20	22	23	
June	18.00	21	22	
July	17.30	20	21	
August	19.20	21	23	
September	20.20	25	23	
October	25.50	29	27	
November	24.30	28	26	
December	25.80	35	27	

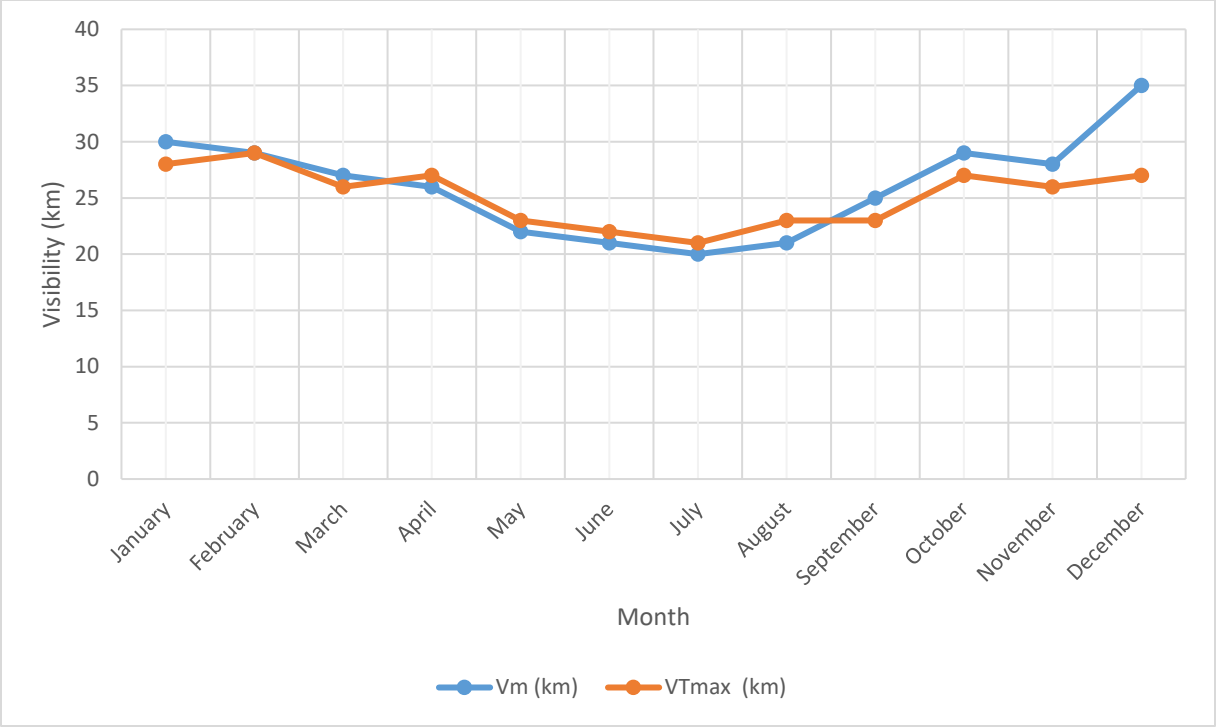

Figure 4.6 Variation of the measured and the predicted values of visibility using the cumulative maximum temperature regression model with the months of the year 2014.

4.2.4 Average Visibility (km) against Average Maximum Temperature (^{0}C)

Table 4.11 and Figure 4.7 present three years average monthly visibilities plotted against corresponding maximum temperature values.

Table 4.11 Average monthly measured maximum temperature and visibility values for three years.

2011 - 2013	
Average T_{max} (^{0}C)	**Average Visibility (km)**
27.533	27.00
27.233	29.00
26.367	26.33
23.200	24.33
20.300	20.33
17.733	19.00
18.200	23.33
17.633	21.33
18.500	23.00
21.333	26.67
23.233	27.67
26.233	30.33

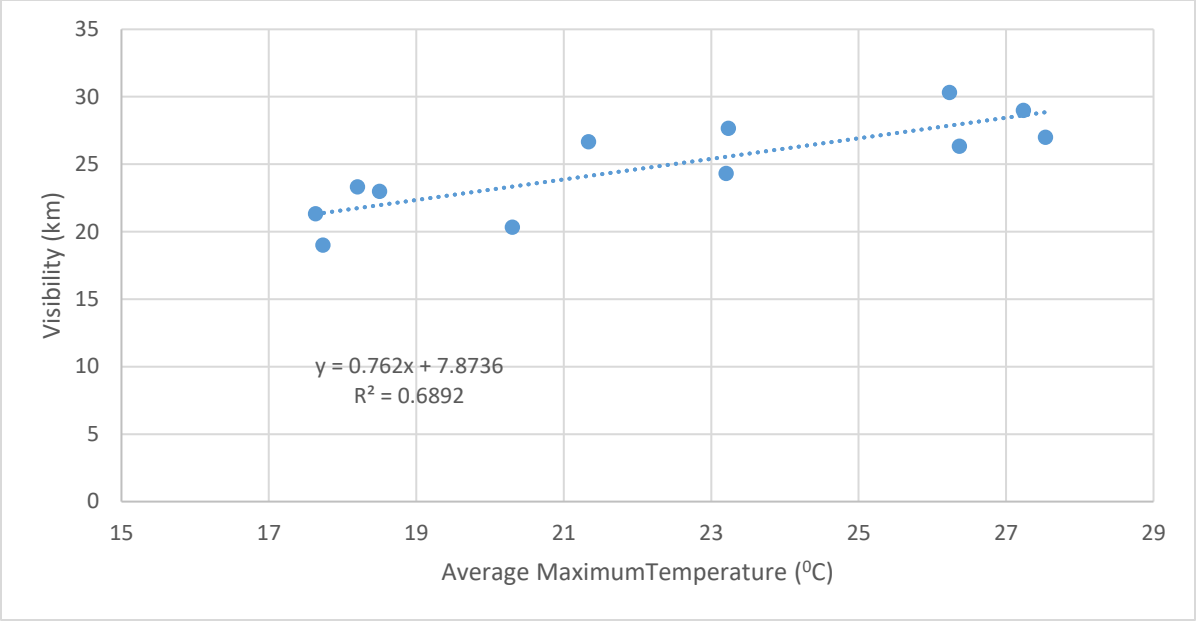

Figure 4.7 Average visibility (km) against average maximum temperature (°C)

As obtained from Figure 4.7, the correlation coefficient is 0.83015 while the standard error is 2.07397.

The average maximum temperature regression model is computed as:

$$V = 0.76201(T_{\max}) + 7.87362 \tag{44}$$

Table 4.12 Measured and predicted visibility values using the average maximum temperature regression model along with their RMSE difference for the year 2014

2014				
Months	**Measured Maximum Temperature T_{max} (°C)**	**Measured Visibility V_m (km)**	**Predicted Visibility $V_{Ave\ Tmax}$ (km)**	**RMSE (km)**
January	27.00	30	28	**2.4832774**
February	28.20	29	29	
March	24.00	27	26	
April	25.50	26	27	
May	20.20	22	23	
June	18.00	21	22	
July	17.30	20	21	
August	19.20	21	23	
September	20.20	25	23	
October	25.50	29	27	
November	24.30	28	26	
December	25.80	35	28	

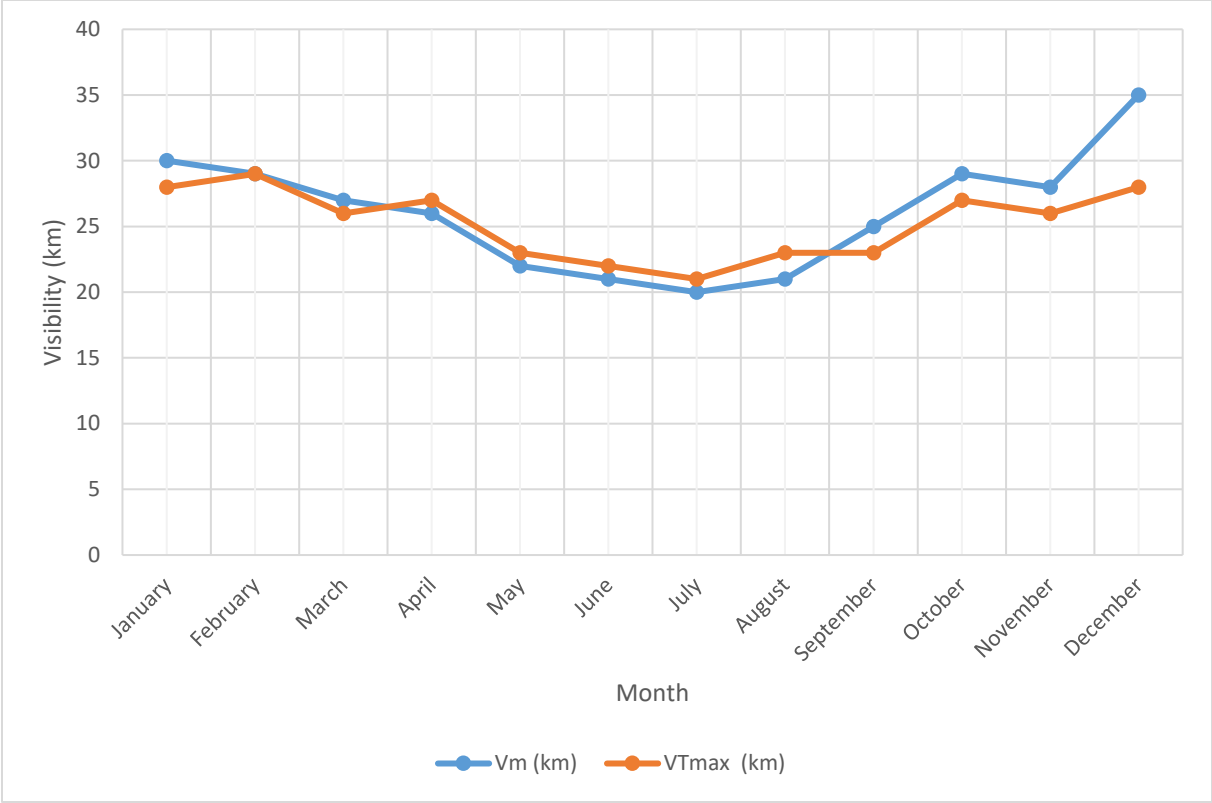

Figure 4.8 Variation of the measured and the predicted values of visibility using the average maximum temperature regression model with the months of the year 2014.

4.2.5 Cumulative Visibility (km) against Cumulative fraction of Sunshine Hours

As shown in Table 4.13 and Figure 4.9, one-to-one monthly visibility values are plotted against calculated values of the fraction of sunshine hours from January 2011 to December 2013.

Table 4.13 Three years measured values of the cumulative monthly fraction of sunshine hours and visibility

2011 - 2013	
n/N	**Visibility (km)**
0.797503	25
0.856292	25
0.709163	21
0.788346	22
0.536062	18
0.580000	16
0.743961	23
0.666075	21
0.623420	20
0.653846	25
0.742857	29
0.828571	30
0.842857	26
0.819188	31
0.808333	28
0.705073	26
0.688995	23
0.570000	20
0.583090	23
0.596616	23
0.645432	24
0.756173	29
0.742857	28
0.785714	28
0.857143	30
0.829091	31
0.750000	30
0.726016	25
0.660287	20
0.610000	21
0.631681	24
0.584007	20
0.641667	25
0.704441	26
0.742857	26
0.828571	33

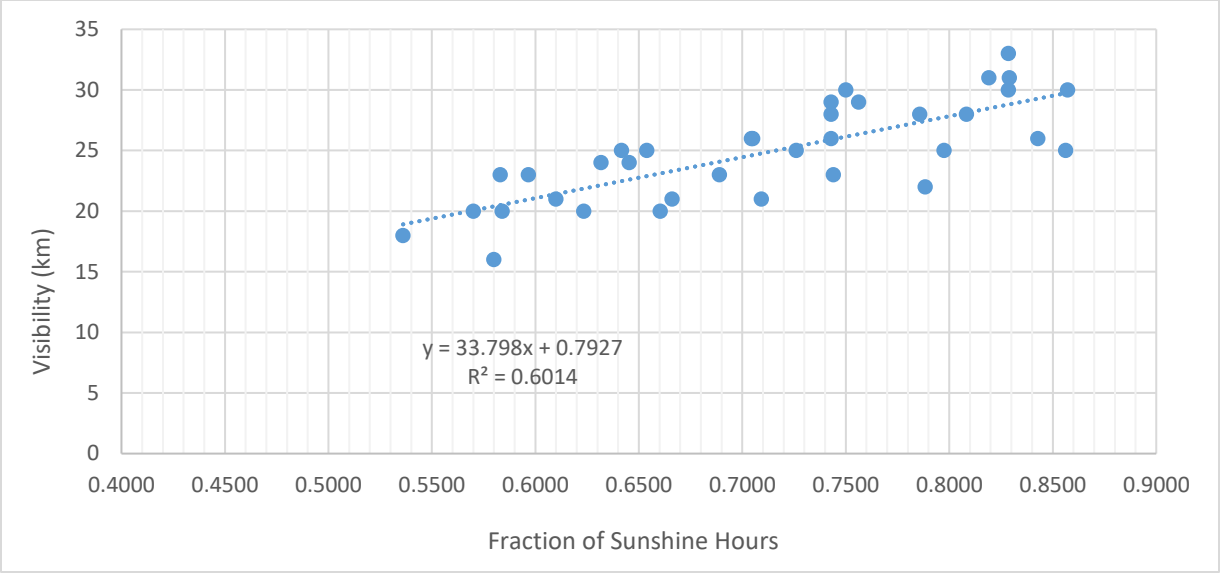

Figure 4.9 Cumulative visibility (km) against cumulative fraction of sunshine hours

The correlation coefficient and standard error values obtained from Figure 4.9 is 0.77549 and 2.60384 respectively. The cumulative fraction of sunshine hours regression model is derived as:

$$V = 33.79843\left(\frac{n}{N}\right) + 0.79270 \tag{45}$$

Table 4.14 Measured and predicted visibility values using the cumulative fraction of sunshine hours regression model along with their RMSE difference for the year 2014

2014				
Months	**Fraction of Sunshine Hours n/N**	**Measured Visibility V_m (km)**	**Predicted Visibility $V_{Cum\ n/N}$ (km)**	**RMSE (km)**
January	0.778571	30	27	**2.38048**
February	0.814286	29	28	
March	0.750000	27	26	
April	0.836207	26	29	
May	0.567854	22	20	
June	0.570000	21	20	
July	0.556098	20	20	
August	0.575022	21	20	
September	0.666667	25	23	
October	0.800000	29	28	
November	0.785714	28	27	
December	0.835714	35	29	

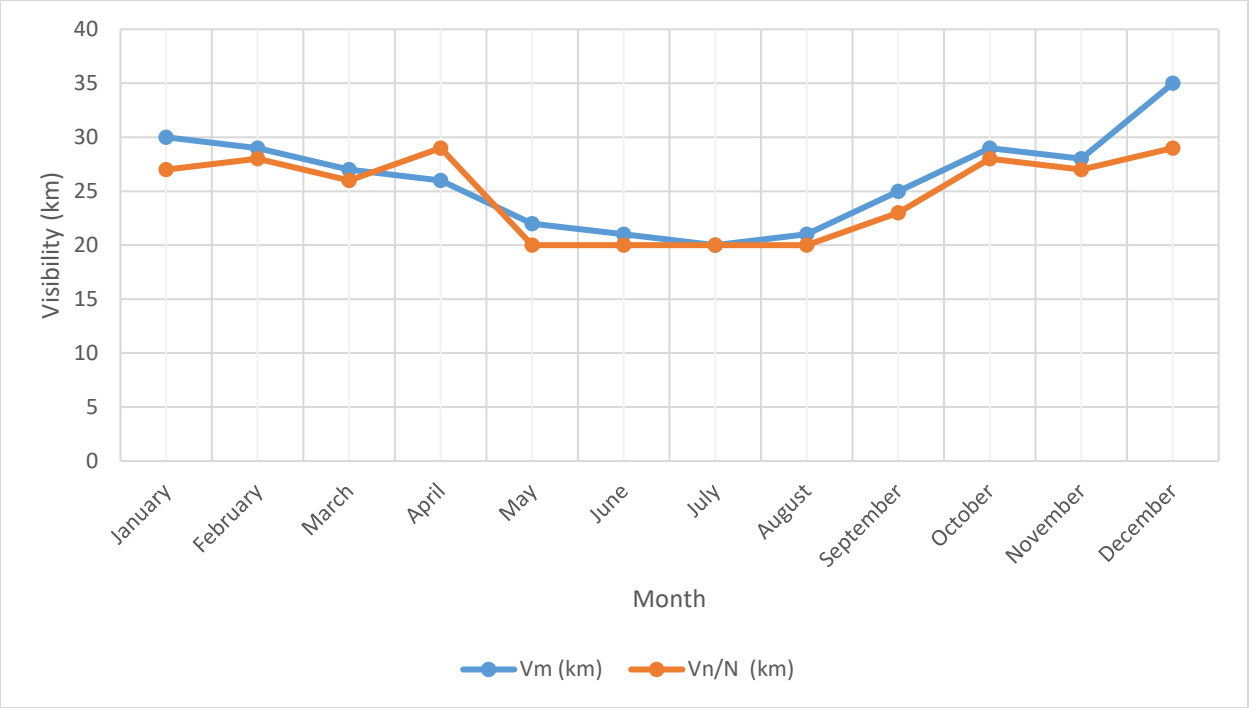

Figure 4.10 Variation of the measured and the predicted values of visibility using the cumulative fraction of sunshine hours regression model with the months of the year 2014.

4.2.6 Average Visibility (km) against Average fraction of Sunshine Hours

In Table 4.15 and Figure 4.11, three years average monthly visibilities plotted against corresponding values of the fraction of sunshine hours are presented.

Table 4.15 Average monthly measured fraction of sunshine hours and visibility for three years.

2011 - 2013	
Average n/N	**Average Visibility (km)**
0.832501	27.00
0.834857	29.00
0.755832	26.33
0.739812	24.33
0.628448	20.33
0.586667	19.00
0.652911	23.33
0.615566	21.33
0.636840	23.00
0.704820	26.67
0.742857	27.67
0.814285	30.33

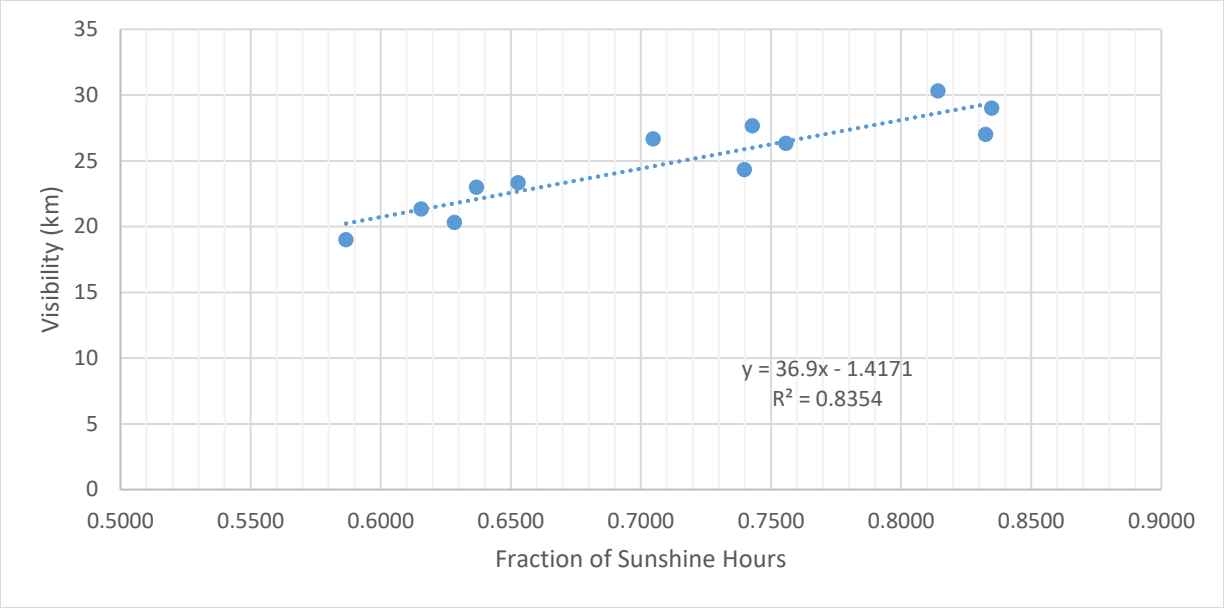

Figure 4.11 Average visibility (km) against average fraction of sunshine hours

The correlation coefficient and the standard error values obtained from Figure 4.11 are 0.91403 and 1.50897 respectively. The average fraction of sunshine hours regression equation is:

$$V = 36.89996\left(\frac{n}{N}\right) - 1.41707 \tag{46}$$

Table 4.16 Measured and predicted visibility values using the average fraction of sunshine hours regression model along with their RMSE difference for the year 2014

2014				
Months	**Fraction of Sunshine Hours n/N**	**Measured Visibility V_m (km)**	**Predicted Visibility $V_{Avg\ n/N}$ (km)**	**RMSE (km)**
January	0.778571	30	27	**2.362907813**
February	0.814286	29	29	
March	0.750000	27	26	
April	0.836207	26	29	
May	0.567854	22	20	
June	0.570000	21	20	
July	0.556098	20	19	
August	0.575022	21	20	
September	0.666667	25	23	
October	0.800000	29	28	
November	0.785714	28	28	
December	0.835714	35	29	

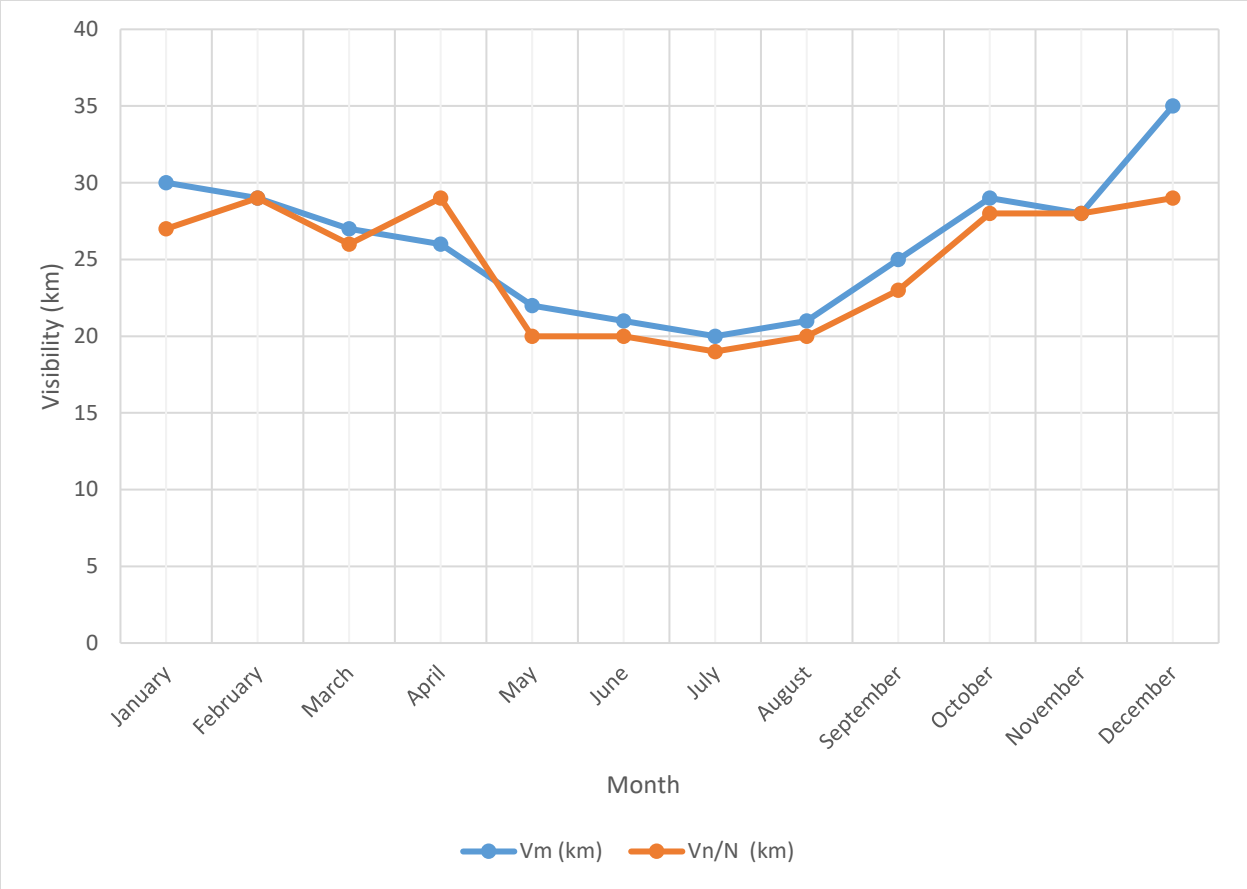

Figure 4.12 Variation of the measured and the predicted values of visibility using the average fraction of sunshine hours regression model with the months of the year 2014.

4.2.7 Cumulative Visibility (km) against Cumulative Multiple Regression Parameters

One-to-one monthly visibility, relative humidity, fraction of sunshine hours and maximum temperature values from January 2011 to December 2013 are presented in Table 4.17.

Table 4.17 Three years measured values of the cumulative monthly relative humidity, fraction of sunshine hours, maximum temperature and visibility

2011 - 2013			
R.H. (%)	**n/N**	**T_{max} (^{0}C)**	**Visibility (km)**
70	0.797503	27.80	25
75	0.856292	28.60	25
76	0.709163	26.80	21
73	0.788346	23.40	22
80	0.536062	20.30	18
85	0.580000	17.70	16
76	0.743961	19.10	23
74	0.666075	19.00	21
76	0.623420	19.20	20
70	0.653846	21.80	25
68	0.742857	22.30	29
68	0.828571	24.30	30
70	0.842857	28.30	26
68	0.819188	26.70	31
73	0.808333	26.10	28
74	0.705073	23.00	26
78	0.688995	19.50	23
73	0.570000	17.90	20
74	0.583090	17.30	23
74	0.596616	16.40	23
69	0.645432	19.00	24
65	0.756173	21.10	29
65	0.742857	23.70	28
66	0.785714	27.40	28
63	0.857143	26.50	30
66	0.829091	26.40	31
66	0.750000	26.20	30
70	0.726016	23.20	25
74	0.660287	21.10	20
70	0.610000	17.60	21
71	0.631681	18.20	24
67	0.584007	17.50	20
67	0.641667	17.30	25
68	0.704441	21.10	26
68	0.742857	23.70	26
64	0.828571	27.00	33

The correlation coefficient and standard error of the data set are obtained as 0.90028 and 1.85053 respectively. The cumulative multiple regression model is computed as:

$$V = 39.91787 - 0.43962(R.H.) + 23.93626\left(\frac{n}{N}\right) - 0.04099(T_{\max}) \tag{47}$$

Table 4.18 Measured and predicted visibility values using the cumulative multiple regression model along with their RMSE difference for the year 2014

2014						
Months	**Measured Relative Humidity R.H. (%)**	**Measured Maximum Temperature T_{max} (^{0}C)**	**Fraction of Sunshine Hours n/N**	**Measured Visibility V_m (km)**	**Predicted Visibility $V_{cum\text{-}mreg}$ (km)**	**RMSE (km)**
January	69	27.00	0.778571	30	27	**2.1015867**
February	67	28.20	0.814286	29	29	
March	71	24.00	0.750000	27	26	
April	67	25.50	0.836207	26	29	
May	76	20.20	0.567854	22	19	
June	73	18.00	0.570000	21	21	
July	78	17.30	0.556098	20	18	
August	76	19.20	0.575022	21	19	
September	71	20.20	0.666667	25	24	
October	67	25.50	0.800000	29	29	
November	67	24.30	0.785714	28	28	
December	64	25.80	0.835714	35	31	

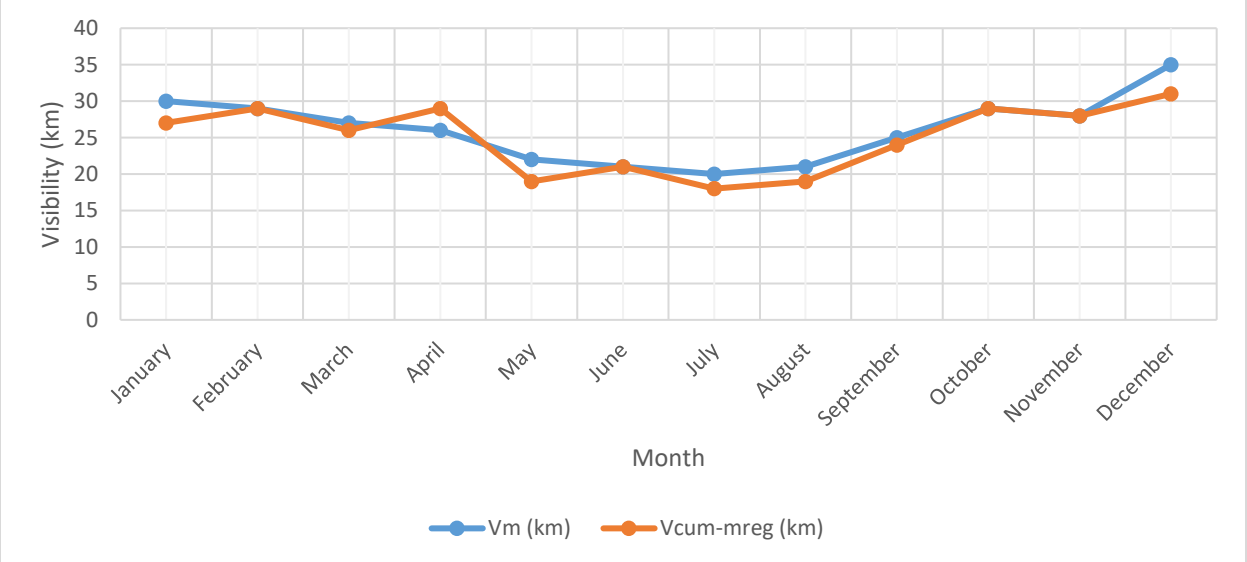

Figure 4.13 Variation of the measured and the predicted values of visibility using the cumulative multiple regression model with the months of the year 2014.

4.2.8 Average Visibility (km) against Average Multiple Regression Parameters

The monthly average values of the relative humidity, the fraction of sunshine hours, the maximum temperature and the visibility for a period of three years was computed and is shown in Table 4.19 below.

Table 4.19 Average monthly measured relative humidity, fraction of sunshine hours, maximum temperature and visibility values for three years.

Year 2011 - 2013			
Average R.H. (%)	**Average n/N**	**Average T_{max} (^oC)**	**Average Visibility (km)**
67.67	0.832501	27.533	27.00
69.67	0.834857	27.233	29.00
71.67	0.755832	26.367	26.33
72.33	0.739812	23.200	24.33
77.33	0.628448	20.300	20.33
76.00	0.586667	17.733	19.00
73.67	0.652911	18.200	23.33
71.67	0.615566	17.633	21.33
70.67	0.636840	18.500	23.00
67.67	0.704820	21.333	26.67
67.00	0.742857	23.233	27.67
66.00	0.814285	26.233	30.33

Table 4.20 Measured and predicted visibility values using the average multiple regression model along with their RMSE difference for the year 2014

2014						
Months	**Measured Relative Humidity R.H. (%)**	**Measured Maximum Temperature T_{max} (^0C)**	**Fraction of Sunshine Hours n/N**	**Measured Visibility V_m (km)**	**Predicted Visibility $V_{Avg\text{-}mul\ reg}$ (km)**	**RMSE (km)**
January	69	27.00	0.778571	30	27	**2.25462488**
February	67	28.20	0.814286	29	29	
March	71	24.00	0.750000	27	26	
April	67	25.50	0.836207	26	30	
May	76	20.20	0.567854	22	19	
June	73	18.00	0.570000	21	20	
July	78	17.30	0.556098	20	18	
August	76	19.20	0.575022	21	19	
September	71	20.20	0.666667	25	24	
October	67	25.50	0.800000	29	29	
November	67	24.30	0.785714	28	28	
December	64	25.80	0.835714	35	31	

Using the multiple regression model as stated in equation (6), the relationship between the four parameters was established for Cape Town and is shown in the equation below as:

$$V = 36.33271 - 0.41889(\text{R.H.}) + 28.08959\left(\frac{\text{n}}{\text{N}}\right) - 0.07882(\text{T}_{\text{max}}) \tag{48}$$

The correlation coefficient and standard error of the data set is computed as 0.96453 and 1.09787 respectively.

Comparing the variation between the measured and predicted values of the mean monthly visibility for the year 2014, the points of noticeable difference are in April and May as shown in Figure 4.14

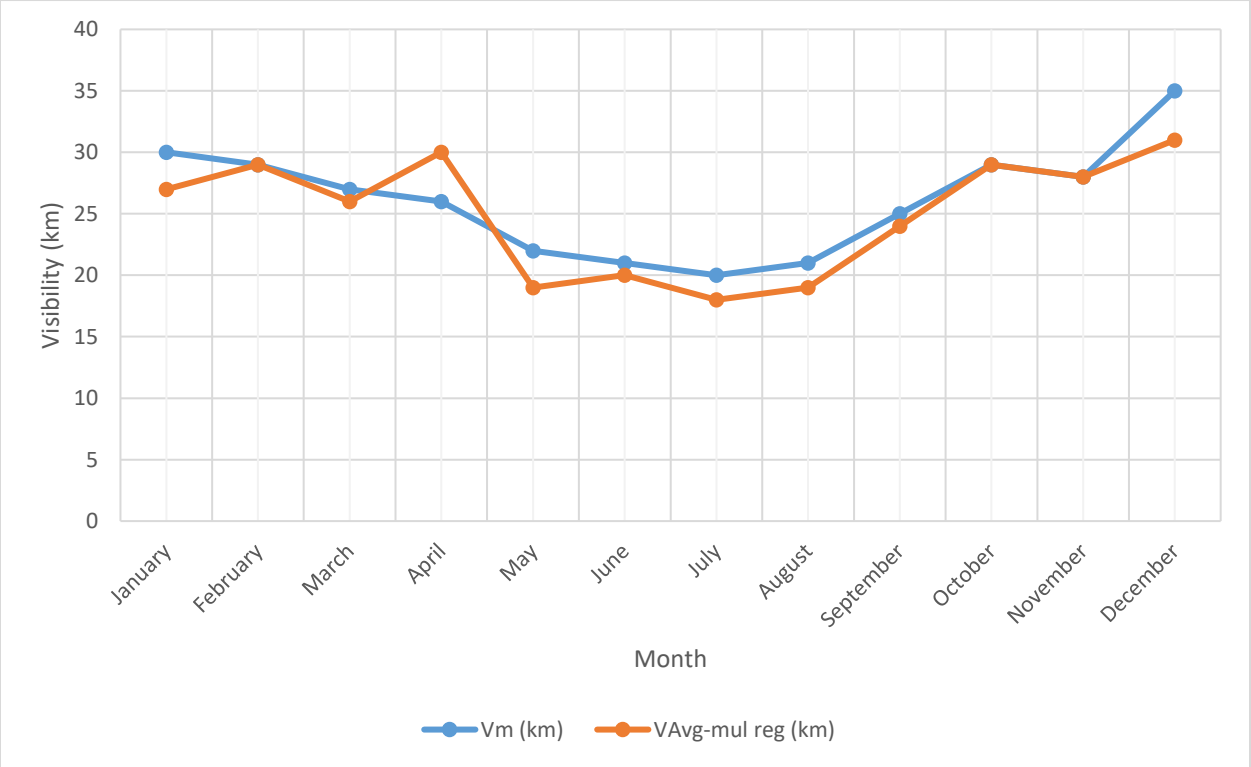

Figure 4.14 Variation of the measured and the predicted values of visibility using the average multiple regression model with the months of the year 2014.

Table 4.21 Model name, regression equations, correlation coefficient, standard error and the RMSE difference between measured and predicted visibility values.

		2011 - 2013			
S/N	**Model Name**	**Regression equations**	**Correlation coefficient**	**Standard error**	**RMSE with 2014**
1	Cumulative R.H.	V = -0.65653 (R.H.) + 71.43793	0.78172	2.57198	2.51661
2	Average R.H.	V = -0.86343 (R.H.) + 86.11686	0.86813	1.84635	1.93649
3	Cumulative T_{max}	V = 0.67550 (T_{max}) + 9.80320	0.63651	3.18085	2.72336
4	Average T_{max}	V = 0.76201 (T_{max}) + 7.87362	0.83015	2.07397	2.48328
5	Cumulative n/N	V = 33.79843 (n/N) + 0.79270	0.77549	2.60384	2.38048
6	Average n/N	V = 36.89996 (n/N) - 1.41707	0.91403	1.50897	2.36291
7	Cumulative Multiple Regression	V = 39.91787 - 0.43962(R.H.) + 23.93626(n/N) - 0.04099(T_{max})	0.90028	1.85053	2.10159
8	**Average Multiple Regression**	**V = 36.33271 - 0.41889 (R.H.) + 28.08959 (n/N) - 0.07882 (T_{max})**	**0.96453**	**1.09787**	**2.25462**

The comparison in Table 4.21 between the single and multiple regression models taking into account the correlation coefficients and the standard errors, shows that the average multiple regression model used to estimate the monthly visibility in this dissertation is the best for Cape Town.

Table 4.22 Comparison between measured and predicted visibility values calculated from various regression equations in Table 4.21

Year 2014									
	Measured Values	**Predicted Values**							
Months	**V_m (km)**	**$V_{Cum\ R.H.}$ (km)**	**$V_{Avg\ R.H.}$ (km)**	**$V_{Cum\ Tmax}$ (km)**	**$V_{Ave\ Tmax}$ (km)**	**$V_{Cum\ n/N}$ (km)**	**$V_{Avg\ n/N}$ (km)**	**$V_{Cum\text{-}mul\ reg}$ (km)**	**$V_{Avg\text{-}mul\ reg}$ (km)**
January	30	26	27	28	28	27	27	27	27
February	29	27	28	29	29	28	29	29	29
March	27	25	25	26	26	26	26	26	26
April	26	27	28	27	27	29	29	29	30
May	22	22	20	23	23	20	20	19	19
June	21	24	23	22	22	20	20	21	20
July	20	20	19	21	21	20	19	18	18
August	21	22	20	23	23	20	20	19	19
September	25	25	25	23	23	23	23	24	24
October	29	27	28	27	27	28	28	29	29
November	28	27	28	26	26	27	28	28	28
December	35	29	31	27	28	29	29	31	31

Using the average multiple regression formula in equation (48), the computation results of monthly average, minimum and maximum visibility for years 2010 – 2015 are as shown in Figures 4.15, 4.16 and 4.17. The highest average visibility occurred in December 2014 with a value of 35 km while the lowest average visibility was found to be 16 km in June and August 2015. The highest minimum visibility (19 km) occurred in December 2015 while the lowest minimum visibility was estimated to be 20 meters in June 2012 as shown in Figure 4.16. The lowest maximum visibility was calculated as 31 km in August 2015 while the highest maximum visibility is estimated to be 45 km in May 2013 as shown in Figure 4.17. The weather-dependent results within this six-year period show that inverse proportionality exists between the visibility and relative humidity while a directly proportional relationship exists between the visibility, maximum temperature and fraction of sunshine hours for the warm-summer Mediterranean climate of Cape Town.

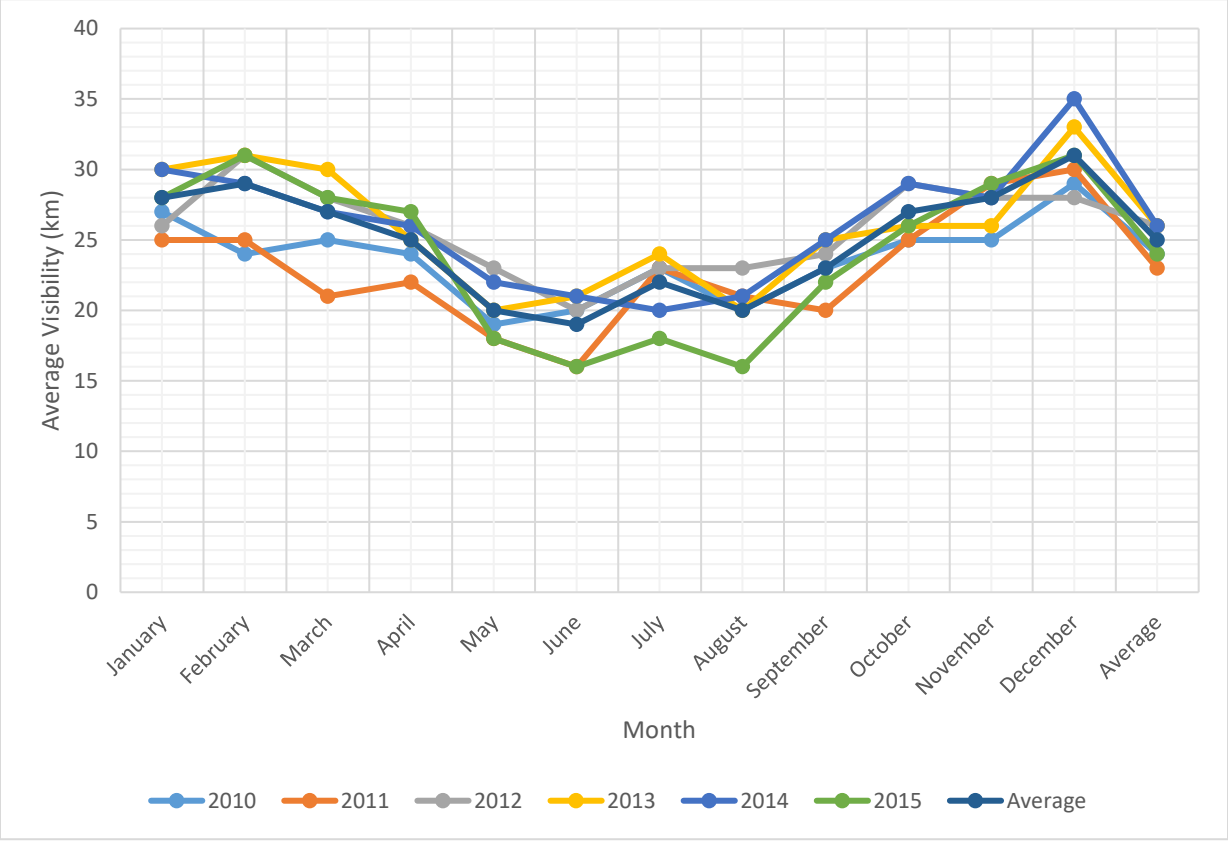

Figure 4.15 Average visibility pattern for years 2010 - 2015

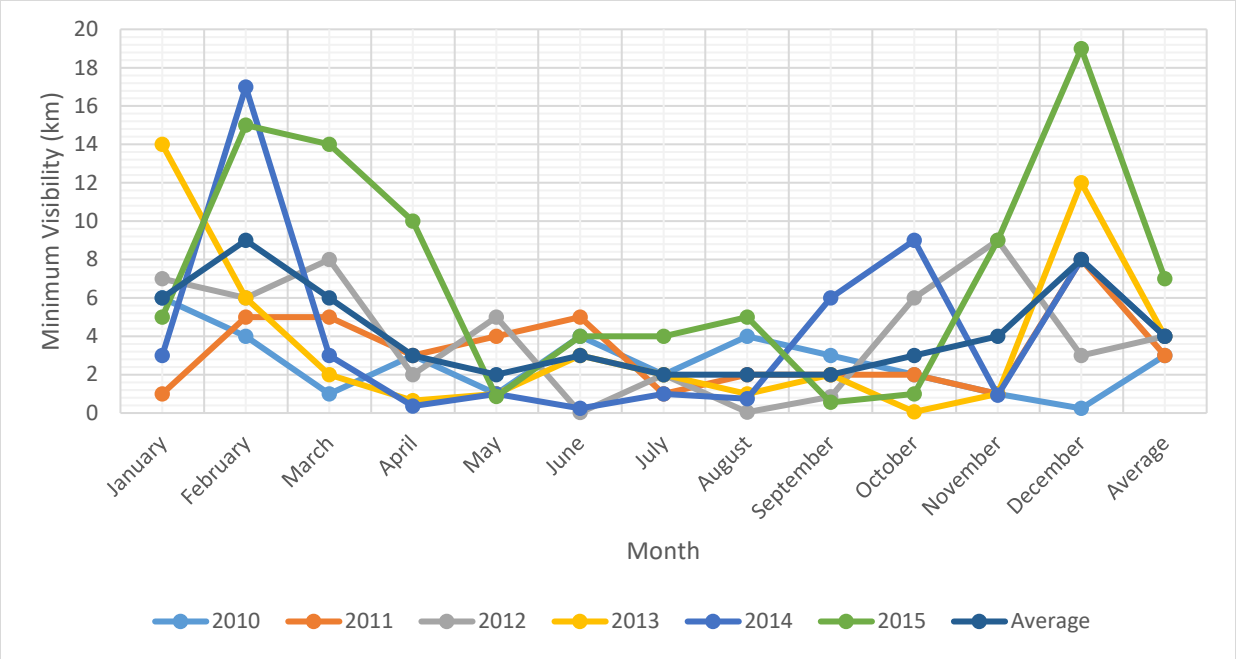

Figure 4.16 Minimum visibility pattern for years 2010 – 2015.

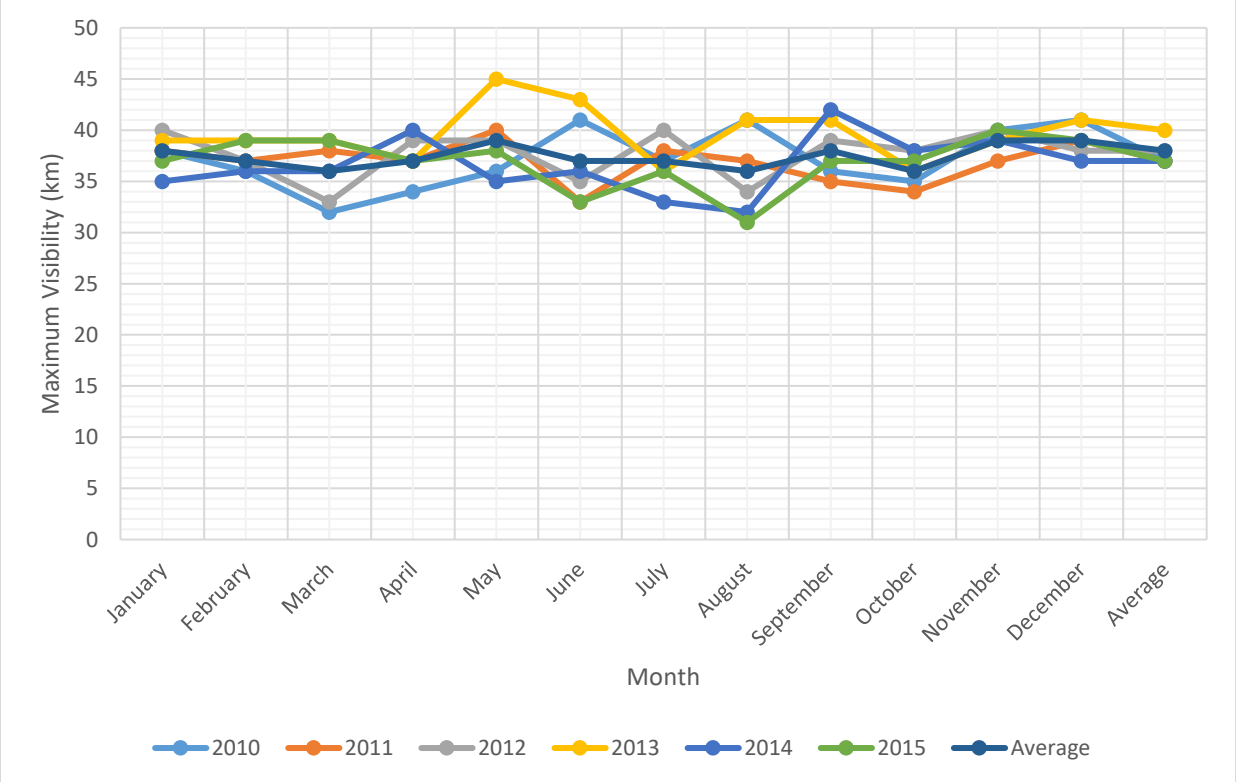

Figure 4.17 Maximum visibility pattern for years 2010 – 2015

4.3 Estimation of the Scattering Attenuation Coefficient for Cape Town

The Kim model in equation (12) and (14) is used to estimate the scattering attenuation coefficient $\beta_{as}(\lambda)$ for each of the monthly visibility values from January 2010 – December 2015. The atmospheric attenuation for three wavelengths (850 nm, 950 nm and 1550 nm) commonly used in commercial OWC systems is calculated. It should be noted that attenuation values of about 0 – 15 dB/km constitute about 94.44% of the scattering attenuation data set while values greater than 15 dB/km make up only 5.56%. The estimated lowest mean minimum attenuation occurred in November and is 0.24666 dB/km on 850 nm wavelength, 0.21345 dB/km on 950 nm wavelength and 0.11303 dB/km on 1550 nm wavelength as shown in Figure 4.18. This corresponds to a period when the maximum visibility is in excess of 38 km.

Conversely, the highest mean maximum atmospheric attenuation occurred in June. This corresponds to the time when visibility values could drop to values far lesser than 4 km. The estimated high attenuation values as shown in Figure 4.20 are 151.15972 dB/km on 850 nm wavelength, 150.96553 dB/km on 950 nm wavelength and 150.32009 dB/km on 1550 nm wavelength. The average scattering atmospheric attenuation as depicted in Figure 4.19 and corresponding to the average visibility of 25 km is 0.40264 dB/km on 850 nm wavelength, 0.34843 dB/km on 950 nm wavelength and 0.18439 dB/km on 1550 nm wavelength.

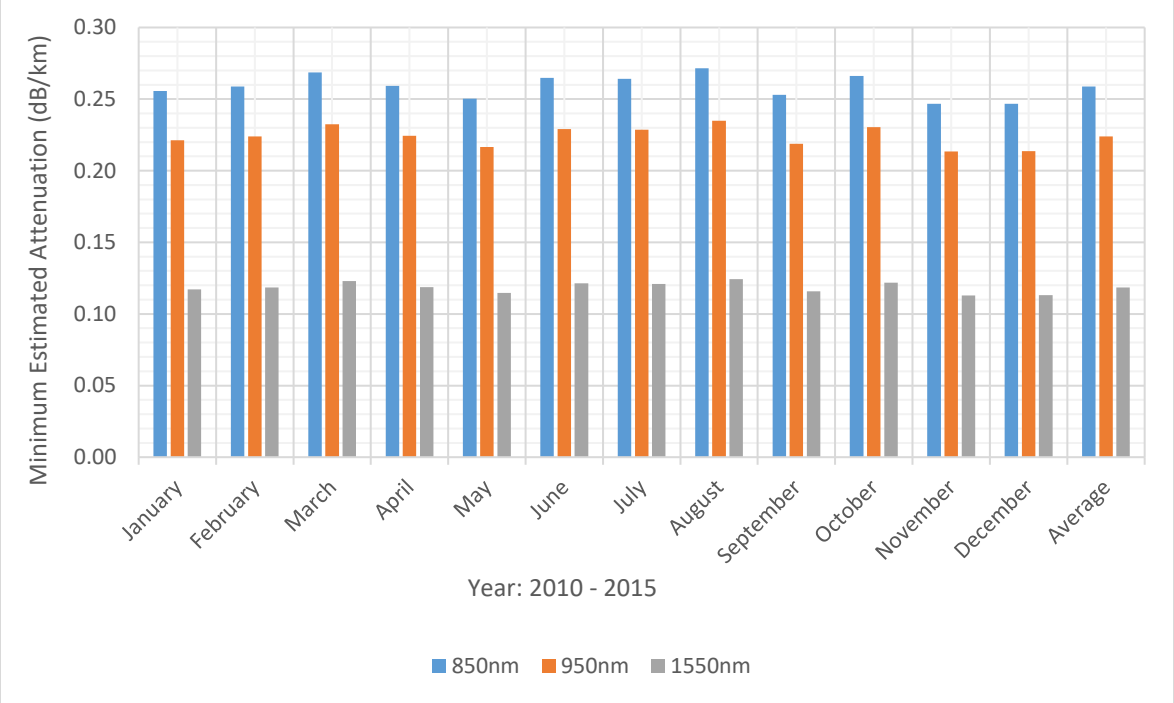

Figure 4.18 Estimated minimum attenuation coefficient (dB/km) for the year 2010 – 2015 at 850 nm, 950 nm and 1550 nm.

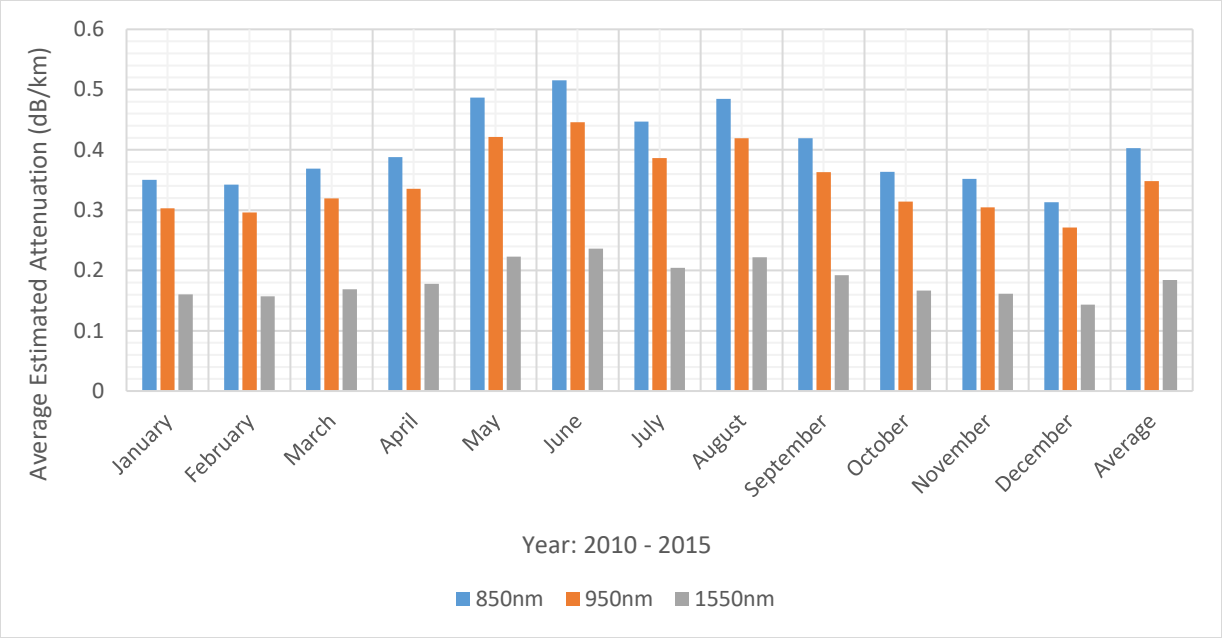

Figure 4.19 Estimated average attenuation coefficient (dB/km) for the year 2010 – 2015 at 850 nm, 950 nm and 1550 nm.

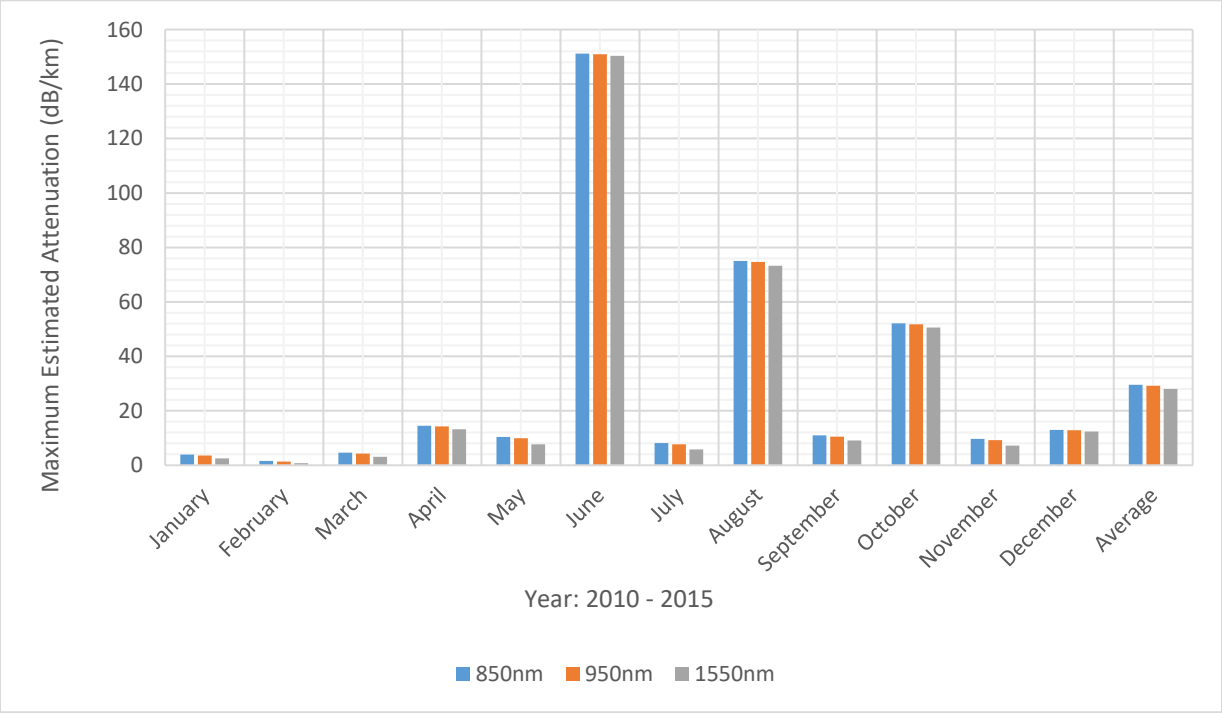

Figure 4.20 Estimated maximum attenuation coefficient (dB/km) for the year 2010 – 2015 at 850 nm, 950 nm and 1550 nm.

4.3.1 Estimation of Scattering Atmospheric Attenuation for Visibilities less than 1 km

For visibility values ranging from 20 – 1000 meters, various models have been proposed to estimate the specific attenuation behavior of the atmosphere at such lengths. The Ijaz and Naboulsi fog models from equation (15), (16), (20) and (21) are the most accurate models for estimating the atmospheric attenuations from thick to light fog weather. In urban areas, smoke emanating from industrial chimneys and fire outbreaks also result in much reduced visibility and the Ijaz Smoke model from equation (20) and (21) estimates the resultant atmospheric attenuation whenever such situations arise. Figures 4.21– 4.23 show the attenuation trend of optical signals on the 850 nm, 950 nm and 1550 nm wavelengths for visibilities ranging from 0 – 1 km. For a visibility of about 250 meters, the Ijaz smoke model estimates the specific attenuation to be 88 dB/km on the 850 nm wavelength while the Naboulsi convection fog model estimates the atmospheric attenuation to be 68 dB/km on the 1550 nm wavelength. From Figures 4.21 - 4.23, it can be deduced that Kruse, Kim and Ferdinandov models do not accurately estimate the specific attenuations for visibilities less than 1 km as compared to the other models used.

Table 4.23 Scattering attenuation coefficients at 850 nm for visibilities between 0 -1 km

Scattering Attenuation Coefficients at 850 nm							
Visibility (km)	**Kruse**	**Naboulsi - Advection fog**	**Naboulsi - Convection fog**	**Kim**	**Ijaz Model - Fog**	**Ferdinandov et al - Model**	**Ijaz Model - Smoke**
0.0206	769.60	784.38	808.87	825.24	859.97	985.38	1035.42
0.0420	370.47	384.72	396.73	404.76	421.80	442.24	507.85
0.0600	256.45	269.30	277.71	283.33	295.26	296.10	355.50
0.2411	60.18	67.02	69.11	70.51	73.48	61.96	88.47
0.2424	59.84	66.66	68.74	70.13	73.08	61.58	87.99
0.3618	39.19	44.66	46.06	46.99	48.96	39.25	58.95
0.5543	24.88	29.15	30.06	29.95	31.96	24.29	38.48
0.6438	21.19	25.10	25.88	24.80	27.52	20.53	33.13
0.7401	18.24	21.83	22.51	20.69	23.94	17.55	28.82
0.8408	15.90	19.22	19.82	17.43	21.07	15.20	25.37
0.8662	15.40	18.65	19.24	16.73	20.45	14.70	24.62
0.9272	14.30	17.43	17.97	15.22	19.11	13.62	23.00
0.9946	13.26	16.25	16.75	13.78	17.81	12.59	21.45

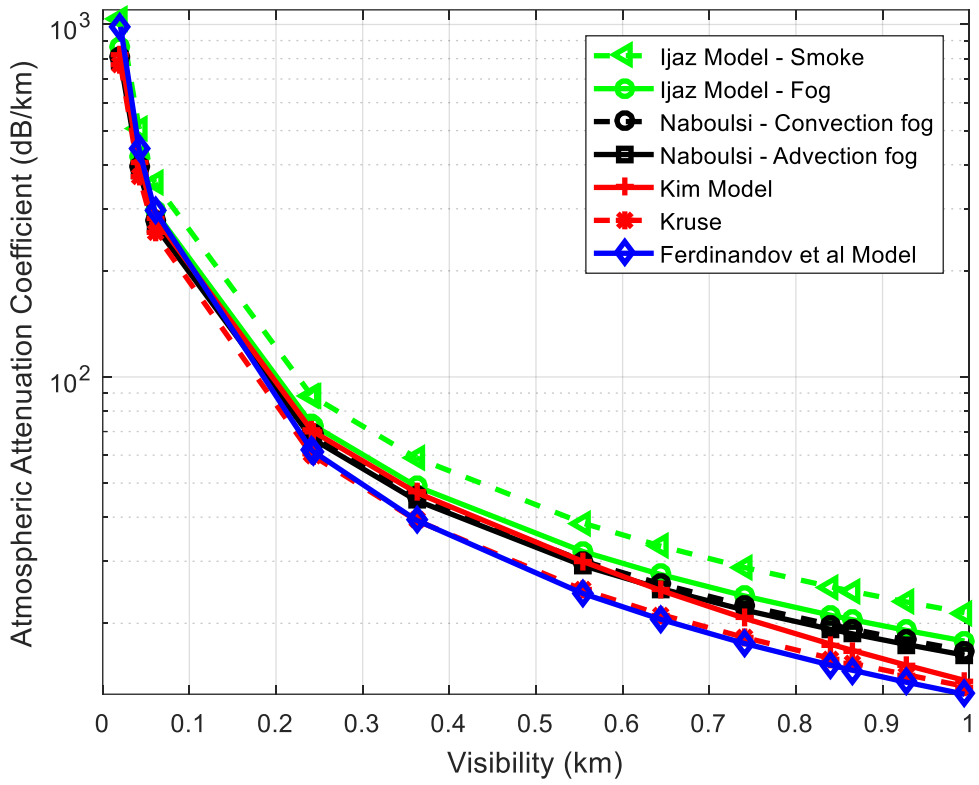

Figure 4.21 Comparison of the models used for calculating the scattering attenuation at 850 nm

Table 4.24 Scattering attenuation coefficient at 950 nm for visibilities between 0 -1 km

Scattering Attenuation Coefficients at 950 nm							
Visibility (km)	**Kruse**	**Naboulsi - Advection fog**	**Naboulsi - Convection fog**	**Kim**	**Ijaz Model - Fog**	**Ferdinandov et al - Model**	**Ijaz Model - Smoke**
0.0206	755.99	784.38	808.87	825.24	869.08	963.68	1097.22
0.0420	362.19	384.72	396.73	404.76	426.26	425.73	538.16
0.0600	250.00	269.30	277.71	283.33	298.38	282.81	376.71
0.2411	57.79	67.02	69.11	70.51	74.26	57.38	93.75
0.2424	57.46	66.66	68.74	70.13	73.86	57.03	93.25
0.3618	37.41	44.66	46.06	46.99	49.48	36.03	62.47
0.5543	23.59	29.15	30.06	29.77	32.30	22.09	40.78
0.6438	20.04	25.10	25.88	24.41	27.81	18.60	35.11
0.7401	17.20	21.83	22.51	20.15	24.19	15.86	30.54
0.8408	14.95	19.22	19.82	16.78	21.29	13.70	26.88
0.8662	14.47	18.65	19.24	16.07	20.67	13.24	26.09
0.9272	13.42	17.43	17.97	14.52	19.31	12.24	24.38
0.9946	12.42	16.25	16.75	13.04	18.00	11.30	22.73

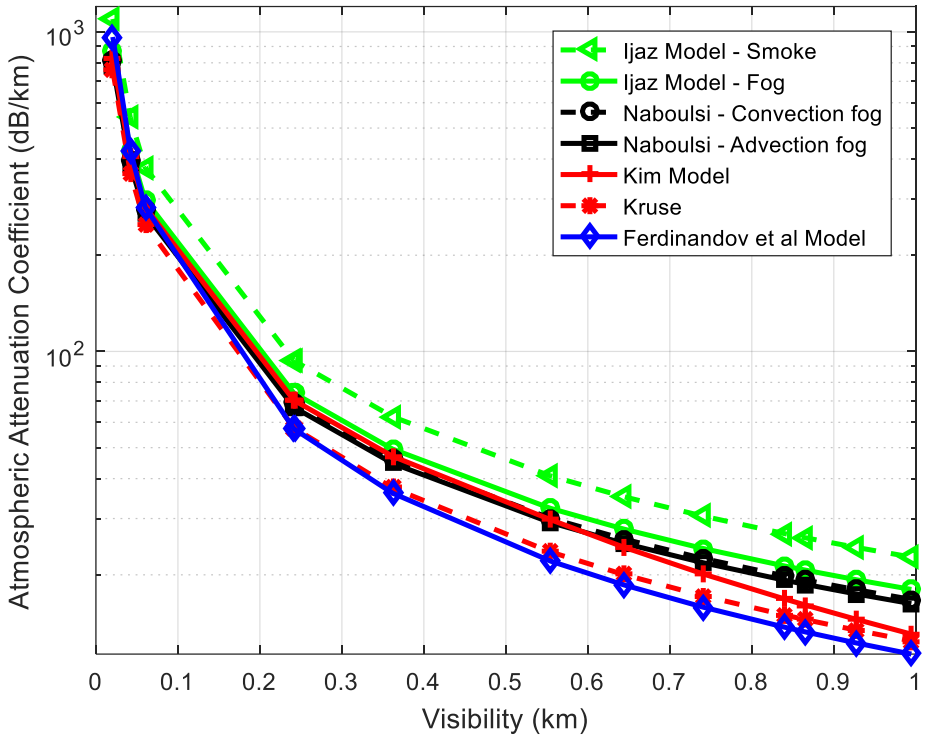

Figure 4.22 Comparison of the models used for calculating the scattering attenuation at 950 nm

Table 4.25 Scattering attenuation coefficient at 1550 nm for visibilities between 0 -1 km

Scattering Attenuation Coefficient at 1550 nm								
Visibility (km)	**Grabner et al Model - Power law**	**Kruse**	**Naboulsi - Advection fog**	**Naboulsi - Convection fog**	**Kim**	**Grabner et al Model - Inverse law**	**Ijaz Model -Fog**	**Ijaz Model - Smoke**
0.0206	636.49	698.91	784.38	808.87	825.24	884.47	910.32	1416.14
0.0420	344.53	327.87	384.72	396.73	404.76	433.81	446.49	694.58
0.0600	253.38	223.48	269.30	277.71	283.33	303.67	312.54	486.21
0.2411	76.44	48.35	67.02	69.11	70.51	75.57	77.78	121.00
0.2424	76.09	48.06	66.66	68.74	70.13	75.17	77.36	120.35
0.3618	53.88	30.51	44.66	46.06	46.99	50.36	51.83	80.63
0.5543	37.31	18.64	29.15	30.06	28.99	32.87	33.83	52.63
0.6438	32.79	15.65	25.10	25.88	22.75	28.30	29.13	45.31
0.7401	29.08	13.28	21.83	22.51	17.91	24.62	25.34	39.42
0.8408	26.06	11.41	19.22	19.82	14.20	21.67	22.30	34.70
0.8662	25.40	11.01	18.65	19.24	13.43	21.03	21.65	33.68
0.9272	23.95	10.15	17.43	17.97	11.78	19.65	20.22	31.46
0.9946	22.54	9.33	16.25	16.75	10.24	18.32	18.85	29.33

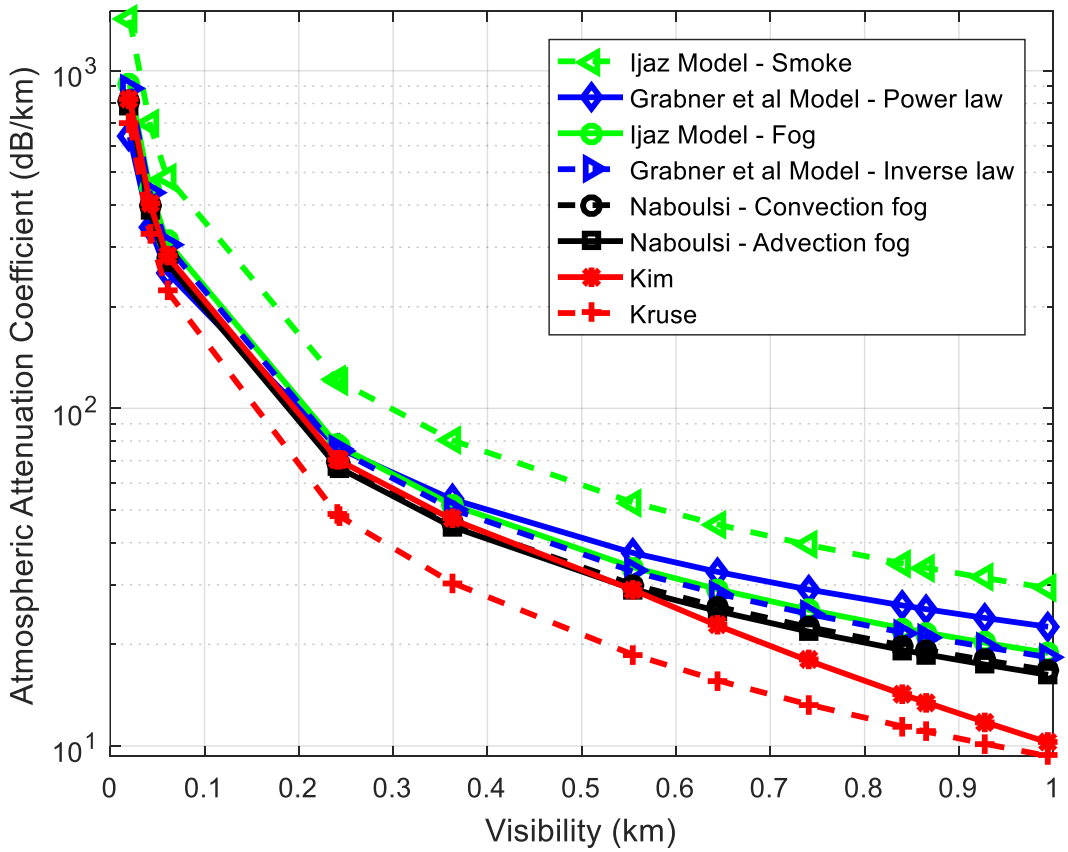

Figure 4.23 Comparison of the models used for calculating the scattering attenuation at 1550 nm

4.4 Probability of encountering various Scattering Atmospheric Attenuation Conditions

It is essential to have an idea of what weather constrictions will be experienced in a given region and at a given time before installing an OWC system. The OWC system installer can anticipate the probability of system outage with the information of the probability of exceeding a specific atmospheric attenuation value once the maximum attenuation the OWC system can withstand is known. The probability of encountering various specific attenuation conditions for 850 nm, 950 nm and 1550 nm wavelength systems is shown in Table 4.26 and Figure 4.24. For an OWC system transmitting optical signals at 850 nm wavelength, the probability of encountering atmospheric attenuation in excess of 1 dB/km is 0.300926 using both Kim and Ferdinandov models. On the other hand, the probability of encountering atmospheric attenuation in excess of 20 dB/km when transmitting at 950 nm wavelength using Kim and Ferdinandov models for estimating specific attenuation is 0.041667 and 0.032407 respectively. The probability of encountering atmospheric attenuation in excess of 150 dB/km when transmitting on the 1550 nm wavelength using Kim model is 0.013889.

Table 4.26 Probability of encountering various atmospheric scattering attenuation conditions.

Probability of Exceeding Different Attenuation Values					
Attenuation Values (dB/km)	**Kim Model – 850 nm**	**Ferdinandov et al Model – 850 nm**	**Kim Model – 950 nm**	**Ferdinandov et al Model – 950 nm**	**Kim Model – 1550 nm**
1	0.300926	0.300925	0.287037	0.287037	0.245370
5	0.157407	0.157407	0.157407	0.157407	0.111111
10	0.111111	0.111111	0.111111	0.111111	0.111111
15	0.055556	0.041667	0.050925	0.037037	0.041667
20	0.041667	0.037037	0.041667	0.032407	0.037037
25	0.032407	0.027778	0.032407	0.027778	0.032407
30	0.027778	0.027778	0.027778	0.027778	0.027778
35	0.027778	0.027778	0.027778	0.027778	0.027778
40	0.027778	0.023148	0.027778	0.023148	0.027778
45	0.027778	0.023148	0.027778	0.023148	0.027778
50	0.023148	0.023148	0.023148	0.023148	0.023148
100	0.013889	0.013889	0.013889	0.013889	0.013889
200	0.013889	0.013889	0.013889	0.013889	0.013889
500	0.004629	0.004630	0.004629	0.004630	0.004629
800	0.004629	0.004630	0.004629	0.004630	0.004629
1000	0.000000	0.000000	0.000000	0.000000	0.000000

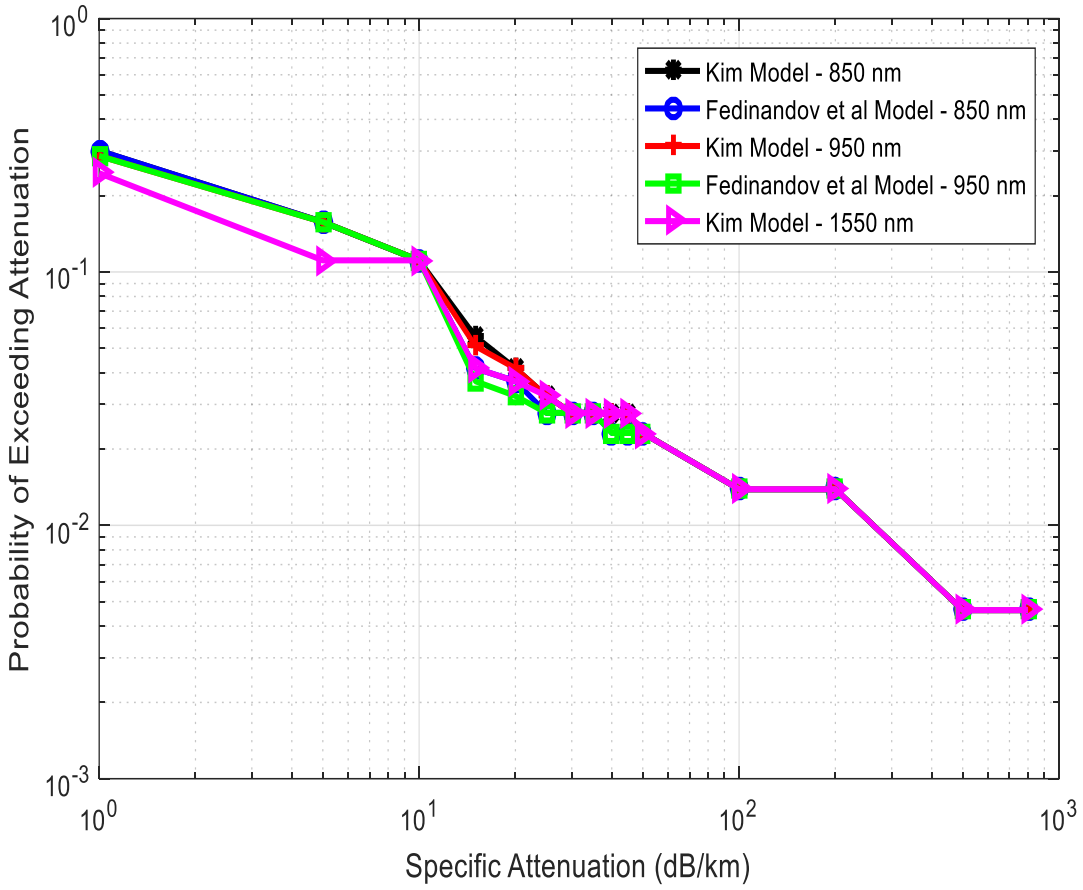

Figure 4.24 Probability of encountering different Atmospheric Scattering Attenuation Conditions.

4.5 Atmospheric Scattering and Turbulence losses for Cape Town.

Figures 4.25 - 4.27 and Tables 4.27 – 4.29 show the comparison and contributions of the scattering attenuation and scintillation losses to the total atmospheric losses. Using the Kim model to evaluate the specific attenuation on an 850 nm wavelength, the scattering atmospheric attenuation has a contribution of 7.7% to the total atmospheric loss for a link distance of 3 km as shown in Figure 4.25. For a propagation distance of 5 km and on a wavelength of 950 nm, the scattering attenuation as evaluated from the Ferdinandov model in Figure 4.26 contributes 6.4% to the total atmospheric loss. The scintillation loss has a contribution of 95.96% to the total atmospheric loss for a wavelength of 1550 nm and a link distance of 7 km in Figure 4.27. The little contributions of scattering losses to the total atmospheric loss is a clear indication that the visibility in a Warm-summer Mediterranean climate has a fairly stable low average value. In these regions, however, the turbulence or scintillation losses are significantly high.

Table 4.27 Atmospheric scattering and turbulence losses using different models at 850 nm

850 nm			
Distance (km)	**Ferdinandov et al Model - Atm. Scattering Losses (dB)**	**Kim Model - Atm. Scattering Losses (dB)**	**Atm. Tur. Loss (dB)**
0.50	0.17600	0.20132	2.79452
1.00	0.35199	0.40264	5.27536
1.50	0.52799	0.60396	7.65013
2.00	0.70398	0.80528	9.95855
2.50	0.87998	1.00660	12.21885
3.00	1.05597	1.20792	14.44153
3.50	1.23197	1.40924	16.63340
4.00	1.40796	1.61056	18.79924
4.50	1.58396	1.81188	20.94258
5.00	1.75995	2.01320	23.06612
5.50	1.93595	2.21452	25.17200
6.00	2.11194	2.41584	27.26197
6.50	2.28794	2.61716	29.33746
7.00	2.46393	2.81848	31.39968
7.50	2.63993	3.01980	33.44964
8.00	2.81592	3.22112	35.48824
8.50	2.99192	3.42244	37.51624
9.00	3.16791	3.62376	39.53432
9.50	3.34391	3.82508	41.54307
10.00	3.51990	4.02640	43.54303
10.50	3.69590	4.22772	45.53467
11.00	3.87189	4.42904	47.51841
11.50	4.04789	4.63036	49.49466
12.00	4.22388	4.83168	51.46375
12.50	4.39988	5.03300	53.42602
13.00	4.57587	5.23432	55.38176
13.50	4.75187	5.43564	57.33123
14.00	4.92786	5.63696	59.27470
14.50	5.10386	5.83828	61.21239
15.00	5.27985	6.03960	63.14451

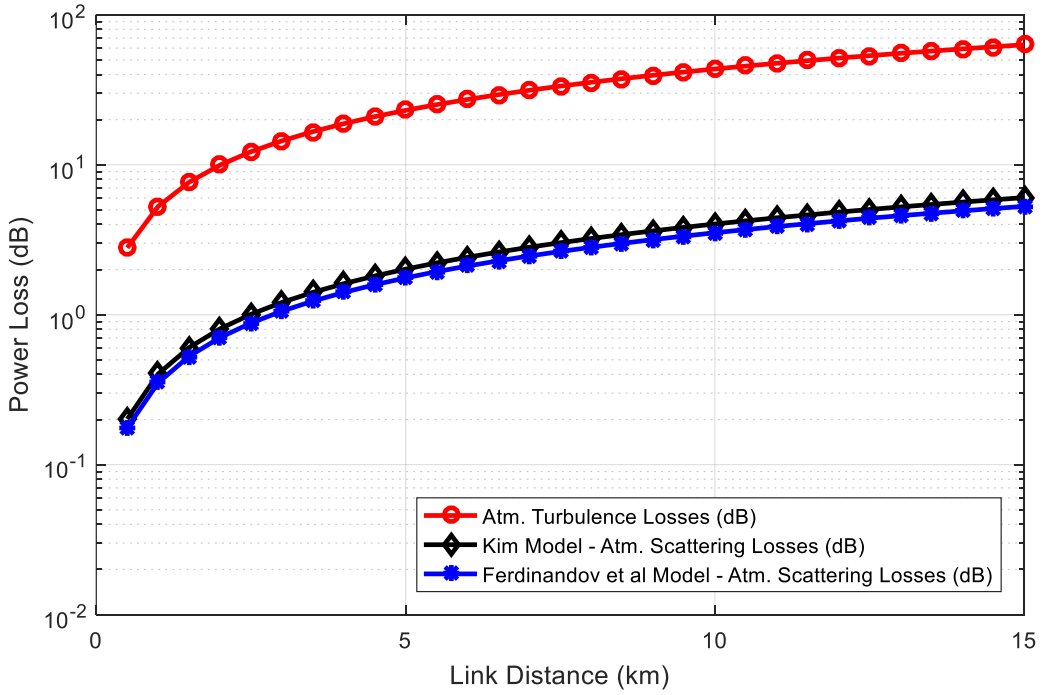

Figure 4.25 Comparison of atmospheric scattering and turbulence losses at 850 nm.

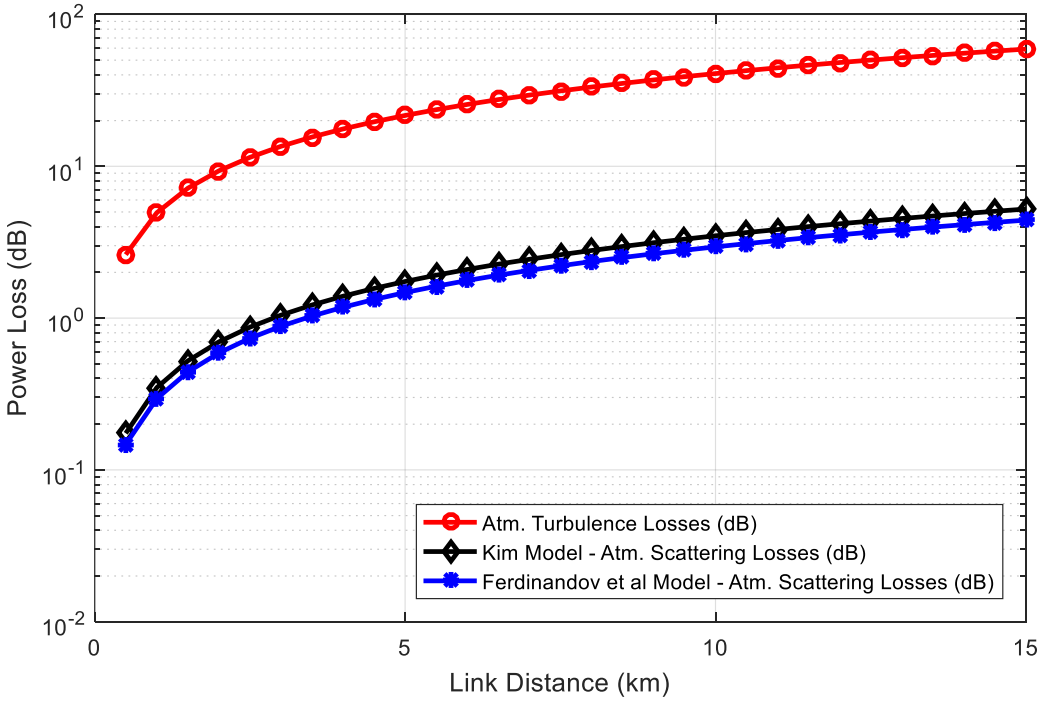

Figure 4.26 Comparison of atmospheric scattering and turbulence losses at 950 nm.

Table 4.28 Atmospheric scattering and turbulence losses using different models at 950 nm

950 nm			
Distance (km)	**Ferdinandov et al Model - Atm. Scattering Losses (dB)**	**Kim Model - Atm. Scattering Losses (dB)**	**Atm. Tur. Loss (dB) (950 nm)**
0.50	0.14730	0.17422	2.61897
1.00	0.29459	0.34843	4.94395
1.50	0.44189	0.52265	7.16954
2.00	0.58918	0.69686	9.33294
2.50	0.73648	0.87108	11.45124
3.00	0.88377	1.04529	13.53429
3.50	1.03107	1.21951	15.58846
4.00	1.17836	1.39372	17.61824
4.50	1.32566	1.56794	19.62693
5.00	1.47295	1.74215	21.61707
5.50	1.62025	1.91637	23.59066
6.00	1.76754	2.09058	25.54933
6.50	1.91484	2.26480	27.49444
7.00	2.06213	2.43901	29.42710
7.50	2.20943	2.61323	31.34828
8.00	2.35672	2.78744	33.25881
8.50	2.50402	2.96166	35.15941
9.00	2.65131	3.13587	37.05071
9.50	2.79861	3.31009	38.93327
10.00	2.94590	3.48430	40.80759
10.50	3.09320	3.65852	42.67411
11.00	3.24049	3.83273	44.53323
11.50	3.38779	4.00695	46.38532
12.00	3.53508	4.18116	48.23072
12.50	3.68238	4.35538	50.06971
13.00	3.82967	4.52959	51.90258
13.50	3.97697	4.70381	53.72959
14.00	4.12426	4.87802	55.55097
14.50	4.27156	5.05224	57.36693
15.00	4.41885	5.22645	59.17768

Table 4.29 Atmospheric scattering and turbulence losses using Kim model at 1550 nm

1550 nm		
Distance (km)	**Kim Model - Atm. Scattering Losses (dB)**	**Atm. Tur. Loss (dB)**
0.50	0.09220	1.96838
1.00	0.18439	3.71580
1.50	0.27659	5.38852
2.00	0.36878	7.01450
2.50	0.46098	8.60659
3.00	0.55317	10.17218
3.50	0.64537	11.71607
4.00	0.73756	13.24162
4.50	0.82976	14.75132
5.00	0.92195	16.24708
5.50	1.01415	17.73041
6.00	1.10634	19.20252
6.50	1.19854	20.66443
7.00	1.29073	22.11699
7.50	1.38293	23.56093
8.00	1.47512	24.99685
8.50	1.56732	26.42532
9.00	1.65951	27.84679
9.50	1.75171	29.26170
10.00	1.84390	30.67041
10.50	1.93610	32.07326
11.00	2.02829	33.47055
11.50	2.12049	34.86256
12.00	2.21268	36.24953
12.50	2.30488	37.63169
13.00	2.39707	39.00925
13.50	2.48927	40.38240
14.00	2.58146	41.75132
14.50	2.67366	43.11617
15.00	2.76585	44.47711

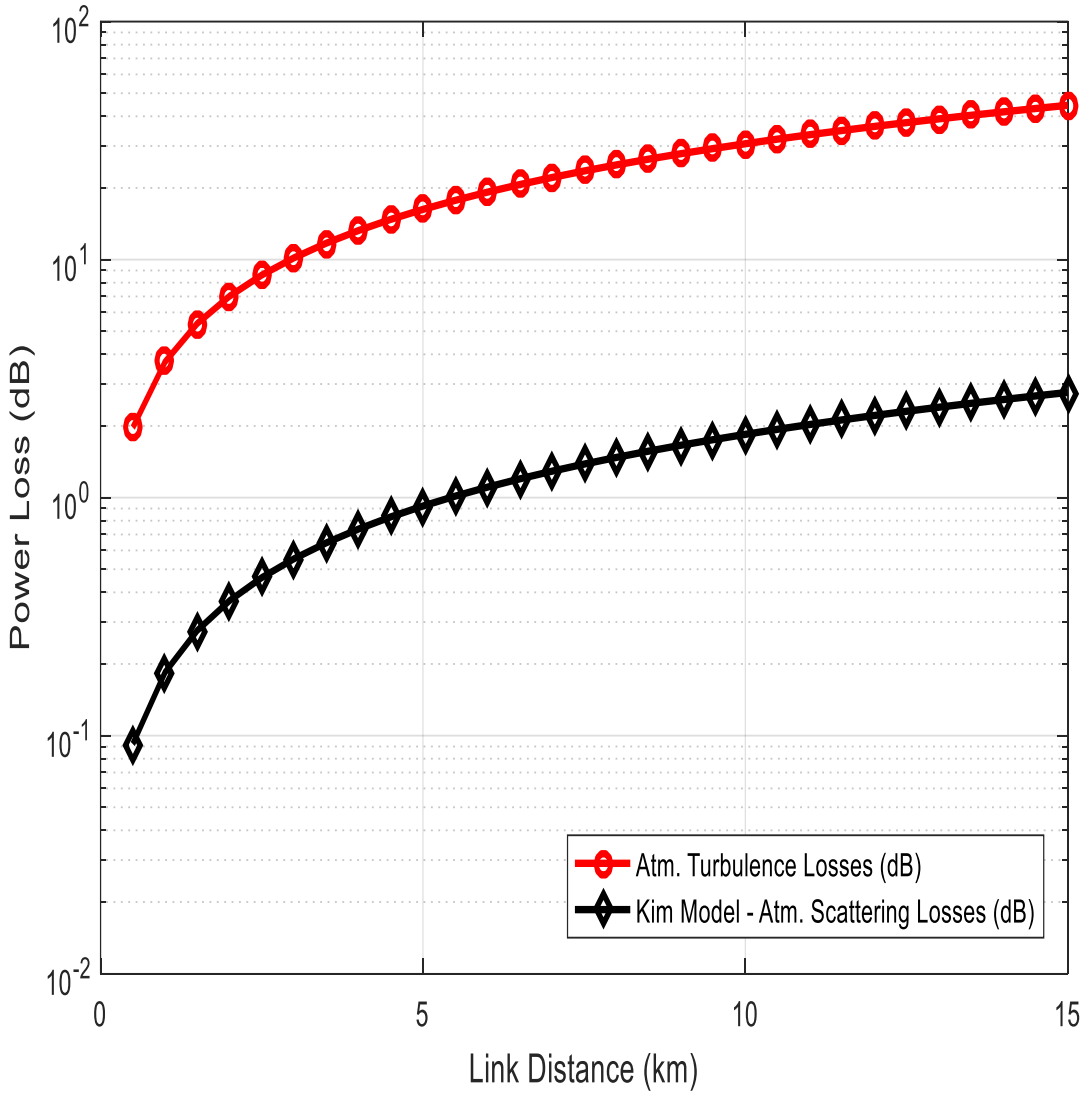

Figure 4.27 Comparison of atmospheric scattering and turbulence losses at 1550 nm.

4.6 Power Scintillation Index at different Measured Refractive Index values

From equation (26), by increasing the diameter of the receiver lens, the collector area of the lens also increases. This causes the reduction of scintillation losses as the increased receiver area allows for the merging of different optical intensities on the major parts of the lens. Substituting the values of the parameters in Table 3.1 into equation (26) appropriately, as the refractive index increases there is a corresponding increase in the power scintillation level at a particular distance as presented in Table 4.30 and Figure 4.28.

Table 4.30 Power scintillation index at different OWCS receivers

Distance (km)	Power S.I. ($m^{-2/3}$)								
	C_n^2 = 2.70189x10^{-15} $m^{-2/3}$			C_n^2 = 9.20233x10^{-15} $m^{-2/3}$			C_n^2 = 2.04320x10^{-14} $m^{-2/3}$		
	OWCS A – 850 nm	OWCS A – 950 nm	OWCS A – 1550 nm	OWCS B – 850 nm	OWCS B – 950 nm	OWCS B – 1550 nm	OWCS C – 850 nm	OWCS C – 950 nm	OWCS C – 1550 nm
0.00	0.00000	0.00000	0.00000	0.00000	0.00000	0.00000	0.00000	0.00000	0.00000
0.50	0.00026	0.00026	0.00025	0.00089	0.00088	0.00084	0.00197	0.00195	0.00186
1.00	0.00195	0.00192	0.00177	0.00663	0.00654	0.00603	0.01472	0.01451	0.01339
1.50	0.00619	0.00607	0.00546	0.02109	0.02068	0.01860	0.04683	0.04592	0.04129
2.00	0.01391	0.01358	0.01194	0.04738	0.04626	0.04068	0.10519	0.10271	0.09032
2.50	0.02585	0.02514	0.02168	0.08804	0.08563	0.07386	0.19547	0.19013	0.16398
3.00	0.04264	0.04133	0.03504	0.14522	0.14077	0.11934	0.32244	0.31255	0.26496
3.50	0.06481	0.06262	0.05228	0.22073	0.21329	0.17805	0.49009	0.47357	0.39532
4.00	0.09281	0.08943	0.07361	0.31611	0.30457	0.25072	0.70186	0.67625	0.55668
4.50	0.12704	0.12208	0.09922	0.43268	0.41579	0.33794	0.96068	0.92317	0.75032
5.00	0.16782	0.16087	0.12923	0.57159	0.54792	0.44015	1.26910	1.21654	0.97727
5.50	0.21546	0.20606	0.16376	0.73382	0.70182	0.55774	1.62931	1.55827	1.23836
6.00	0.27020	0.25786	0.20289	0.92026	0.87824	0.69100	2.04326	1.94997	1.53424
6.50	0.33226	0.31646	0.24669	1.13165	1.07782	0.84018	2.51262	2.39308	1.86546
7.00	0.40185	0.38201	0.29522	1.36867	1.30109	1.00547	3.03887	2.88882	2.23246
7.50	0.47914	0.45467	0.34852	1.63190	1.54856	1.18703	3.62333	3.43828	2.63557
8.00	0.56428	0.53456	0.40664	1.92187	1.82064	1.38498	4.26714	4.04238	3.07509
8.50	0.65740	0.62178	0.46961	2.23903	2.11770	1.59943	4.97132	4.70194	3.55123
9.00	0.75862	0.71643	0.53744	2.58378	2.44007	1.83046	5.73679	5.41770	4.06418
9.50	0.86806	0.81859	0.61016	2.95650	2.78803	2.07812	6.56435	6.19028	4.61407
10.00	0.98580	0.92834	0.68777	3.35751	3.16183	2.34248	7.45470	7.02022	5.20102
10.50	1.11192	1.04574	0.77030	3.78708	3.56168	2.62355	8.40849	7.90803	5.82509
11.00	1.24651	1.17085	0.85774	4.24549	3.98779	2.92137	9.42628	8.85413	6.48634
11.50	1.38963	1.30372	0.95010	4.73294	4.44032	3.23595	10.50858	9.85888	7.18480
12.00	1.54134	1.44439	1.04739	5.24964	4.91942	3.56730	11.65582	10.92263	7.92050
12.50	1.70170	1.59289	1.14960	5.79578	5.42522	3.91541	12.86842	12.04565	8.69342
13.00	1.87074	1.74927	1.25674	6.37151	5.95783	4.28030	14.14672	13.22820	9.50357

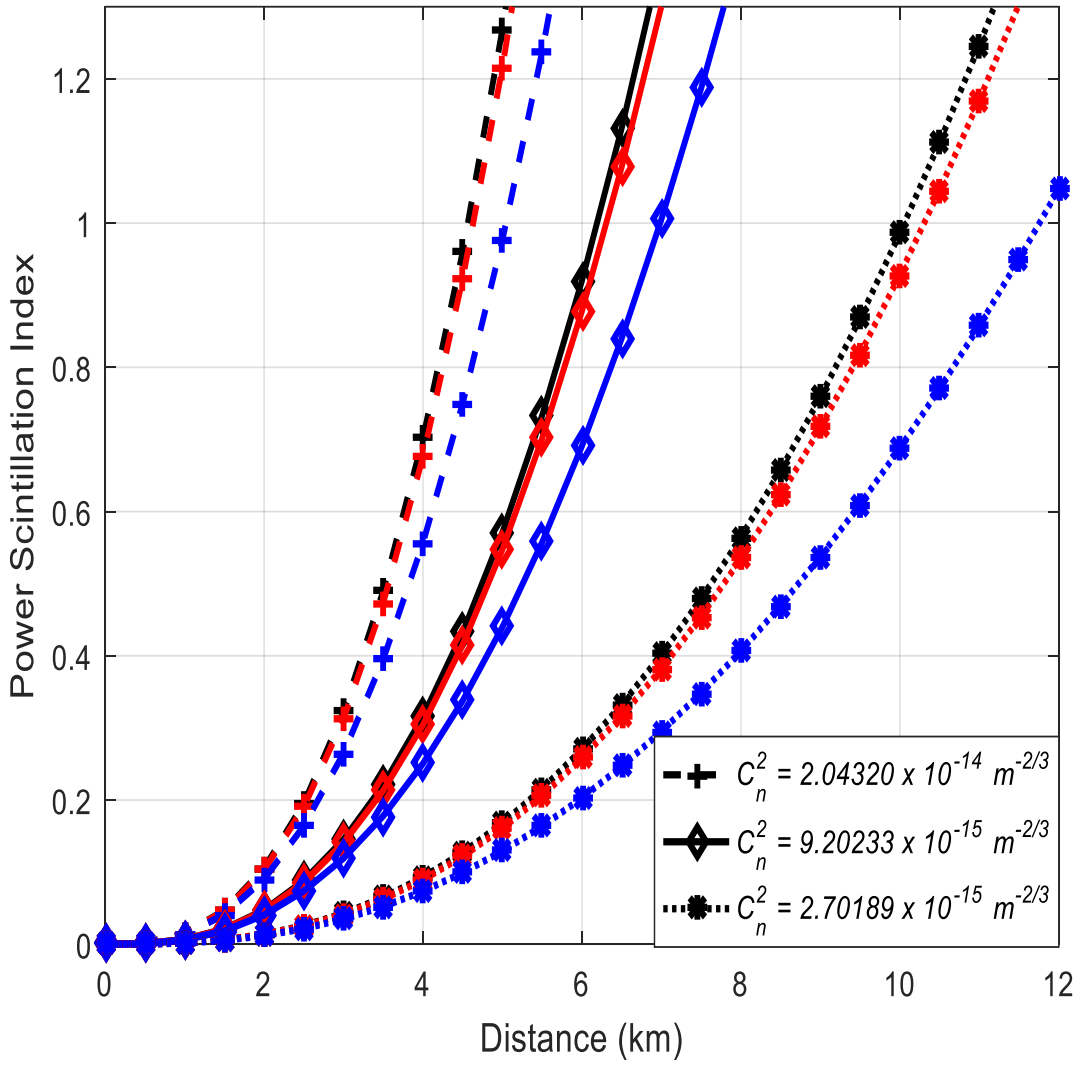

Figure 4.28 Power scintillation index at OWC receivers versus link distance.

4.7 Power Loss due to Turbulence

Tables 4.31 – 4.33 and Figures 4.29 – 4.31, show the dependence of power loss due to turbulence on the power scintillation index for various upper bound outage probabilities at different wavelength values by utilizing equation (27). As the power scintillation index increases, the atmospheric turbulence loss due to irradiance fluctuations increases as well. The fading loss and the outage probability have an inversely proportional relationship while the turbulence power loss increases greatly with increase in the link length. The wavelengths have little or no impact on the fading loss characteristic dependence on the power scintillation index as observed from the figures below.

Table 4.31 Atmospheric turbulence losses for various upper bound probabilities at 850 nm

FSO B - 850nm							
Distance (km)	**Power S.I. ($m^{-2/3}$)**	**Atmospheric Turbulence Losses (A_{turb} (L)) (dB)**					
		$P_{ub} = 10^{-7}$	**$P_{ub} = 10^{-4}$**	**$P_{ub} = 10^{-3}$**	**$P_{ub} = 10^{-2}$**	**$P_{ub} = 10^{-1}$**	**$P_{ub} = 2x10^{-1}$**
0.00	0.0000	0.0000	0.0000	0.0000	0.0000	0.0000	0.0000
0.50	0.0009	0.6743	0.4829	0.4016	0.3028	0.1677	0.1108
1.00	0.0066	1.8501	1.3275	1.1055	0.8357	0.4668	0.3115
1.50	0.0211	3.3076	2.3788	1.9843	1.5050	0.8494	0.5734
2.00	0.0474	4.9586	3.5754	2.9879	2.2742	1.2979	0.8869
2.50	0.0880	6.7423	4.8749	4.0816	3.1180	1.7999	1.2449
3.00	0.1452	8.6094	6.2420	5.2364	4.0148	2.3439	1.6404
3.50	0.2207	10.5175	7.6463	6.4268	4.9452	2.9187	2.0655
4.00	0.3161	12.4308	9.0614	7.6302	5.8915	3.5134	2.5121
4.50	0.4327	14.3205	10.4655	8.8281	6.8388	4.1181	2.9724
5.00	0.5716	16.1642	11.8415	10.0054	7.7748	4.7239	3.4393
5.50	0.7338	17.9461	13.1769	11.1511	8.6900	5.3239	3.9065
6.00	0.9203	19.6561	14.4632	12.2574	9.5777	5.9125	4.3692
6.50	1.1317	21.2885	15.6954	13.3196	10.4334	6.4857	4.8235

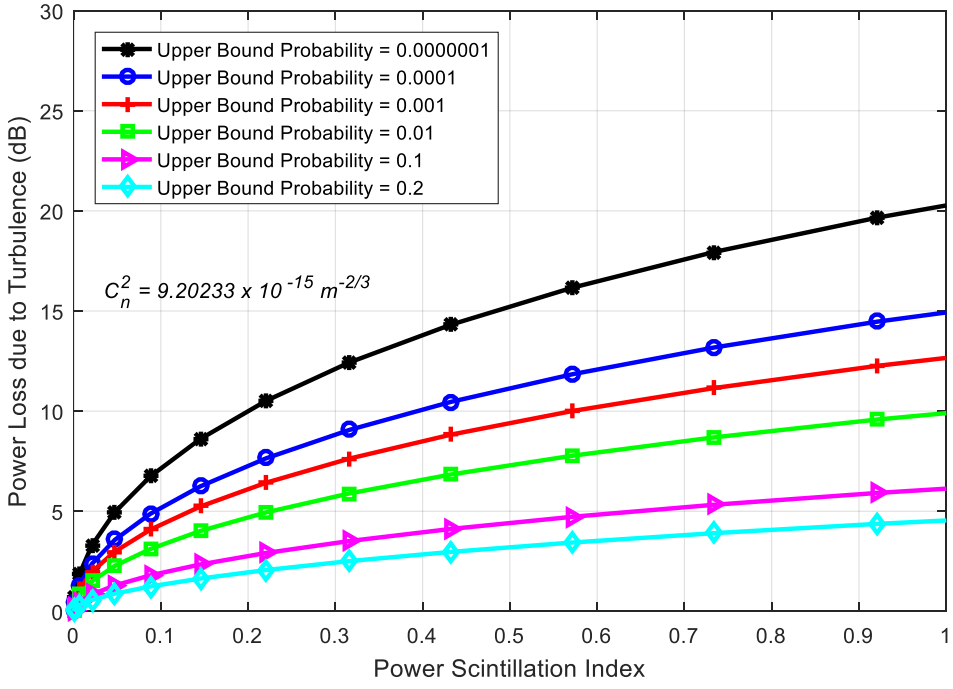

Figure 4.29 Power loss caused by turbulence plotted for various probabilities at 850 nm.

Table 4.32 Atmospheric turbulence losses for various upper bound probabilities at 950 nm

FSO B - 950 nm							
Distance (km)	**Power S.I. ($m^{-2/3}$)**	**$A_{turb}(L)$ (dB)**					
		$P_{ub} = 10^{-7}$	**$P_{ub} = 10^{-4}$**	**$P_{ub} = 10^{-3}$**	**$P_{ub} = 10^{-2}$**	**$P_{ub} = 10^{-1}$**	**$P_{ub} = 2x10^{-1}$**
0.00	0.0000	0.0000	0.0000	0.0000	0.0000	0.0000	0.0000
0.50	0.0009	0.6714	0.4808	0.3998	0.3015	0.1669	0.1103
1.00	0.0065	1.8367	1.3178	1.0974	0.8296	0.4634	0.3092
1.50	0.0207	3.2753	2.3555	1.9647	1.4901	0.8408	0.5674
2.00	0.0463	4.8999	3.5328	2.9521	2.2466	1.2817	0.8755
2.50	0.0856	6.6509	4.8081	4.0254	3.0744	1.7738	1.2261
3.00	0.1408	8.4806	6.1475	5.1565	3.9525	2.3058	1.6125
3.50	0.2133	10.3484	7.5216	6.3209	4.8622	2.8671	2.0270
4.00	0.3046	12.2206	8.9056	7.4975	5.7869	3.4472	2.4620
4.50	0.4158	14.0695	10.2787	8.6685	6.7123	4.0368	2.9102
5.00	0.5479	15.8742	11.6247	9.8197	7.6269	4.6276	3.3647
5.50	0.7018	17.6197	12.9319	10.9407	8.5216	5.2130	3.8198
6.00	0.8782	19.2962	14.1920	12.0240	9.3901	5.7876	4.2707
6.50	1.0778	20.8982	15.4003	13.0650	10.2280	6.3477	4.7138

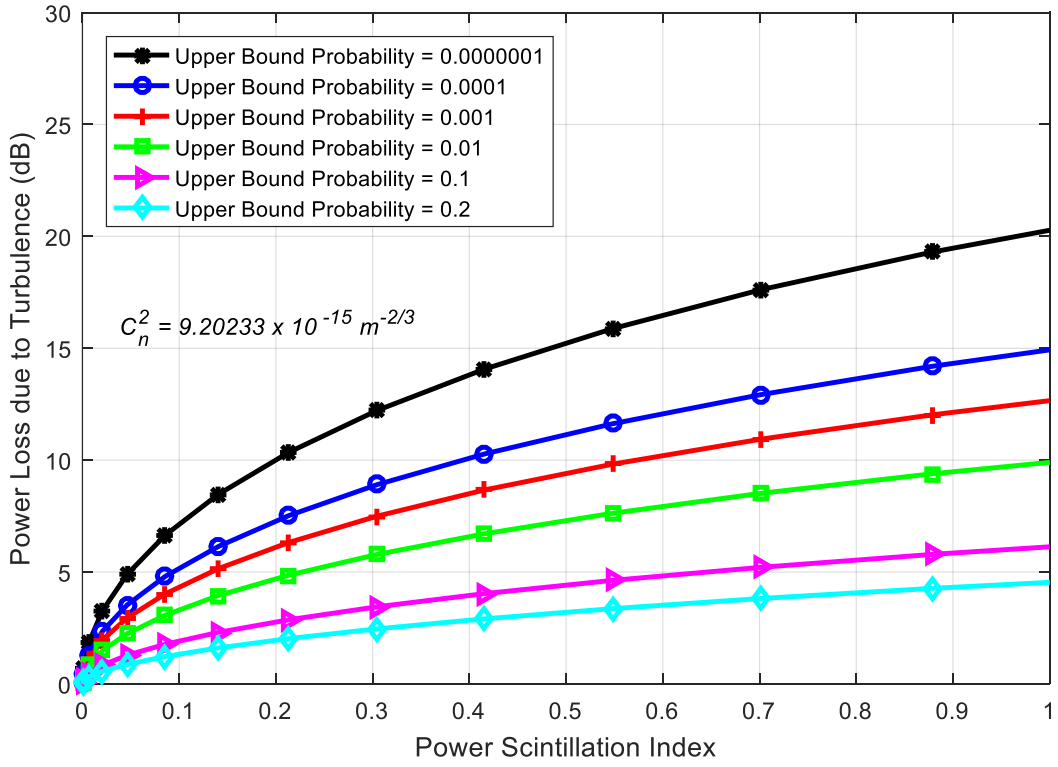

Figure 4.30 Power loss caused by turbulence plotted for various probabilities at 950 nm.

Table 4.33 Atmospheric turbulence losses for various upper bound probabilities at 1550 nm

FSO B – 1550 nm							
Distance (km)	**Power S.I. ($m^{-2/3}$)**	**$A_{turb}(L)$ (dB)**					
		$P_{ub} = 10^{-7}$	**$P_{ub} = 10^{-4}$**	**$P_{ub} = 10^{-3}$**	**$P_{ub} = 10^{-2}$**	**$P_{ub} = 10^{-1}$**	**$P_{ub} = 2x10^{-1}$**
0.00	0.0000	0.0000	0.0000	0.0000	0.0000	0.0000	0.0000
0.50	0.0008	0.6555	0.4694	0.3903	0.2943	0.1629	0.1076
1.00	0.0060	1.7642	1.2656	1.0539	0.7966	0.4447	0.2965
1.50	0.0186	3.1052	2.2325	1.8618	1.4115	0.7955	0.5362
2.00	0.0407	4.5955	3.3117	2.7664	2.1040	1.1979	0.8164
2.50	0.0739	6.1823	4.4662	3.7372	2.8517	1.6404	1.1304
3.00	0.1193	7.8264	5.6678	4.7510	3.6371	2.1136	1.4720
3.50	0.1780	9.4963	6.8939	5.7884	4.4455	2.6088	1.8354
4.00	0.2507	11.1662	8.1253	6.8337	5.2645	3.1183	2.2146
4.50	0.3379	12.8157	9.3469	7.8735	6.0835	3.6352	2.6043
5.00	0.4402	14.4294	10.5466	8.8974	6.8938	4.1534	2.9995
5.50	0.5577	15.9956	11.7155	9.8975	7.6888	4.6679	3.3959
6.00	0.6910	17.5068	12.8472	10.8679	8.4634	5.1747	3.7899
6.50	0.8402	18.9582	13.9376	11.8051	9.2143	5.6708	4.1787
7.00	1.0055	20.3475	14.9845	12.7066	9.9391	6.1540	4.5602
7.50	1.1870	21.6743	15.9871	13.5714	10.6367	6.6228	4.9326

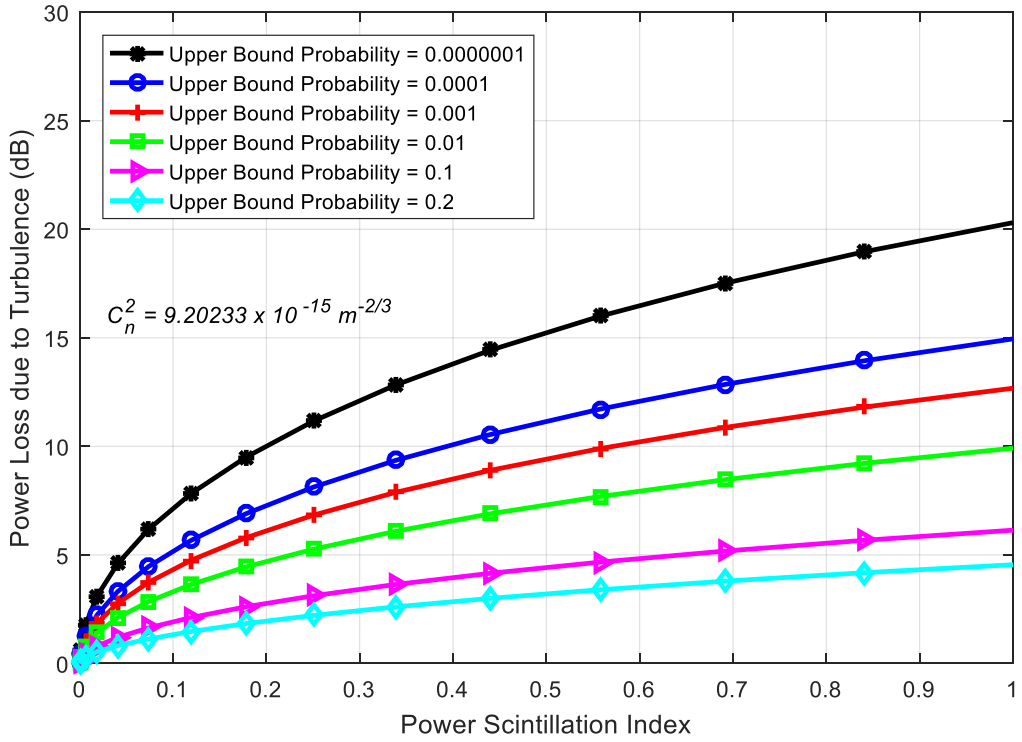

Figure 4.31 Power loss caused by turbulence plotted for various probabilities at 1550 nm.

4.8 Link Margin versus Link distance (Link Budget Analysis)

The achievable link length as a function of the power link margin for various visibility values is shown in Figures 4.32 - 4.34 and Tables 4.34 – 4.36 for typical commercially used OWC systems whose specifications are listed in Table 3.1. The graphs and tables are generated from computations using equations (12), (17), (27), (28), (29), (30) and (31). For optical signals being transmitted on the 850 nm wavelength and with an average visibility of 25 km, the link length of 3 km must have a link margin of 5 dB as shown in Figure 4.32. Reliable connection between the transmitter and receiver over a propagation distance of 3 km and on a 1550 nm wavelength with a visibility of 10 km will require a link margin of ~7.5 dB as shown in Figure 4.34. As seen in Tables 4.34 - 4.36 and for a visibility of 5 km, the link margin has a value below zero for link lengths greater than 3km. This simply indicates that the power of the received signal is lesser than the sensitivity of the receiver at such distances.

For an OWC system link distance to be available, the power link margin must be equal to or greater than the total atmospheric loss comprising of scattering and turbulence losses. The points in Figure 4.35 where the link margin intersect with the total atmospheric loss lines denote the points of optimal link length for different optical signal wavelengths. The optimal link distance of 2.85 km is achieved for the 850 nm wavelength using Kim model while for the 950 nm wavelength the optical beam has a maximum link length of 3.00 km using the Ferdinandov model. For the 1550 nm wavelength, the optimal link distance is 3.6 km.

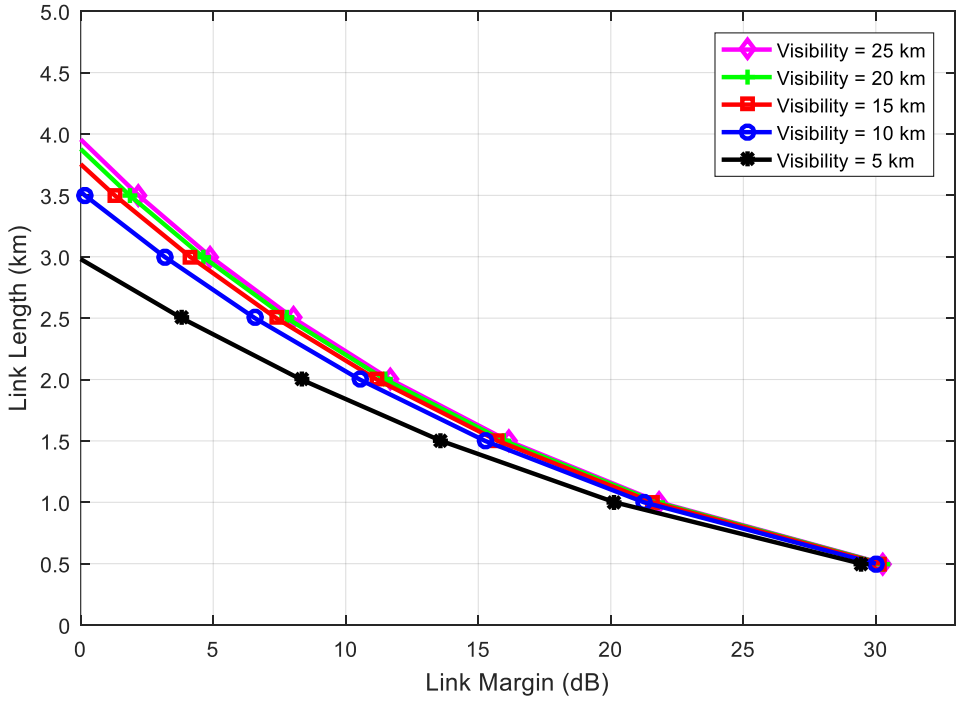

Figure 4.32 Link range against link margin for different values of visibility at 850 nm.

Table 4.34 Link Margin for various visibilities at 850 nm

Link Length (km)	850 nm				
	Link Margin (dB) (V = 5 km)	Link Margin (dB) (V = 10 km)	Link Margin (dB) (V = 15 km)	Link Margin (dB) (V = 20 km)	Link Margin (dB) (V = 25 km)
0.50	29.44664	29.99894	30.15983	30.24027	30.28854
1.00	20.14657	21.25117	21.57295	21.73383	21.83037
1.50	13.60208	15.25898	15.74165	15.98297	16.12778
2.00	8.31796	10.52716	11.17072	11.49248	11.68556
2.50	3.81081	6.57231	7.37676	7.77896	8.02031
3.00	-0.15203	3.16177	4.12711	4.60975	4.89937
3.50	-3.70810	0.15800	1.28423	1.84731	2.18520

Table 4.35 Link Margin for various visibilities at 950 nm

Link Length (km)	950 nm				
	Link Margin (dB) (V = 5 km)	Link Margin (dB) (V = 10 km)	Link Margin (dB) (V = 15 km)	Link Margin (dB) (V = 20 km)	Link Margin (dB) (V = 25 km)
0.50	29.73389	30.22792	30.36715	30.43676	30.47853
1.00	20.68404	21.67209	21.95055	22.08977	22.17331
1.50	14.35945	15.84152	16.25921	16.46804	16.59335
2.00	9.26690	11.24300	11.79992	12.07836	12.24544
2.50	4.92845	7.39857	8.09472	8.44277	8.65162
3.00	1.11750	4.08165	4.91703	5.33469	5.58531
3.50	-2.29838	1.15979	2.13440	2.62167	2.91406
4.00	-5.40636	-1.45416	-0.34032	0.21656	0.55072

Table 4.36 Link Margin for various visibilities at 1550 nm

Link Length (km)	1550 nm				
	Link Margin (dB) (V = 5 km)	Link Margin (dB) (V = 10 km)	Link Margin (dB) (V = 15 km)	Link Margin (dB) (V = 20 km)	Link Margin (dB) (V = 25 km)
0.50	30.73666	31.03740	31.11108	31.14792	31.17002
1.00	22.56710	23.16858	23.31594	23.38962	23.43382
1.50	17.03070	17.93292	18.15396	18.26448	18.33078
2.00	12.63539	13.83835	14.13307	14.28043	14.36883
2.50	8.91327	10.41697	10.78537	10.96957	11.08007
3.00	5.65281	7.45725	7.89933	8.12037	8.25297
3.50	2.73681	4.84199	5.35775	5.61563	5.77033
4.00	0.09116	2.49708	3.08652	3.38124	3.55804
4.50	-2.33536	0.37130	1.03442	1.36598	1.56488

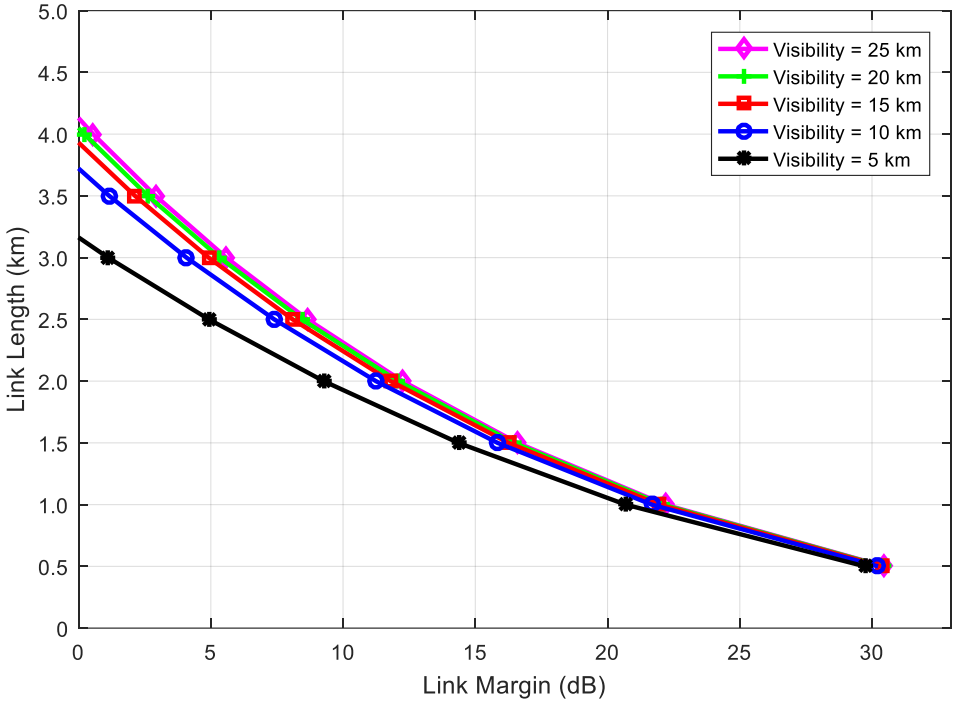

Figure 4.33 Link range against link margin for different values of visibility at 950 nm.

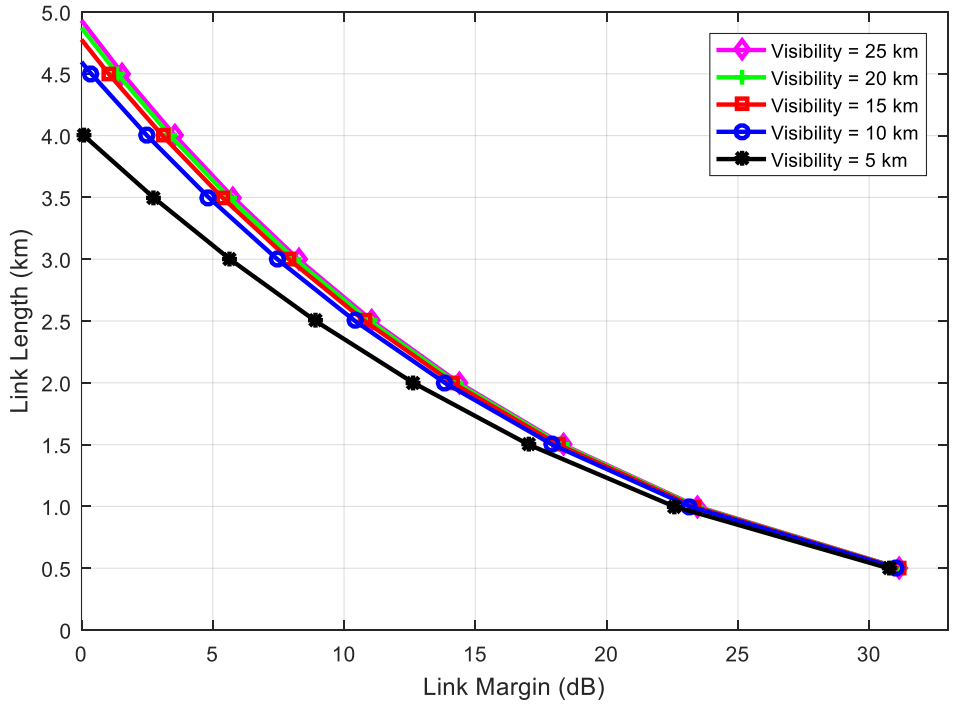

Figure 4.34 Link range against link margin for different values of visibility at 1550 nm.

Table 4.37 Power link margin and total atmospheric power losses for different models

Distance (km)	Power Link Margin (M(L)) (dB)	Ferdinandov et al Model (850nm)- Total Power Losses (dB)	Kim Model (850nm) - Total Power Losses (dB)	Ferdinandov et al Model (950nm)- Total Power Losses (dB)	Kim Model (950nm) - Total Power Losses (dB)	Kim Model (1550nm) - Total Power Losses (dB)
0.50	30.02	2.97052	2.99584	2.76626	2.79318	2.06057
1.00	24.00	5.62735	5.67800	5.23854	5.29238	3.90019
1.50	20.48	8.17812	8.25409	7.61142	7.69218	5.66511
2.00	17.98	10.66253	10.76383	9.92212	10.02980	7.38328
2.50	16.04	13.09882	13.22545	12.18772	12.32232	9.06757
3.00	14.46	15.49750	15.64945	14.41806	14.57958	10.72535
3.50	13.12	17.86536	18.04264	16.61953	16.80797	12.36143
4.00	11.96	20.20720	20.40980	18.79660	19.01196	13.97918
4.50	10.94	22.52653	22.75446	20.95259	21.19487	15.58108
5.00	10.02	24.82607	25.07932	23.09002	23.35922	17.16903
5.50	9.19	27.10795	27.38652	25.21090	25.50702	18.74455
6.00	8.44	29.37391	29.67781	27.31687	27.63991	20.30886
6.50	7.74	31.62540	31.95462	29.40927	29.75923	21.86297
7.00	7.10	33.86361	34.21816	31.48923	31.86611	23.40772
7.50	6.50	36.08957	36.46944	33.55771	33.96151	24.94385
8.00	5.94	38.30416	38.70936	35.61553	36.04625	26.47197
8.50	5.41	40.50816	40.93868	37.66343	38.12107	27.99263
9.00	4.92	42.70223	43.15808	39.70202	40.18658	29.50630
9.50	4.45	44.88698	45.36815	41.73188	42.24336	31.01340
10.00	4.00	47.06293	47.56943	43.75349	44.29189	32.51431
10.50	3.58	49.23056	49.76239	45.76730	46.33262	34.00935
11.00	3.17	51.39030	51.94745	47.77372	48.36596	35.49884
11.50	2.79	53.54254	54.12502	49.77311	50.39227	36.98304
12.00	2.42	55.68763	56.29543	51.76580	52.41188	38.46221
12.50	2.06	57.82589	58.45902	53.75209	54.42509	39.93656
13.00	1.72	59.95763	60.61608	55.73225	56.43217	41.40632
13.50	1.39	62.08310	62.76687	57.70656	58.43340	42.87167
14.00	1.08	64.20256	64.91166	59.67523	60.42899	44.33278
14.50	0.77	66.31624	67.05067	61.63848	62.41916	45.78983
15.00	0.48	68.42436	69.18411	63.59653	64.40413	47.24296

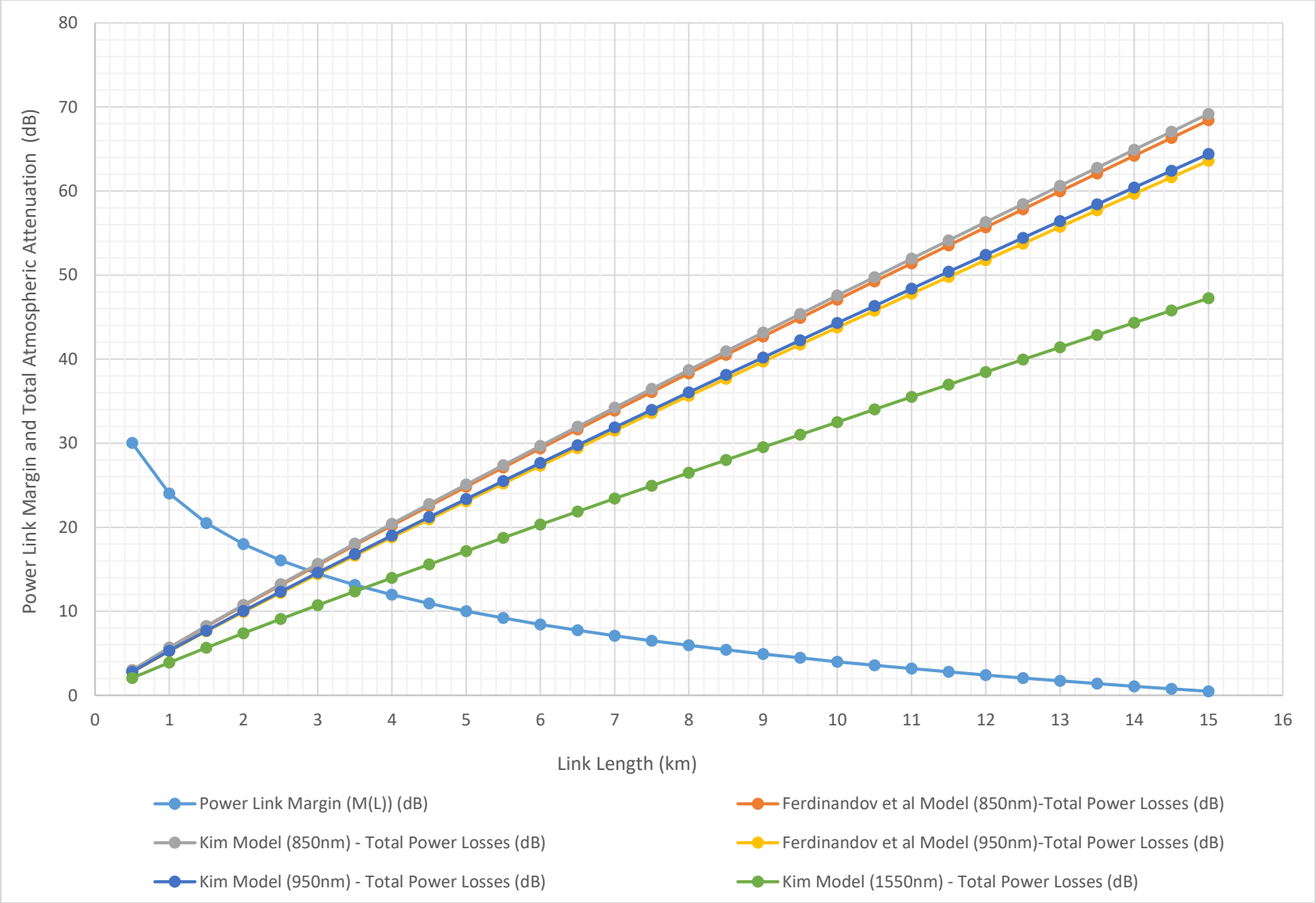

Figure 4.35 Power link margin and total atmospheric attenuation versus link length.

4.9 Minimum Required Visibility

For the correct operation of an OWC system, the minimum required visibility $V_{\min}(L)$ must be calculated. The minimum required visibility is important for estimating the OWC system's availability. A pertinent condition for the OWC system availability is that for all optimal OWCS link path lengths, the average visibility value must be greater than the corresponding required minimum visibility. Figures 4.36 - 4.39 are generated from relations stated from equations (33) – (39). For an average visibility of 25 km and a link distance of 4 km, the minimum required visibility as shown in Figure 4.36 and Table 4.38 for 850 nm, 950 nm and 1550 nm wavelengths are 3.23 km, 2.79 km and 1.48 km respectively. For visibilities lesser than 1 km, the relations in equation (34), (35) and (39) for the Naboulsi fog models, and the Ijaz fog and smoke models estimate the minimum required visibilities better as compared to the other models in Figures 4.37 – 4.39.

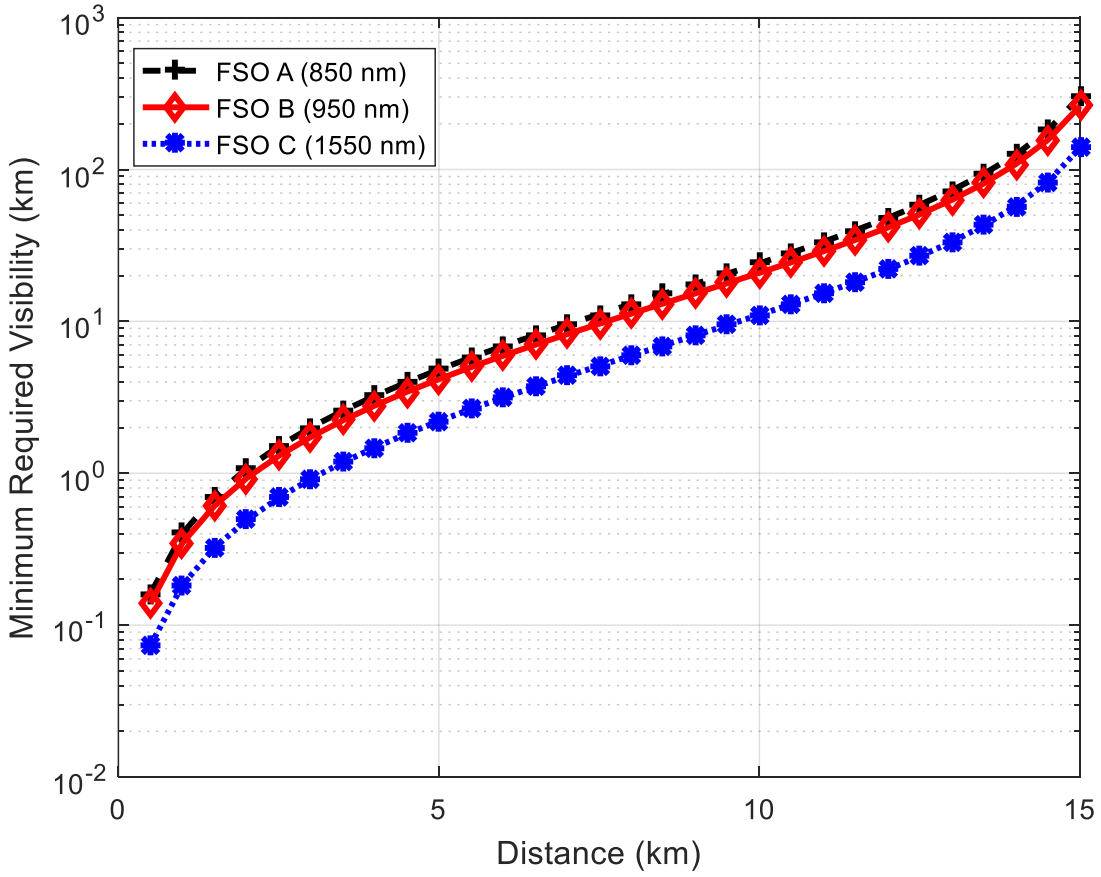

Figure 4.36 Minimum required visibility for correct operation of OWC systems in dependence on link length of 0 – 15 km

Table 4.38 Minimum required visibilities at different wavelengths

Distance (km)	Min. Req. Visibility (V_{min}) 850 nm	Min. Req. Visibility (V_{min}) 950 nm	Min. Req. Visibility (V_{min}) 1550 nm
0.50	0.16068	0.13905	0.07358
1.00	0.40198	0.34786	0.18408
1.50	0.70666	0.61153	0.32361
2.00	1.07317	0.92869	0.49145
2.50	1.50354	1.30113	0.68854
3.00	2.00188	1.73238	0.91675
3.50	2.57390	2.22739	1.17871
4.00	3.22690	2.79247	1.47774
4.50	3.96987	3.43542	1.81798
5.00	4.81381	4.16575	2.20446
5.50	5.77205	4.99498	2.64328
6.00	6.86084	5.93719	3.14189
6.50	8.10005	7.00958	3.70938
7.00	9.51420	8.23334	4.35698
7.50	11.13377	9.63488	5.09866
8.00	12.99714	11.24739	5.95198
8.50	15.15319	13.11318	6.93933
9.00	17.66519	15.28700	8.08969
9.50	20.61640	17.84090	9.44118
10.00	24.11863	20.87164	11.04501
10.50	28.32555	24.51220	12.97155
11.00	33.45431	28.95050	15.32024
11.50	39.82196	34.46089	18.23627
12.00	47.91037	41.46039	21.94032
12.50	58.48926	50.61509	26.78487
13.00	72.86879	63.05876	33.36990
13.50	93.47470	80.89058	42.80628
14.00	125.35678	108.48052	57.40652
14.50	181.05205	156.67776	82.91189
15.00	302.63361	261.89130	138.58957

Table 4.39 Minimum required visibilities estimated from different models at 850 nm

Distance (km)	Minimum Required Visibility (V_{min}) 850 nm						
	Kruse	Naboulsi - Advection fog	Naboulsi - Convection fog	Kim	Ijaz Model - Fog	Ferdinandov et al - Model	Ijaz Model - Smoke
0.0206	0.003445	0.005767	0.005947	0.003445	0.006322	0.002693	0.007612
0.0420	0.007867	0.013169	0.013580	0.007867	0.014438	0.006237	0.017383
0.0600	0.011958	0.020015	0.020641	0.011958	0.021945	0.009554	0.026422
0.2411	0.064017	0.107155	0.110501	0.064017	0.117482	0.053010	0.141451
0.2424	0.064445	0.107871	0.111240	0.064445	0.118268	0.053373	0.142396
0.3618	0.106381	0.178066	0.183627	0.106381	0.195228	0.089218	0.235058
0.5543	0.183719	0.307517	0.317121	0.183719	0.337155	0.156395	0.405940
0.6438	0.223353	0.373859	0.385535	0.223353	0.409891	0.191221	0.493516
0.7401	0.268444	0.449333	0.463367	0.268444	0.492640	0.231103	0.593147
0.8408	0.318217	0.532646	0.549282	0.318217	0.583983	0.275409	0.703125
0.8662	0.331187	0.554356	0.571670	0.331187	0.607785	0.286998	0.731783
0.9272	0.363009	0.607621	0.626598	0.363009	0.666184	0.315504	0.802096
0.9946	0.399266	0.668310	0.689183	0.399266	0.732722	0.348102	0.882210

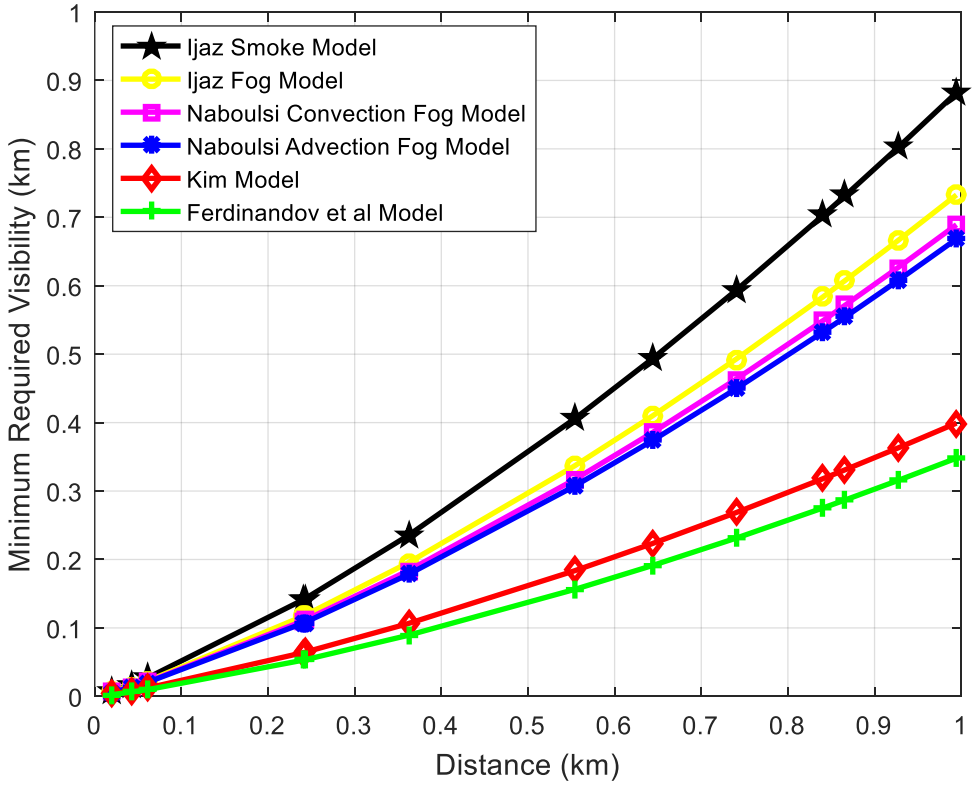

Figure 4.37 Minimum required visibility at 850 nm for correct operation of OWC systems in dependence on link length of 0 – 1 km.

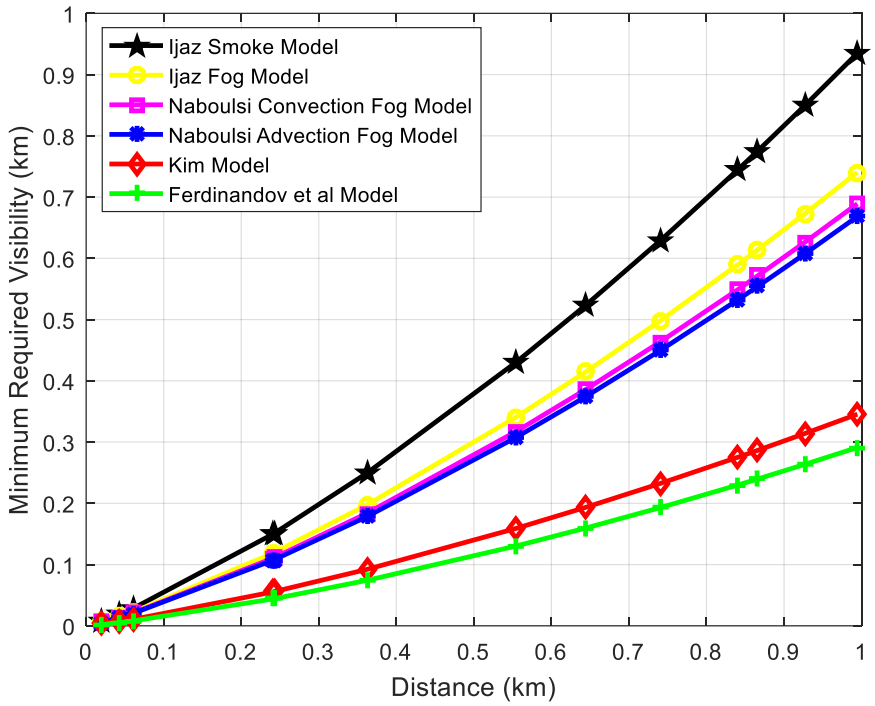

Figure 4.38 Minimum required visibility at 950 nm for correct operation of OWC systems in dependence on link length of 0 – 1 km.

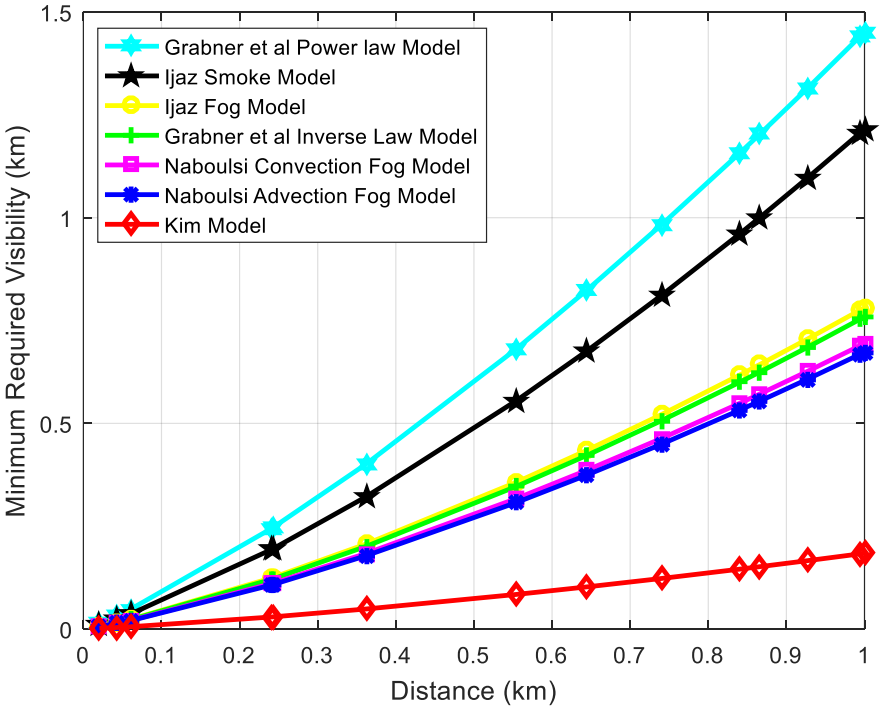

Figure 4.39 Minimum required visibility at 1550 nm for correct operation of OWC systems in dependence on link length of 0 – 1 km.

4.10 Link Availability

The optical link availability depends significantly on the atmospheric attenuation conditions. For an OWCS link to be available, the link margin must be greater than or equal to the total atmospheric attenuation for a particular link length as stated in equation (32). The link availability graphs in Figures 4.40 – 4.44 are derived from equation (40). Various models used to calculate the link availability for visibility values less than 1 km are presented in Figures 4.40 – 4.42. As previously stated, the Naboulsi and Ijaz models predict the link availability during foggy weather and smoky conditions better than the other models for the 850 nm, 950 nm and 1550 nm wavelengths. As shown in Figures 4.43 – 4.44, the optical signals being transmitted on the 1550 nm wavelength have better link availability over a specific propagation distance as compared to the other two wavelengths considered in this work. The link availability results for different link lengths are presented in Tables 4.41 – 4.44. The OWCS link availability reduces with increase in propagation path distance.

Table 4.40 Estimated link Availabilities using different models at 850 nm

Link Length (km)	**850 nm Link Availability (%)**						
	Kruse	**Naboulsi - Advection fog**	**Naboulsi - Convection fog**	**Kim**	**Ijaz Model - Fog**	**Ferdinandov et al - Model**	**Ijaz Model - Smoke**
0.0206	100.0000	100.0000	100.0000	100.0000	100.0000	100.0000	100.0000
0.0420	100.0000	100.0000	100.0000	100.0000	100.0000	100.0000	100.0000
0.0600	100.0000	100.0000	99.5370	100.0000	99.5370	100.0000	99.5370
0.2411	98.6111	98.6111	98.6111	98.6111	98.6111	99.0741	98.6111
0.2424	98.6111	98.6111	98.6111	98.6111	98.6111	99.0741	98.6111
0.3618	98.6111	98.6111	98.6111	98.6111	98.6111	98.6111	98.6111
0.5543	98.6111	97.6852	97.6852	98.6111	97.6852	98.6111	97.2222
0.6438	98.6111	97.2222	97.2222	98.6111	97.2222	98.6111	97.2222
0.7401	97.6852	97.2222	97.2222	97.6852	97.2222	98.6111	96.7593
0.8408	97.6852	97.2222	97.2222	97.6852	96.7593	97.6852	96.2963
0.8662	97.6852	96.7593	96.7593	97.6852	96.7593	97.6852	96.2963
0.9272	97.2222	96.7593	96.7593	97.2222	96.2963	97.6852	95.8333
0.9946	97.2222	96.2963	96.2963	97.2222	96.2963	97.6852	94.9074

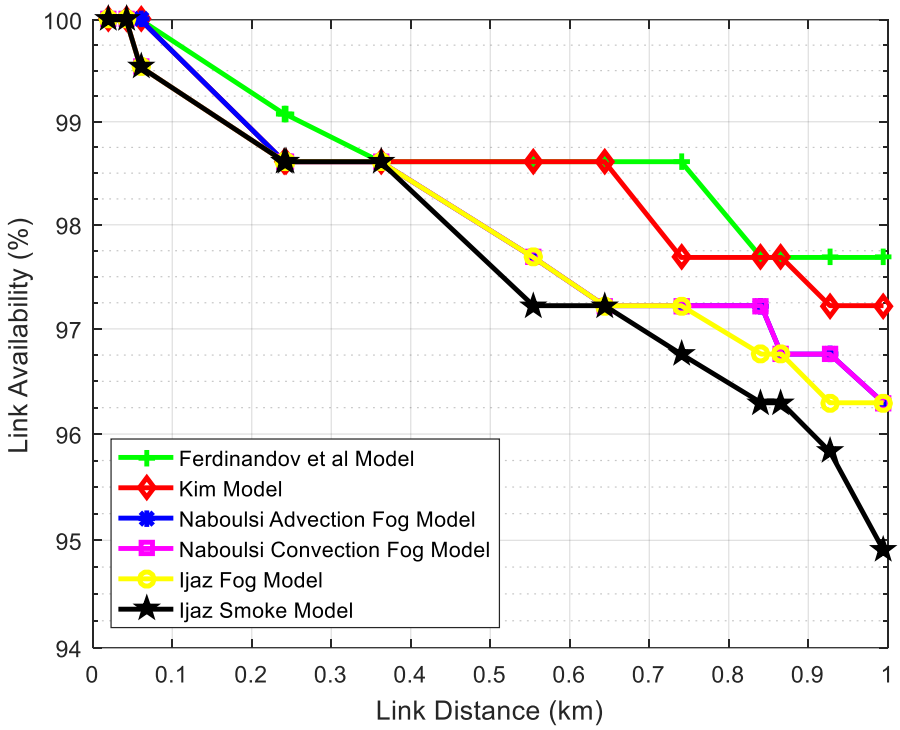

Figure 4.40 Availability of OWC links in dependence on the link distance at 850 nm for visibilities ranging from 0 – 1 km

Table 4.41 Estimated link Availabilities using different models at 950 nm

Link Length (km)	950 nm Link Availability (%)						
	Kruse	Naboulsi - Advection fog	Naboulsi - Convection fog	Kim	Ijaz Model - Fog	Ferdinandov et al - Model	Ijaz Model - Smoke
0.0206	100.0000	100.0000	100.0000	100.0000	100.0000	100.0000	100.0000
0.0420	100.0000	100.0000	100.0000	100.0000	100.0000	100.0000	100.0000
0.0600	100.0000	100.0000	99.5370	100.0000	99.5370	100.0000	99.5370
0.2411	99.0741	98.6111	98.6111	99.0741	98.6111	99.0741	98.6111
0.2424	99.0741	98.6111	98.6111	99.0741	98.6111	99.0741	98.6111
0.3618	98.6111	98.6111	98.6111	98.6111	98.6111	98.6111	97.6852
0.5543	98.6111	97.6852	97.6852	98.6111	97.6852	98.6111	97.2222
0.6438	98.6111	97.2222	97.2222	98.6111	97.2222	98.6111	97.2222
0.7401	98.6111	97.2222	97.2222	98.6111	97.2222	98.6111	96.7593
0.8408	97.6852	97.2222	97.2222	97.6852	96.7593	98.6111	95.8333
0.8662	97.6852	96.7593	96.7593	97.6852	96.7593	98.6111	95.8333
0.9272	97.6852	96.7593	96.7593	97.6852	96.2963	97.6852	95.3704
0.9946	97.6852	96.2963	96.2963	97.6852	95.8333	97.6852	94.4444

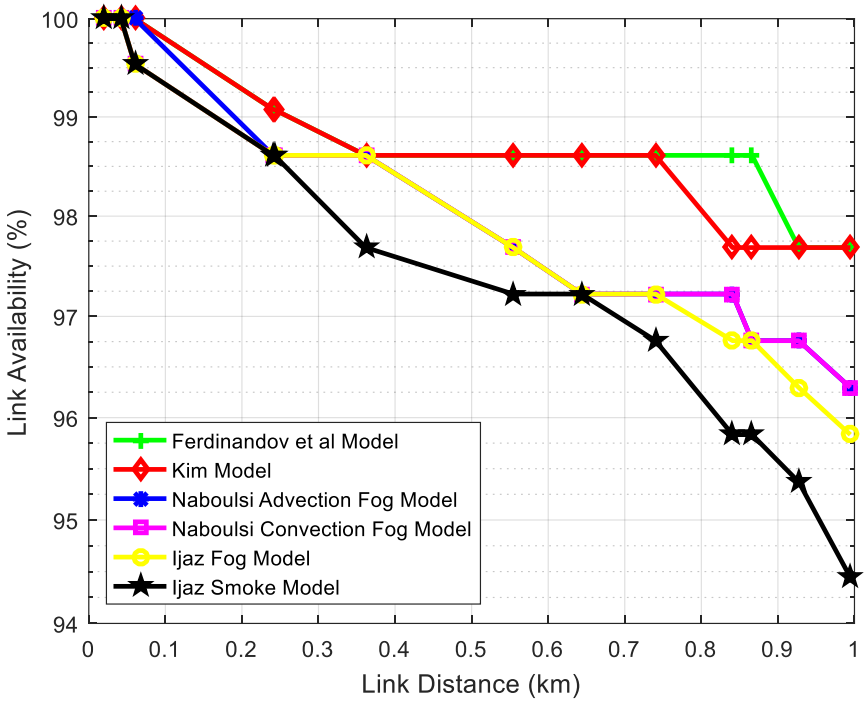

Figure 4.41 Availability of OWC links in dependence on the link distance at 950 nm for visibilities ranging from 0 – 1 km

Table 4.42 Estimated link Availabilities using different models at 1550 nm

Link Length (km)	1550 nm Link Availability (%)							
	Grabner et al Model - Power law	Kruse	Naboulsi - Advection fog	Naboulsi - Convection fog	Kim	Grabner et al Model - Inverse law	Ijaz Model - Fog	Ijaz Model - Smoke
0.0206	100.000	100.000	100.000	100.000	100.000	100.000	100.000	100.000
0.0420	99.537	100.000	100.000	100.000	100.000	100.000	100.000	99.537
0.0600	99.074	100.000	100.000	99.537	100.000	99.537	99.537	99.537
0.2411	97.685	99.537	98.611	98.611	99.537	98.611	98.611	98.611
0.2424	97.685	99.537	98.611	98.611	99.537	98.611	98.611	98.611
0.3618	97.222	99.074	98.611	98.611	99.074	98.611	98.611	97.685
0.5543	96.296	98.611	97.685	97.685	98.611	97.685	97.685	96.759
0.6438	95.833	98.611	97.222	97.222	98.611	97.222	97.222	96.296
0.7401	94.444	98.611	97.222	97.222	98.611	97.222	97.222	95.833
0.8408	93.519	98.611	97.222	97.222	98.611	96.759	96.759	94.444
0.8662	93.519	98.611	96.759	96.759	98.611	96.759	96.759	93.519
0.9272	93.519	98.611	96.759	96.759	98.611	96.296	96.296	93.519
0.9946	93.519	98.611	96.296	96.296	98.611	95.833	95.833	93.519
1.0000	93.519	98.611	96.296	96.296	98.611	95.833	95.833	93.519

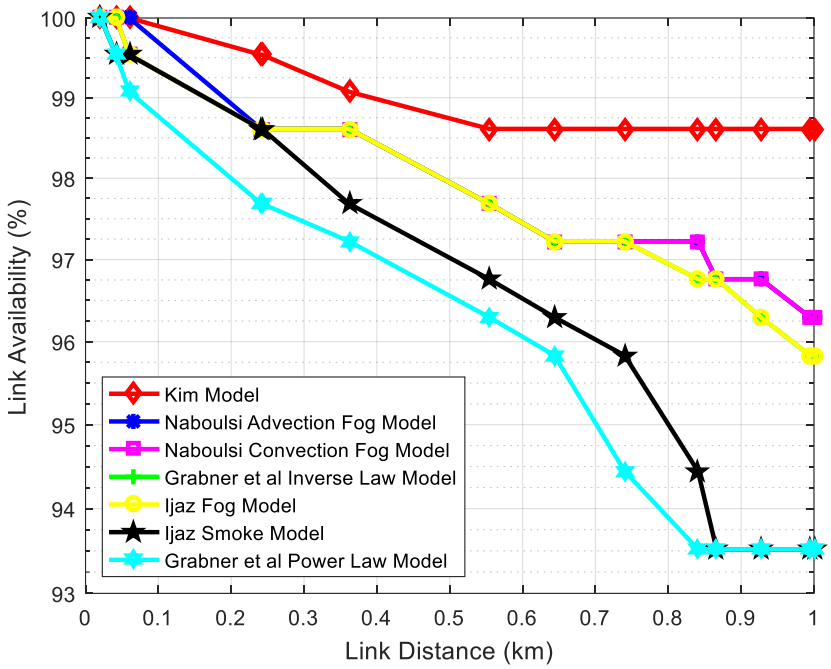

Figure 4.42 Availability of OWC links in dependence on the link distance at 1550nm for visibilities ranging from 0 – 1 km

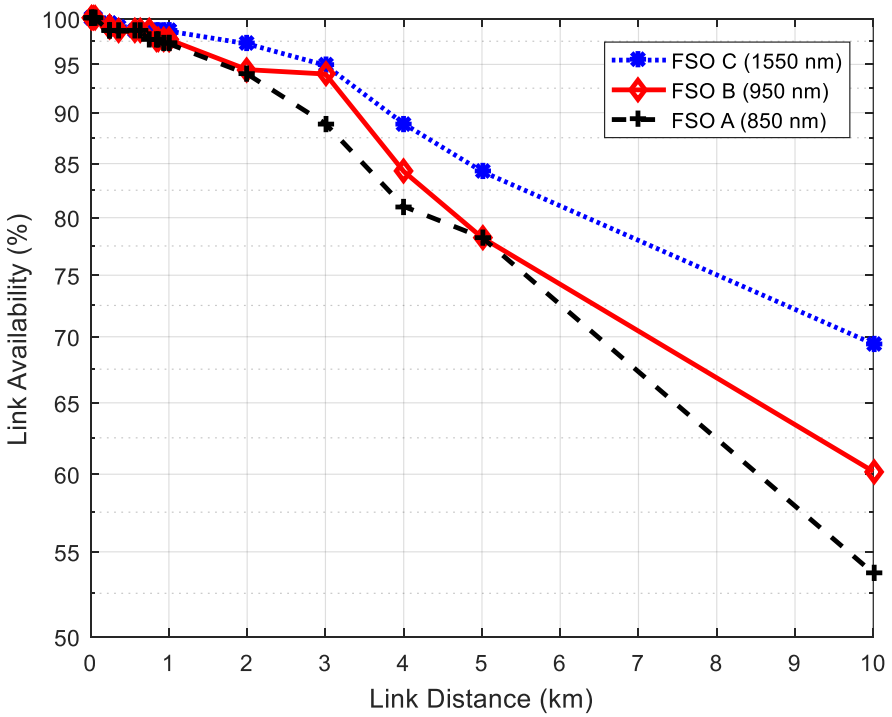

Figure 4.43 Availability of OWC links in dependence on the link distance at different wavelengths.

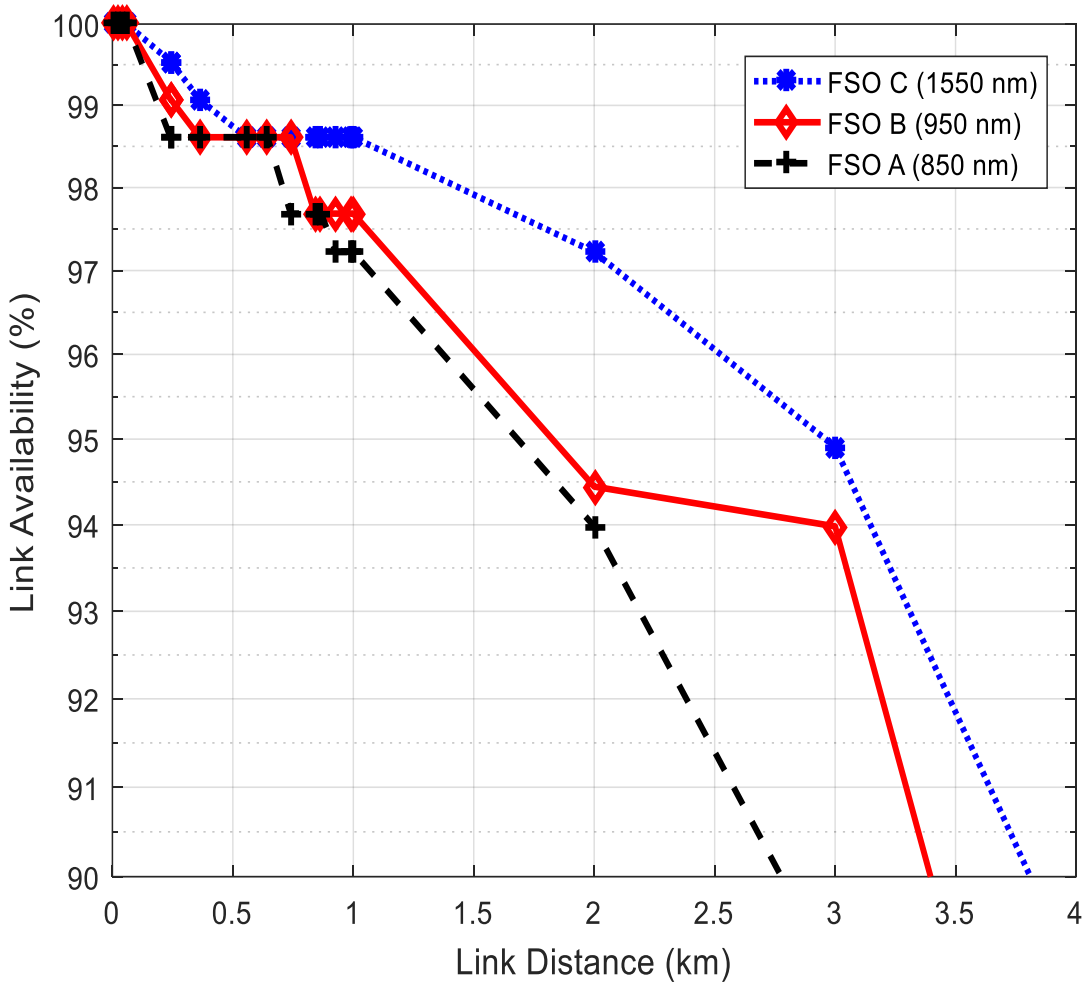

Figure 4.44 Availability of OWC links in dependence on the link distance at different wavelengths.

Table 4.43 FSO System Availability Estimation in Cape Town

Link Length (km)	850 nm Link Availability (%)	950 nm Link Availability (%)	1550 nm Link Availability (%)
0.0000	100.0000	100.0000	100.0000
0.0206	100.0000	100.0000	100.0000
0.0420	100.0000	100.0000	100.0000
0.0600	100.0000	100.0000	100.0000
0.2411	98.6111	99.0741	99.5370
0.2424	98.6111	99.0741	99.5370
0.3618	98.6111	98.6111	99.0741
0.5543	98.6111	98.6111	98.6111
0.6438	98.6111	98.6111	98.6111
0.7401	97.6852	98.6111	98.6111
0.8408	97.6852	97.6852	98.6111
0.8662	97.6852	97.6852	98.6111
0.9272	97.2222	97.6852	98.6111
0.9946	97.2222	97.6852	98.6111
1	97.2222	97.6852	98.6111
2	93.9815	94.4444	97.2222
3	88.8889	93.9815	94.9074
4	81.0185	84.2593	88.8889
5	78.2407	78.2407	84.2593
10	53.7037	60.1852	69.4444

4.11 Summary

In this chapter, the determination of visibility using different single and multiple regression models and the estimation of the scattering attenuation coefficient for Cape Town were discussed. The probability of encountering various scattering atmospheric attenuation conditions, turbulence losses and power scintillation index values were calculated and graphically depicted. Lastly, the analysis of the link budget, minimum required visibility and link availability were presented. The OWC system link availability reduces with increase in propagation distance.

Chapter 5

APPLICATIONS TO CROSS M-QAM OWC SYSTEMS

5.1 Introduction

This chapter presents discussions on the bit error rate (BER) equation for analyzing the performance of cross M-ary quadrature amplitude modulated (QAM) OWC systems over the lognormal channel. A description of the proposed cross M-QAM OWC system model will be presented. Cross M-QAM signal constellation diagrams at the transmitter and receiver will be presented and BER performance results for cross M-QAM OWC systems using various parameters will be examined as well at the end of the chapter.

5.2 OWC Channel Model

From the processed six year (2010 - 2015) data sets, the computed average refractive index structure parameter (C_n^2) ranges from 2.70189x10^{-15} to 2.04320x10^{-14} m$^{-2/3}$. Slotting the refractive index values into equations (22) – (26) for different wavelength values considered in this work, the power scintillation index ($\sigma_{P-S.I.}$) values range from 0 – 1.2 for link lengths of up to 10 km. The scintillation index ($\sigma_{S.I.}$), also known as the Rytov variance or log irradiance variance is the standard for characterizing turbulence models [37-39]. For $\sigma_{S.I.} < 1.2$, the atmospheric channel fading strength is categorized as weak and the log-normal distribution is utilized to model this channel. The gamma-gamma and negative exponential models are required to characterize the atmospheric channel turbulence strength for $\sigma_{S.I.}$ values greater than 1.2 [40].

The log intensity I of the optical radiation from the laser beam propagating through the turbulent channel is viewed to have a normally distributed mean value of $\frac{-\sigma_l^2}{2}$ as assumed by the log-normal model. The Probability density function of the received light intensity (irradiance) $I = I_o \exp(l)$ is given by [40, 41].

$$P_I(I) = \frac{1}{I\,\sigma_{S.I.}\sqrt{2\pi}} \exp\left\{ \frac{-\left(\ln\frac{I}{I_o} + \frac{\sigma_{S.I.}}{2}\right)^2}{2\,\sigma_{S.I.}} \right\} \quad I \geq 0 \tag{49}$$

where I and I_0 represents the irradiance at the receiver and turbulence-free irradiance respectively.

5.3 Cross M-QAM OWC System Model

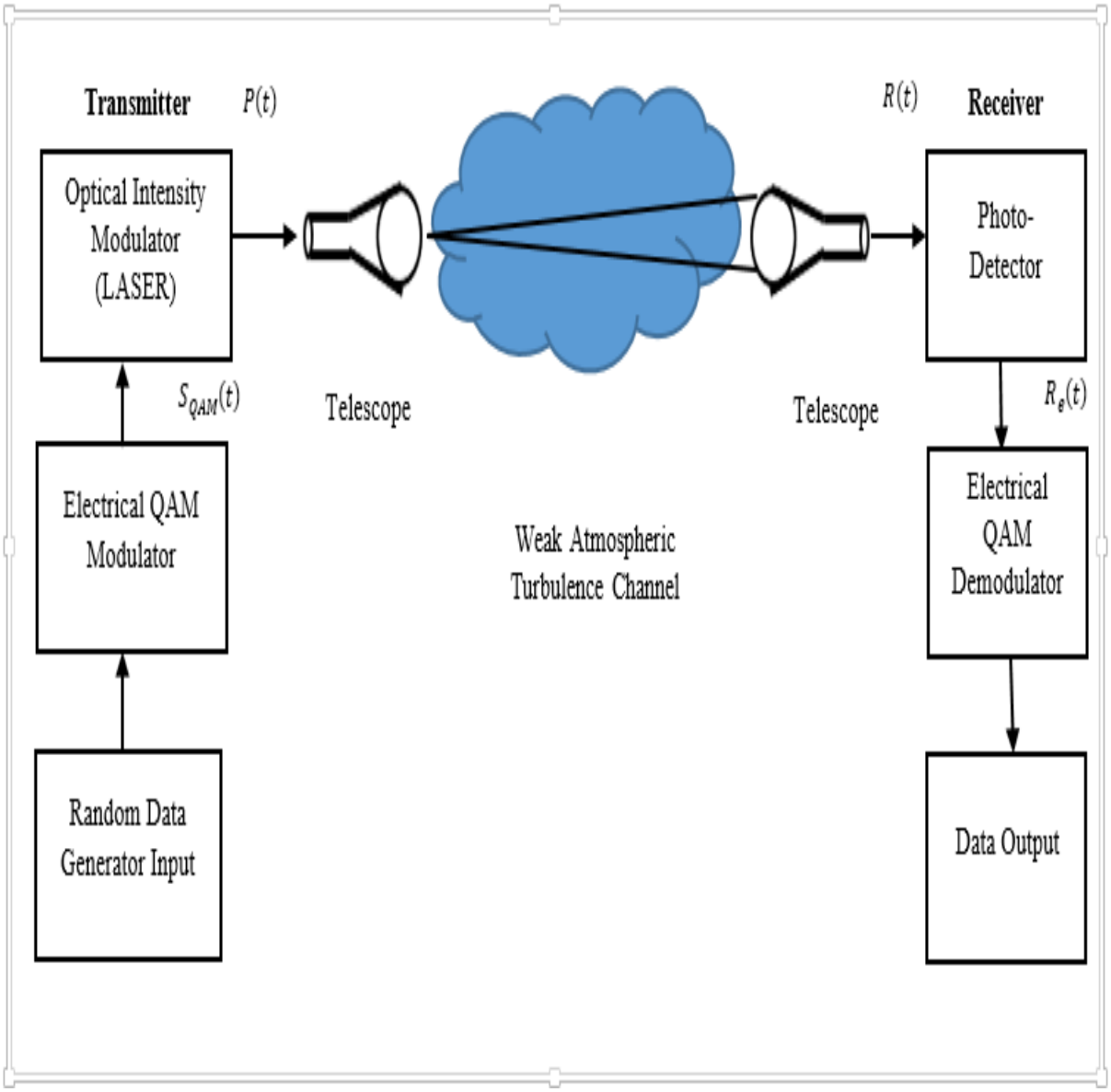

Figure 5.1 Block diagram of a cross M-QAM optical wireless communication system operating over a weak atmospheric turbulence channel.

A typical optical wireless communication system using cross QAM is shown in Figure 5.1. At the transmission section, a random generator produces the information bits. The electrical QAM modulator modulates each block of $\log_2 M$ data bits by up-converting the QAM signal to an intermediate carrier frequency. The information bit streams are modulated using $M = M_I \times M_Q$ QAM where M_I and M_Q

represent the in-phase and quadrature signals respectively. The signal output of the electrical QAM modulator can be given as [39]:

$$S_{QAM}(t) = A_I(t)\cos(2\pi f_c t) - A_Q(t)\sin(2\pi f_c t) \tag{50}$$

where $A_I(t) = \sum_{\infty}^{\infty} \alpha_i g(t - iT_s)$ and $A_Q(t) = \sum_{\infty}^{\infty} \beta_i g(t - iT_s)$ are the in-phase and quadrature signal components respectively; α_i and β_i are the in-phase and the quadrature information signal components of the i th amplitude symbol respectively. $g(t)$ represents the signal shaping pulse while the symbol time interval is denoted by T_s. The optical intensity modulator uses the QAM signal output of the electrical QAM modulator to modulate the laser intensity of the light source (LED) of the transmitter. The telescope in the transmitting section influences the orientation and magnitude of the modulated laser beam. The radiated optical intensity can be expressed as:

$$P(t) = P_{tx}\left\{1 + I_m\left[A_I(t)\cos(2\pi f_c t) - A_Q(t)\sin(2\pi f_c t)\right]\right\} \tag{51}$$

where I_m represents the modulation index (to achieve high efficiency I_m is assumed to be equal to 1). P_{tx} represents the average transmitted optical power. As the transmitted optical signal traverses the atmospheric turbulence channel, there is a relatively significant reduction in the signal link length amongst other distortion effects such as scattering and absorption. The detected optical intensity at the receiver can be written as:

$$R(t) = a_L X_s(t) P(t) \tag{52}$$

where a_L denotes the signal link loss factor and $X_s(t)$ is the stationary random process signal scintillation resulting from atmospheric turbulence. The link loss factor a_L is a constant that takes various complexities such as the molecular absorption and scattering of the transmitted optical signal, the divergence angle of the transmitter and the aperture area of the receiver into consideration. It may be expressed as:

$$a_L = \frac{A_r}{\pi\left(\frac{\theta L}{2}\right)^2} e^{(-\alpha_a L)} \tag{53}$$

where A_r, θ, L and α_a represents the area of the receiver, divergence angle (in radians), the signal link length between the transmitter and receiver and the total extinction coefficient, respectively [39]. At the receiver, the optical field of the narrowed laser beam is focused onto a photodetector by a telescope. The received signal intensity at the input of the photodetector can be expressed as [39]:

$$R(t) = a_L X_s(t) P_{tx} \{1 + I_m[A_I(t)\cos(2\pi f_c t) - A_Q(t)\sin(2\pi f_c t)]\} \tag{54}$$

The received optical signal is then converted to an electrical signal by the photodetector. The bandpass filter removes the DC term $a_L X_s(t) P_{tx}$. The electrical signal output of the photodetector can be written as:

$$R_e(t) = G\Re a_L X_s(t) P_{tx} I_m S_{QAM}(t) + n(t) \tag{55}$$

This can be further expanded as:

$$R_e(t) = G\Re a_L X_s(t) P_{tx} \{I_m[A_I(t)\cos(2\pi f_c t) - A_Q(t)\sin(2\pi f_c t)]\} + n(t) \tag{56}$$

where $\Re$ represents the photodetector's responsivity, G is the average gain and $n(t)$ is the total noise at the receiver. $n(t)$ is modelled as the zero-mean additive white Gaussian noise (AWGN) with spectral density N_o and variance σ_n^2. Demodulation of the electrical signals by the electrical QAM demodulator takes place thereafter. The bits produced by this process are given as data output.

5.4 Bit Error Rate Cross M-QAM Equation

The atmospheric turbulence channel can be designed as a slow fading channel. The general expression for the system BER can thus be expressed as:

$$BER = \int_0^{\infty} BER_{inst}\, P_I(I) dI \tag{57}$$

where BER_{inst} represents the bit error rate of the system devoid of turbulence characteristics. It may be called the instantaneous BER of the system. $P_I(I)$ denotes the probability distribution function of I which can be derived by analysis.

Therefore, the BER expression for the general cross M-ary QAM as given in equation (30) in [42] is:

$$P_{M(BER)} = \frac{1}{2m+1}\left(\sum_{k=1}^{m+1} P_M(i_k) + \sum_{k=1}^{m} P_M(q_k) \right) \tag{58}$$

where M ≥ 32 i.e. M= 2^N (N ≥ 5) and N is an odd integer.

The BER of the system is then computed with $P_I(I)$ for the Log-normal turbulence channel in the equation below where:

$$BER = \int_0^{\infty} P_{M(BER)} P_I(I) dI \tag{59}$$

and substituting for P_M from equation (58) in equation (59), we have that the BER of the system is:

$$BER = \frac{1}{2m+1}\left[\left(\sum_{k=1}^{m+1} \int_0^{\infty} P_M(i_k) P_I(I) dI \right) + \left(\sum_{k=1}^{m} \int_0^{\infty} P_M(q_k) P_I(I) dI \right) \right] \tag{60}$$

5.5 Cross M-QAM Signal Constellations

The transmitted and received symbols constellation diagrams for the cross 32-QAM scheme in a weak atmospheric turbulence channel are presented in Figures 5.2 – 5.3. Figure 5.3 depicts the scattering of the symbols about their respective constellation positions at the receiver after being affected by the weak turbulence in the log-normal channel.

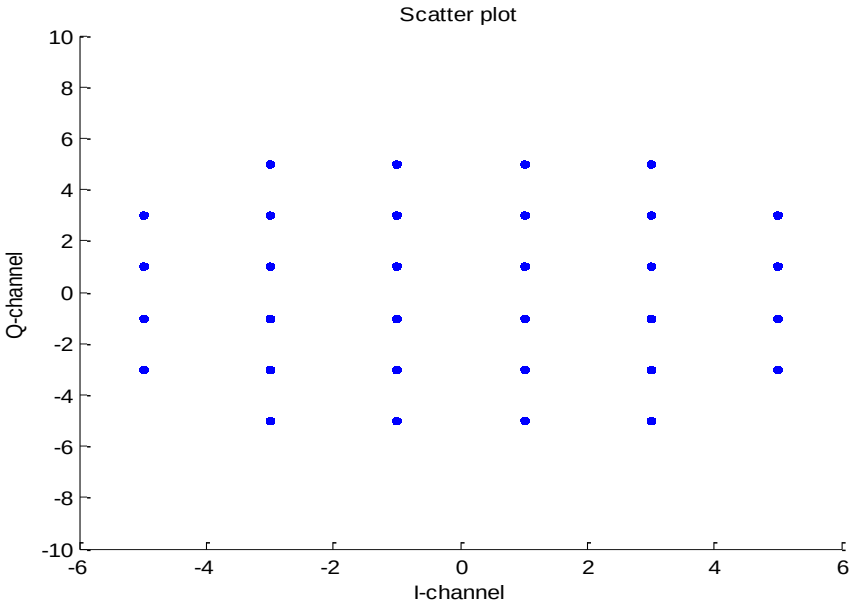

Figure 5.2 Transmitted Constellation diagram for Cross 32-QAM in a weak atmospheric turbulence channel.

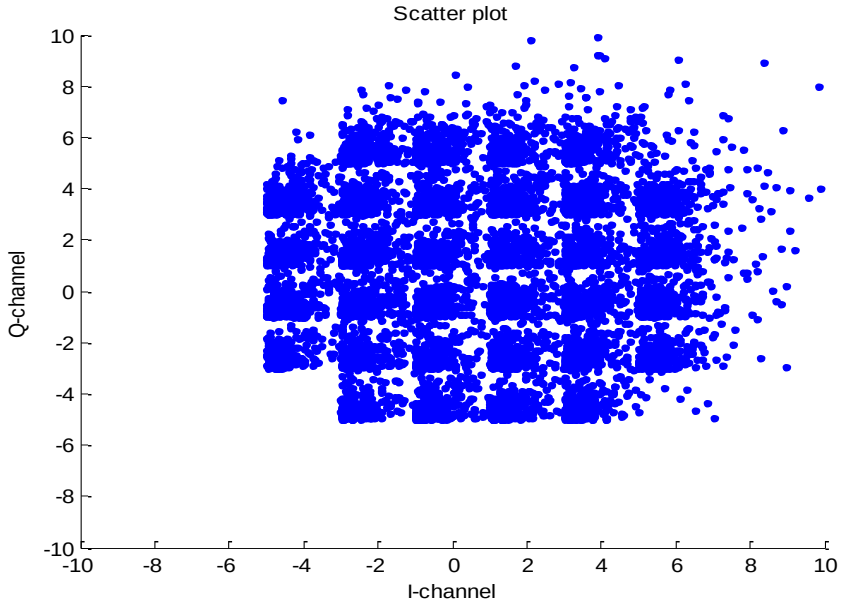

Figure 5.3 Received Constellation diagram for Cross 32-QAM in a weak atmospheric turbulence channel.

5.6 BER Performance of OWC Cross M-QAM System

The bit error rate performance for various OWC cross M-ary QAM systems are presented in Figures 5.4 – 5.7. In Figure 5.4, the cross 32-QAM OWCS is designed to transmit at 1550 nm while it is subjected to measured minimum, average and maximum refractive index values corresponding to power scintillation index values of 0.12, 0.4 and 0.9 respectively. For a link length of 2500 m and in order to attain a BER of 10^{-4}, an SNR of ~19 dB, 27 dB and 39 dB will be needed for refractive index values of 2.70189 x 10^{-15} $m^{-2/3}$, 9.20233 x 10^{-15} $m^{-2/3}$ and 2.04320 x 10^{-14} $m^{-2/3}$ respectively. This means that more power will be needed to maintain a certain BER as the turbulence in the atmosphere increases.

Figure 5.5 shows that the SNR requirements needed to attain a certain BER increases as the value of the odd bit M-ary QAM increase in a weak turbulence channel. In a weak atmospheric situation with a measured refractive index value of 9.20233 x 10^{-15} $m^{-2/3}$ and corresponding scintillation index value of 0.56, for example, ~22 dB of SNR is required to achieve a BER of 10^{-3} for cross 8-QAM while ~28 dB would be needed to attain the same level of BER for cross 32-QAM. For a transmitting wavelength of 1550 nm for a cross 32-QAM OWCS, attaining link lengths of 1000 m, 2000 m and 3000 m for a BER of 10^{-4} would require an SNR of ~17 dB, 24 dB and 32 dB respectively as shown in Figure 5.6. It can be deduced from Figure 5.7 that in order to attain a BER of 10^{-3}, transmitting wavelengths of 850 nm, 950 nm and 1550 nm require an SNR of ~37 dB, 34 dB and 27 dB respectively. It can be concluded that it is better to transmit at 1550 nm since lesser power would be needed to propagate optical signals to the receiver.

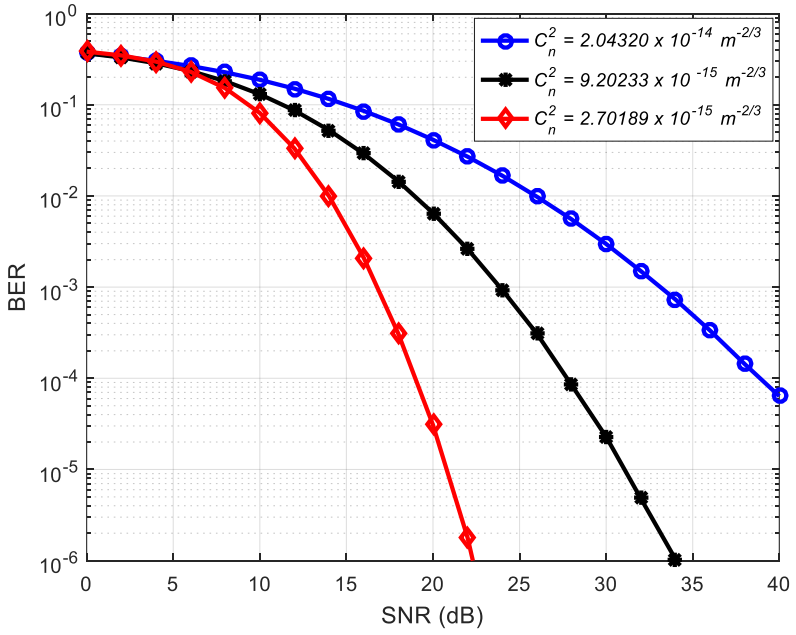

Figure 5.4 BER against SNR for cross 32-QAM under weak atmospheric turbulence for various measured refractive index values.

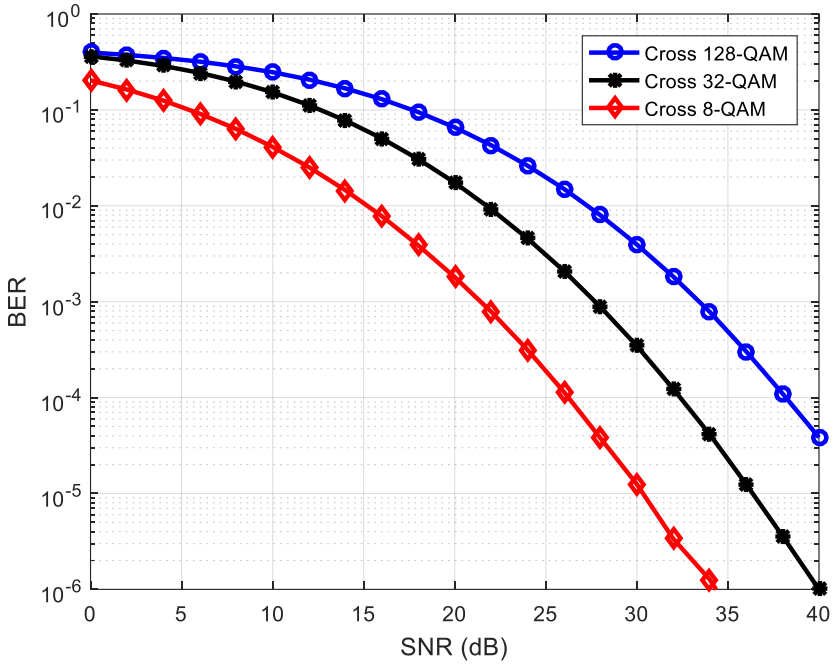

Figure 5.5 BER against SNR for cross 8-QAM, 32-QAM and 128-QAM under weak atmospheric turbulence.

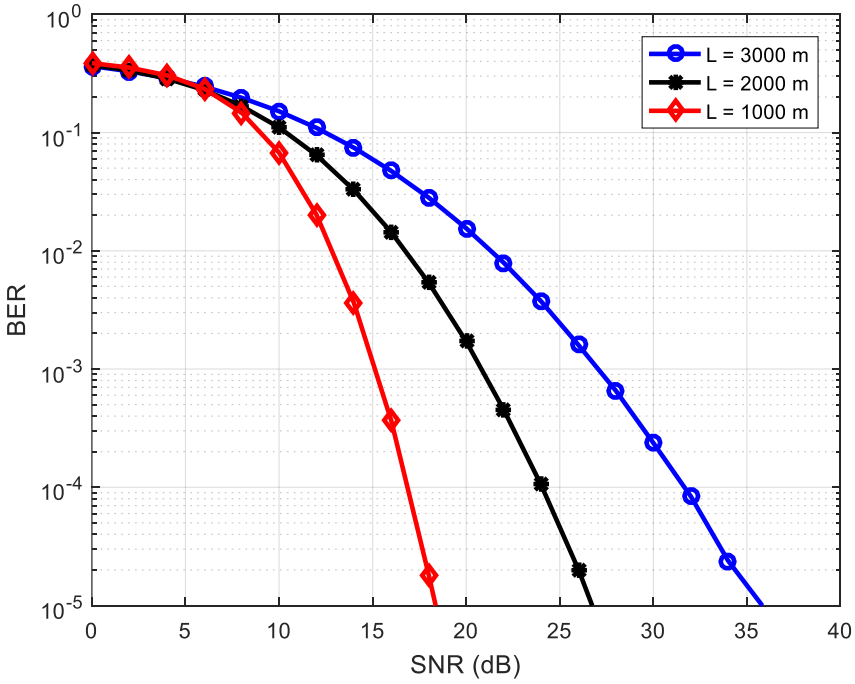

Figure 5.6 BER against SNR for cross 32-QAM for different propagation distances under weak atmospheric turbulence.

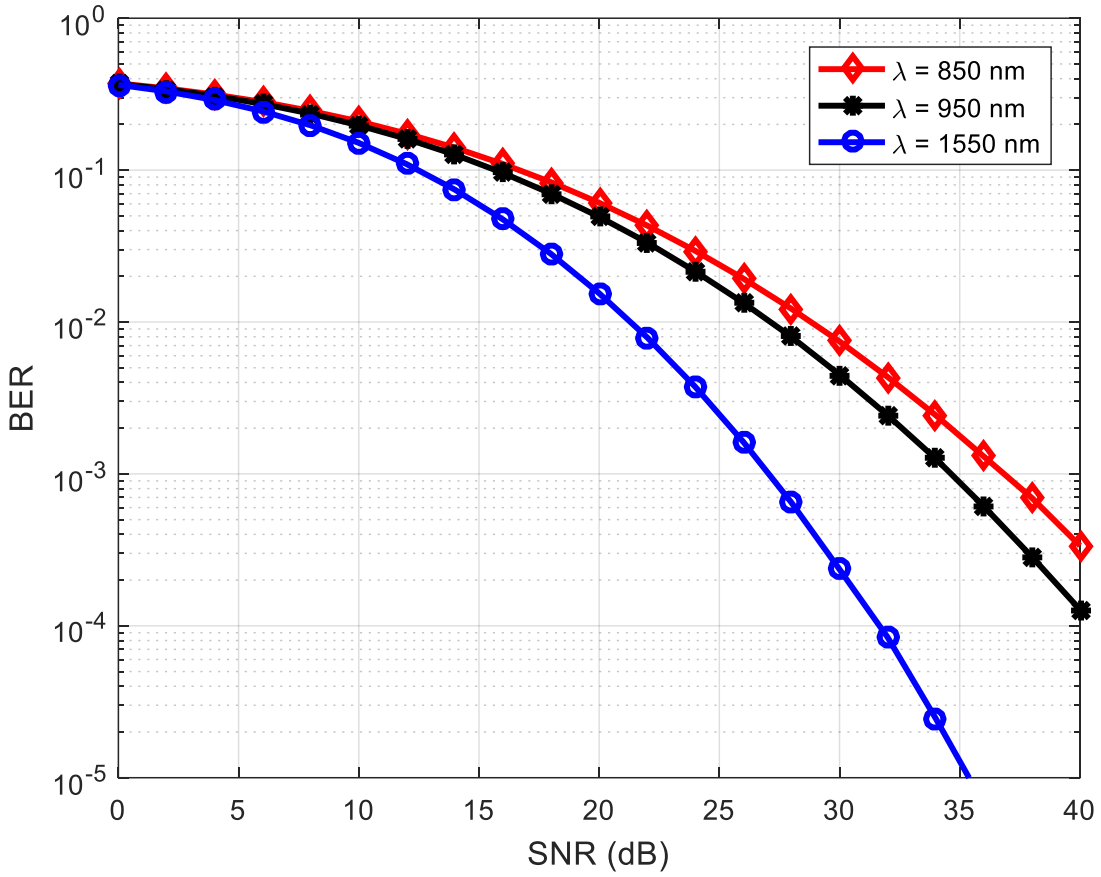

Figure 5.7 BER against SNR for cross 32-QAM for various wavelengths under weak atmosphere turbulence.

5.7 Summary

The BER cross M-QAM equation for evaluating the performance of cross M-QAM OWC systems was presented in this chapter. The proposed cross M-QAM OWC system model was described. Vivid constellation diagrams of cross M-QAM optical signals about their respective symbol positions at the transmitter and when they are detected at the receiver are also given. The BER performance of OWC cross M-QAM systems for various measured parameters were discussed. It was concluded that it is better to transmit at 1550 nm since lesser power would be needed to propagate optical signals to the receiver.

Chapter 6
CONCLUSIONS AND FUTURE WORK

6.1 Conclusions

In this dissertation, an in-depth performance analysis was carried out on OWC systems in a warm-summer Mediterranean climatic region with Cape Town as the case study. Models for predicting visibilities in such climatic regions from other weather parameters such as relative humidity, maximum temperature and fraction of sunshine hours were investigated. The atmospheric scattering attenuation coefficients were estimated using different models such as the Kim, Kruse, Ferdinandov et al, Naboulsi, Ijaz, and Grabner et al models over visibilities ranging from 0 - 50 km. These estimated scattering attenuation computations amongst others were carried out on commonly used commercial OWC systems transmitting at 850, 950 and 1550 nm wavelengths. Scintillation effects leading to power losses on OWC systems as well as the required link budget analysis were also investigated. The minimum required visibility relations and their corresponding link availability estimations from various models were derived. Finally, the analyzed results were applied to cross M-ary QAM OWC systems and their bit error rate performance analyses were presented.

Various single and multiple regression models were examined and used to predict the visibility in Cape Town. The average multiple regression model was adjudged to be the best and most suitable model to determine the visibility in Cape Town based on the fact that it had the highest correlation coefficient and the lowest standard error. The predicted average monthly visibility values from this model were compared to the measured values and a low root mean square error of 2.25 km was obtained for the year 2014. The average multiple regression model was then used to estimate the minimum, average and maximum monthly visibility values for a six year period (2010 – 2015). The highest average visibility occurred in December 2014 with a value of 35 km while the average minimum visibility in June 2012 was estimated to be 16 km. The results obtained within this six-year period show that an inverse proportionality exists between the visibility and relative humidity while a directly proportional relationship exists between the visibility, maximum temperature and fraction of sunshine hours for the warm-summer Mediterranean climate of Cape Town.

The Kim model was used to estimate the scattering attenuation coefficient for each of the monthly visibility values from January 2010 – December 2015. During this six-year period, the estimated lowest mean attenuation occurred in November and was determined to be 0.24666 dB/km on the 850 nm wavelength, 0.21345 dB/km on 950 nm wavelength and 0.11303 dB/km on 1550 nm wavelength. This corresponds to a period when the maximum visibility is in excess of 38 km. Conversely, the highest mean atmospheric attenuation occurred in June. This corresponds to the time when visibility values could drop to values far

less than 4 km. The estimated high attenuation values are 151.15972 dB/km on 850 nm wavelength, 150.96553 dB/km on 950 nm wavelength and 150.32009 dB/km on 1550 nm wavelength. The average scattering atmospheric attenuation corresponding to the average visibility of 25 km is 0.40264 dB/km on 850 nm wavelength, 0.34843 dB/km on 950 nm wavelength and 0.18439 dB/km on 1550 nm wavelength.

For visibility values ranging from 20 – 1000 meters, various models were utilized to estimate the specific attenuation behavior of the atmosphere at such periods. The Ijaz and Naboulsi fog models were adjudged to be the most accurate models for estimating the atmospheric attenuations from thick to light fog weather. The Ijaz smoke model was used to estimate the resultant atmospheric attenuation due to smoke emanating from industrial chimneys and fire outbreaks which also result in much reduced visibility. For a visibility of about 250 meters, the Ijaz smoke model estimates the specific attenuation to be 88 dB/km on the 850 nm wavelength while the Naboulsi convection fog model estimates the atmospheric attenuation to be 68 dB/km on the 1550 nm wavelength. It was deduced that the Kruse, Kim and Ferdinandov models do not accurately estimate the specific attenuations for visibilities less than 1 km as compared to the other models investigated.

It is imperative to estimate the probability of exceeding a specific atmospheric attenuation value in a warm-summer Mediterranean climatic region at any given time before installing an OWC equipment so as to accurately predict the system's outage probability. For an OWC system transmitting optical signals on the 850 nm wavelength, the probability of encountering atmospheric attenuation in excess of 1 dB/km was calculated to be 0.300926 using both Kim and Ferdinandov models. On the other hand, the probability of encountering atmospheric attenuation in excess of 20 dB/km when transmitting on the 950 nm wavelength using both Kim and Ferdinandov models to estimate the specific attenuation, was 0.041667 and 0.032407, respectively. The probability of encountering atmospheric attenuation in excess of 150 dB/km when transmitting on the 1550 nm wavelength using Kim model was computed to be 0.013889.

Using the Kim model to evaluate the specific attenuation on the 850nm wavelength, the scattering atmospheric attenuation had a contribution of 7.7% to the total atmospheric loss for a link distance of 3 km. The scintillation loss was also computed to have a contribution of 95.96% to the total atmospheric loss for a link distance of 7 km and on a wavelength of 1550 nm. The little contributions of scattering losses to the total atmospheric loss clearly indicated that the visibility in a warm-summer Mediterranean climate has a fairly stable low average value. This means that the turbulence or scintillation losses are significantly high in this region. It was deduced that the fading loss and the outage probability have an inversely proportional relationship while the turbulence power loss increases greatly with increase in the link length. It was also observed that the wavelengths had very little or no impact on the fading loss characteristics as well as the power scintillation index.

In the link budget analysis performed for optical signals being transmitted on the 850 nm wavelength and with an average visibility of 25 km, the link length of 3 km must have a link margin of 5 dB. Also, reliable connection between the transmitter and receiver over a propagation distance of 3 km and on a 1550 nm wavelength with a visibility of 10 km will require a link margin of ~7.5 dB. It is generally accepted that for an OWC link to be available, the link margin must be greater than or equal to the total atmospheric attenuation for a particular link length. Of all the various models used to calculate the link availability for visibility values less than 1 km, the Naboulsi and Ijaz models predicted the link availability during foggy weather and smoky conditions better than the other models for the three wavelengths considered. Results showed that the OWC link availability reduces with increase in the propagation distance. It was also deduced that the optical signals being transmitted on the 1550 nm wavelength had better link availability over a specific propagation distance as compared to the 850 and 950 nm wavelengths.

Finally, a bit-error-rate (BER) performance analysis was conducted on cross M-QAM OWC systems using the results generated from the previous sections. It was deduced that in order to attain a certain bit error rate value, transmitting wavelengths of 850 nm and 950 nm require a higher SNR than at the 1550 nm wavelength. It can therefore be concluded that it is more power efficient to transmit optical signals on the 1550 nm wavelength using the spectral efficient cross QAM OWC system.

6.2 Future Work

The main objectives of this dissertation as stated in chapter one have been completed. However, more research work can be done to attain the 99.999% link availability of OWC systems in all weather conditions. They include:

Capacity analysis for quadrature spatial modulation (QSM) multiple input and output (MIMO) OWC systems over various atmospheric turbulence channels: Utilizing the inherent advantages in QSM systems and transmitting over the free space channel is one of the efficient methods of achieving better link availability during periods of severe turbulence.

Performance analysis of Index modulation OWC systems over lognormal and gamma-gamma turbulence channels: Using a low-complexity detection technique, OWC systems employing the use of index modulation in the transmission of optical signals is one of the possible ways of achieving improved system performance over other older modulation schemes.

References

[1] A. G. Bell, "On the production and reproduction of sound by light," American Journal of Science, vol. 20, pp. 305-324, 1880.

[2] D. Killinger, "Free space optics for laser communication through the air," Optics and Photonics News, vol. 13, pp. 36-42, 2002.

[3] F. E. Goodwin, "A review of operational laser communication systems," Proceedings of the IEEE, vol. 58, pp. 1746-1752, 1970.

[4] H. Hemmati, "Interplanetary laser communications," Optics and Photonics News, vol. 18, pp. 22-27, 2007.

[5] Z. Sodnik, B. Furch, and H. Lutz, "Free-space laser communication activities in Europe: SILEX and beyond," in Lasers and Electro-Optics Society, 2006. LEOS 2006. 19th Annual Meeting of the IEEE, 2006, pp. 78-79.

[6] C. Colvero, M. Cordeiro, G. De Faria, and J. Von der Weid, "Experimental comparison between far-and near-infrared wavelengths in free-space optical systems," Microwave and optical technology letters, vol. 46, pp. 319-323, 2005.

[7] B. Flecker, E. Leitgeb, S. S. Muhammad, C. Chlestil, E. Duca, and V. Carrozzo, "Measurement of light attenuation in fog and snow conditions for terrestrial FSO links," in 15th IST Mobile and Wireless Communications Summit, 2006.

[8] S. Hardy, "Free-space optics systems are finding their niches," Lightwave, pp. 33-36, 2005.

[9] E. J. Korevaar, I. I. Kim, and B. McArthur, "Atmospheric propagation characteristics of highest importance to commercial free space optics," in Proceedings of SPIE, 2003, pp. 1-12.

[10] A. Usman, K. Olaore, and G. Ismaila, "Estimating visibility using some Meteorological data at Sokoto, Nigeria," Int. J. Basic Appli. Sci, vol. 1, pp. 810-815, 2013.

[11] I. I. Kim, B. McArthur, and E. J. Korevaar, "Comparison of laser beam propagation at 785 nm and 1550 nm in fog and haze for optical wireless communications," in Information Technologies 2000, 2001, pp. 26-37.

[12] M. Al Naboulsi, "Fog attenuation prediction for optical and infrared waves," Optical Engineering, vol. 43, pp. 319-329, 2004.

[13] E. Ferdinandov, K. Dimitrov, A. Dandarov, and I. Bakalski, "A general model of the atmospheric scattering in the wavelength interval 300–1100 nm," Radioengineering, vol. 18, pp. 517-521, 2009.

[14] M. Grabner and V. Kvicera, "Case study of fog attenuation on 830 nm and 1550 nm free-space optical links," in Antennas and Propagation (EuCAP), 2010 Proceedings of the Fourth European Conference on, 2010, pp. 1-4.

[15] M. Ijaz, "Experimental Characterisation and Modelling of Atmospheric Fog and Turbulence in FSO," Northumbria University, 2013.

[16] A. Prokes, "Atmospheric effects on availability of free space optics systems," Optical Engineering, vol. 48, pp. 1-10, 2009.

[17] A. Bekkali, C. B. Naila, K. Kazaura, K. Wakamori, and M. Matsumoto, "Transmission analysis of OFDM-based wireless services over turbulent radio-on-FSO links modeled by gamma–gamma distribution," IEEE Photonics Journal, vol. 2, pp. 510-520, 2010.

[18] N. H. M. Noor, A. Naji, and W. Al-Khateeb, "Theoretical analysis of multiple transmitters/receivers on the performance of free space optics (FSO) link," in Space Science and Communication (IconSpace), 2011 IEEE International Conference on, 2011, pp. 291-295.

[19] X. Wu, P. Liu, and M. Matsumoto, "A study on atmospheric turbulence effects in full-optical free-space communication systems," in Wireless Communications Networking and Mobile Computing (WiCOM), 2010 6th International Conference on, 2010, pp. 1-5.

[20] S. A. Zabidi, M. R. Islam, W. Al Khateeb, and A. W. Naji, "Investigating of rain attenuation impact on free space optics propagation in tropical region," in Mechatronics (ICOM), 2011 4th International Conference On, 2011, pp. 1-6.

[21] M. Niu, J. Cheng, and J. F. Holzman, "Diversity reception for coherent free-space optical communications over K-distributed atmospheric turbulence channels," in Wireless Communications and Networking Conference (WCNC), 2010 IEEE, 2010, pp. 1-6.

[22] T. Yamashita, M. Morita, M. Shimizu, D. Eto, K. Shiratama, and S. Murata, "The new tracking control system for Free-Space Optical Communications," in Space Optical Systems and Applications (ICSOS), 2011 International Conference on, 2011, pp. 122-131.

[23] M. Gregory and S. Badri-Hoeher, "Characterization of maritime RF/FSO channel," in Space Optical Systems and Applications (ICSOS), 2011 International Conference on, 2011, pp. 21-27.

[24] W. O. Popoola, "Subcarrier intensity modulated free-space optical communication systems," Northumbria University, 2009.

[25] S. Bloom, E. Korevaar, J. Schuster, and H. Willebrand, "Understanding the performance of free-space optics [Invited]," Journal of optical Networking, vol. 2, pp. 178-200, 2003.

[26] H. Willebrand and B. S. Ghuman, Free space optics: enabling optical connectivity in today's networks: SAMS publishing, 2002.

[27] R. M. Gagliardi and S. Karp, "Optical communications," New York, Wiley-Interscience, 1976.

[28] W. K. Pratt, "Laser Communication Systems," 1969.

[29] S. Betti, G. De Marchis, and E. Iannone, Coherent optical communications systems: Wiley-Interscience, 1995.

[30] O. Bouchet, H. Sizun, C. Boisrobert, and F. De Fornel, Free-space optics: propagation and communication vol. 91: John Wiley & Sons, 2010.

[31] I. E. Commission, "IEC 60825-1 Safety of laser products-part 1: equipment classification and, requirements," Geneva, Switzerland: International Electrotechnical Commission, 2007.

[32] P. Anokye, "Free space optical communication over the Ghanaian Turbulent Atmospheric Channel," KWAME NKRUMAH UNIVERSITY OF SCIENCE AND TECHNOLOGY, KUMASI, 2014.

[33] I. Recommendation, "1: Propagation data required for the design of terrestrial free-space optical links," International Telecommunication Union Radiocommunication Sector (ITU-R) Std, 1817.

[34] J. Mohale, M. R. Handura, T. O. Olwal, and C. N. Nyirenda, "Feasibility study of free-space optical communication for South Africa," Optical Engineering, vol. 55, pp. 1-10, 2016.

[35] P. W. Kruse, L. D. McGlauchlin, and R. B. McQuistan, "Elements of infrared technology: Generation, transmission and detection," New York: Wiley, 1962.

[36] L. C. Andrews, R. L. Phillips, and C. Y. Hopen, Laser beam scintillation with applications vol. 99: SPIE press, 2001.

[37] M. Faridzadeh, A. Gholami, Z. Ghassemlooy, and A. Gatri, "BPSK-SIM-PPM modulation for free space optical communications," in Telecommunications (IST), 2014 7th International Symposium on, 2014, pp. 794-798.

[38] K. P. Peppas and C. K. Datsikas, "Average symbol error probability of general-order rectangular quadrature amplitude modulation of optical wireless communication systems over atmospheric turbulence channels," Journal of Optical Communications and Networking, vol. 2, pp. 102-110, 2010.

[39] B. T. Vu, N. T. Dang, T. C. Thang, and A. T. Pham, "Bit error rate analysis of rectangular QAM/FSO systems using an APD receiver over atmospheric turbulence channels," Journal of Optical Communications and Networking, vol. 5, pp. 437-446, 2013.

[40] X. Tang, S. Rajbhandari, W. O. Popoola, Z. Ghassemlooy, E. Leitgeb, S. Muhammad, et al., "Performance of BPSK subcarrier intensity modulation free-space optical communications using a log-normal atmospheric turbulence model," in Photonics and Optoelectronic (SOPO), 2010 Symposium on, 2010, pp. 1-4.

[41] W. O. Popoola, Z. Ghassemlooy, J. Allen, E. Leitgeb, and S. Gao, "Free-space optical communication employing subcarrier modulation and spatial diversity in atmospheric turbulence channel," IET optoelectronics, vol. 2, pp. 16-23, 2008.

[42] P. K. Vitthaladevuni, M.-S. Alouini, and J. C. Kieffer, "Exact BER computation for cross QAM constellations," IEEE Transactions on Wireless Communications, vol. 4, pp. 3039-3050, 2005.